



Synthesis and Evaluation of Acetylcholinesterase Inhibitory Activity of
Chromone Derivatives

Paptawan Suwanhom

A Thesis Submitted in Partial Fulfillment of the Requirements for the
Degree of Master of Pharmacy in Pharmaceutical Sciences
Prince of Songkla University

2017

Copyright of Prince of Songkla University

This is to certify that the work here submitted is the result of the candidate's own investigations. Due acknowledgement has been made of any assistance received.

..... Signature

(Assist. Prof. Dr. Luelak Lomlim)

Major Advisor

..... Signature

(Miss Paptawan Suwanhom)

Candidate

I hereby certify that this work has not been accepted in substance for any degree, and is not being currently submitted in candidature for any degree.

..... Signature

(Miss Paptawan Suwanhom)

Candidate

ชื่อวิทยานิพนธ์ การสังเคราะห์และศึกษาฤทธิ์ยับยั้งเอนไซม์อะเซทิลโคลีนเอสเทอเรสของ
อนุพันธ์โครโมน

ผู้เขียน นางสาวภาพตะวัน สุวรรณหอม

สาขาวิชา เกษษศาสตร์

ปีการศึกษา 2560

บทคัดย่อ

โรคอัลไซเมอร์เป็นโรคที่พบมากถึง 30% ของประชากรโลกที่มีอายุเกิน 65 ปี และปัจจุบันมีรายงานว่ามีคนไทยถึง 600,000 คน เป็นโรคอัลไซเมอร์ สาเหตุสำคัญในการเกิดโรคคาดว่าเกี่ยวข้องกับ การลดลงของสารสื่อประสาทอะเซทิลโคลีน โดยมีเอนไซม์อะเซทิลโคลีนเอสเทอเรสและเอนไซม์บิวทิลโคลีนเอสเทอเรสทำลายสารสื่อประสาทนี้ด้วยกระบวนการย่อยสลายด้วยน้ำ ยาที่มีฤทธิ์ยับยั้งการทำงานของเอนไซม์เป็นกลุ่มยาหลักที่ใช้ในการรักษาโรคอัลไซเมอร์ในปัจจุบัน เช่น โดเนเพซิล, ทาครีน และกาแลนทามีน

ในงานวิจัยนี้ได้มีการออกแบบและสังเคราะห์อนุพันธ์ของโครโมน จำนวน 12 ชนิดโดยใช้สาร *N*-(4-((2-เมทอกซีเบนซิล)เอทิล)อะมิโน)บิวทิล)-5-ไฮดรอกซี-4-ออกโซ-4*H*-โครมิน-2-คาร์บอกซาไมด์ (A) และยาโดเนเพซิล เป็นสารต้นแบบ สารที่สังเคราะห์ได้นำไปพิสูจน์โครงสร้าง IR, ¹H-NMR, ¹³C-NMR และ mass spectrometry จากนั้นนำสารไปทดสอบฤทธิ์ยับยั้งเอนไซม์อะเซทิลโคลีนเอสเทอเรสและเอนไซม์บิวทิลโคลีนเอสเทอเรส ตามวิธีการของ Ellman โดยเลือกสารสังเคราะห์ที่มีฤทธิ์ที่ดีที่สุดมาศึกษาจลนพลศาสตร์ของเอนไซม์และศึกษาอันตรกิริยาระหว่างลิแกนด์และเอนไซม์โดยใช้วิธีการทางคอมพิวเตอร์

อนุพันธ์โครโมน-2-คาร์บอกซามิโด-แอลคิลเอมีน (7-18) ให้ค่าเปอร์เซ็นต์การยับยั้งเอนไซม์อะเซทิลโคลีนเอสเทอเรสและเอนไซม์บิวทิลโคลีนเอสเทอเรสมากกว่า 50% ที่ความเข้มข้น 100 ไมโครโมลาร์ สารหมายเลข 7-18 แสดงค่า IC₅₀ ในการยับยั้งเอนไซม์อะเซทิลโคลีนเอสเทอเรสอยู่ในระดับนาโนโมลาถึงไมโครโมลาร์ (IC₅₀=0.09-9.16 μM) สามารถยับยั้งได้ดีกว่าเอนไซม์บิวทิลโคลีนเอสเทอเรส (IC₅₀=12.09-44.56 μM) จากการศึกษาพบว่าสารหมายเลข 14 (IC₅₀= 0.09±0.02 μM) มีฤทธิ์ยับยั้งเอนไซม์อะเซทิลโคลีนเอสเทอเรสสูงที่สุดและมีความแรงในการออกฤทธิ์ที่สูงกว่ายาทาครีนและจากการศึกษาจลนพลศาสตร์ของเอนไซม์และศึกษาอันตรกิริยาระหว่างลิแกนด์กับเอนไซม์พบว่า สารหมายเลข 14 มีการยับยั้งในลักษณะไม่สามารถแข่งขันได้โดยตรง (uncompetitive) และมีการยับยั้งโดยจับกับเอนไซม์ทั้งสองตำแหน่ง (dual-binding site)

Thesis Title	Synthesis and evaluation of acetylcholinesterase inhibitory activity of chromone derivatives
Author	Miss Paptawan Suwanhom
Major Program	Pharmaceutical Sciences
Academic Year	2017

ABSTRACT

Alzheimer's disease (AD) is considered as one of the biggest global public burden. An estimate 30% of the world's population over age of 65 are affected by AD. Nowadays, six hundred thousand of Thai people were suffered from this disease. Cause of this disease is proposed to be associated with reduced level of the neurotransmitter acetylcholine (ACh). Cholinesterase, namely acetylcholinesterase (AChE) and butyrylcholinesterase (BChE), destroy ACh through hydrolysis. Cholinesterase inhibitors (ChEI) portray the main group of drugs currently used for the treatment of AD such as donepezil, tacrine and galanthamine.

In this research, 12 chromone derivatives were designed and synthesized using compound *N*-(4-((2-methoxybenzyl)ethyl)amino)butyl)-5-hydroxy-4-oxo-4*H*-chromene-2-carboxamide (**A**) and donepezil were used as references. Structure of target compounds was characterized with IR, ¹H-NMR, ¹³C-NMR spectroscopy and mass spectrometry. Cholinesterase inhibitory activity of chromone derivatives (**7-18**) was evaluated using the Ellman's method. In addition, the kinetic study for characterization of AChE inhibition and molecular docking studies demonstrated interactions between enzyme and ligand were evaluated by using computer program.

Chromone derivatives (**7-18**) showed percent inhibition of AChE and BChE higher than 50% at 100 μM. Most of the synthesized compound exhibited potent AChE inhibitory activities at the nanomolar to micromolar range (IC₅₀ 0.09-9.16 μM) and demonstrated weak BChE inhibitory activities at the micromolar range (IC₅₀ 12.09-44.56 μM). Compound **14** was the most potent AChEI, it exerted IC₅₀ in nanomolar range, higher activity than the clinical used drug tacrine. Enzyme kinetic study and molecular docking revealed that compound **14** was uncompetitive inhibitor and dual-binding site inhibitor.

ACKNOWLEDGMENT

The success of this research have occurred with the help of many people, so I would like to express my gratefulness.

I would like to thank my advisor, Assist. Prof. Dr. Luelak Lomlim for giving an opportunity, kindness, valuable guidance, continual suggestion, and encouragement throughout the course of my graduate study.

I would like to thank my co-advisor, Assoc. Prof. Dr. Vannajan Sanghiran Lee for suggestions and support in the study of molecular docking.

I would like to thank Dr. Trerapat Nualnoi for suggestions and support in the study of enzyme kinetic.

I would also like to thank:

The examination committee members of this thesis for their valuable time,
Thesis financial support from Graduate School, Prince of Songkla University (PSU).

Our colleagues from Laboratory at the New Chemistry Building Department of Chemistry, Faculty of Science, University of Malaya, who provided insight and expertise that greatly assisted the research.

All staffs of the Department of Pharmaceutical Chemistry, Pharmaceutical Laboratory Service Center, Central Laboratory Unit, for their help in technical aspects of this thesis,

Miss Jiraporn Kara for suggestion and training *in vitro* assay and my friends for helps and encouragement.

Finally, my family for their love, understanding, encouragement, and supporting in everything.

Paptawan Suwanhom

CONTENTS

	Page
CHAPTER 1 INTRODUCTION	1
1. Background, Rationale and Objectives	1
1.1 Alzheimer's disease	1
1.1.1 Symptoms	1
1.1.2 Causes	1
1.1.3 Acetylcholine (ACh)	3
1.1.4 Acetylcholinesterase (AChE)	4
1.1.5 Butyrylcholinesterase (BChE)	6
1.2 Cholinesterase Inhibitors	9
1.2.1 Mechanism of cholinesterase Inhibition	9
1.2.2 Clinical Pharmacology of the cholinesterase Inhibition	12
1.3 Rationale	15
2. Review literatures	17
3. Objectives	25
CHAPTER 2 EXPERIMENT	26
1. Instruments	26
2. Chemicals	26
3. Methods	28
3.1 Synthesis and characterization	28
3.2 Acetylcholinesterase inhibitory activity	45
3.3 Butyrylcholinesterase inhibitory activity	46
3.4 The kinetic study for characterization of AChE inhibition	46
3.5 Molecular docking studies	46

CONTENTS (continued)

CHAPTER 3 RESULTS AND DISCUSSION	48
1. Synthesis of chromone derivatives	48
2. Evaluation for <i>in vitro</i> inhibitory activities AChE and BChE	51
3. Kinetic study for the inhibition of AChE	64
4. Molecular docking study	67
CHAPTER 4 CONCLUSION	75
BIBLIOGRAPHY	77
APPENDIX	80
VITAE	140

LIST OF TABLES

Table	Page
Table 1. Modes of inhibition (competitive, non-competitive, uncompetitive and mixed-type inhibition)	10
Table 2. Acetylcholinesterase inhibitory activity of 7, 4'-O-modified genistein derivatives.	18
Table 3. Activity of AChEI and BChEI of 7-aminoalkyl-substituted flavonoid derivatives.	20
Table 4. Structure of the chromone-2-carboxamido-alkylamine derivatives.	25
Table 5. The synthesized of chromone derivatives (7-18)	51
Table 6. % Inhibition of AChE and BChE of chromone derivatives.	54
Table 7. Inhibition concentration at 50% to AChE (electric eel) of chromone derivatives.	57
Table 8. Inhibition concentration at 50% to BChE (horse serum) of chromone derivatives.	59
Table 9. Inhibition concentration at 50% to AChE (human) of chromone derivatives.	61
Table 10. AChE and BChE inhibitory activity and selectivity index of chromone derivatives.	62
Table 11. Comparison between compound 14 and 15 by t-test	63
Table 12. Data of Michaelis-Menten with plotting between velocity (V) and concentration of substrate [S] acetylthiocholine (ATCI)	65
Table 13. Affinity of binding energy of compound 14, A (Liu Q. et al. 2015.), tacrine and donepezil.	67
Table 14. Binding energy, key enzyme-ligand interactions and distance of compound 14, A (Liu Q. et al. 2015.), tacrine and donepezil.	73

LIST OF FIGURES

Figure	Page
Figure 1. The chemical structure of acetylcholine	3
Figure 2. Acetylcholine in cholinergic synapse.	3
Figure 3. Cholinesterase activity in the cortex and hippocampus of human AD brain.	4
Figure 4. Structure of active site of <i>TcAChE</i>	5
Figure 5. Mechanism of ACh hydrolysis catalyzed by AChE	5
Figure 6. Structure of active site of <i>HuBChE</i> .	6
Figure 7. The kinetic enzyme of Michaelis-Menten between concentration of substrate [S] and reaction velocity (V)	8
Figure 8. The kinetic enzyme of Lineweaver-Burk between 1/[S] and reaction 1/(V)	8
Figure 9. Structure and molecular docking study of tacrine- <i>TcAChE</i> .	12
Figure 10. Structure and molecular docking study of galanthamine- <i>TcAChE</i> .	13
Figure 11. Structure and molecular docking study of NAP- <i>TcAChE</i> .	14
Figure 12. Structure and molecular docking study of donepezil.	15
Figure 13. The structure of <i>N</i> -(4-((2-methoxybenzyl)ethyl)amino)butyl)-5-hydroxy-4-oxo-4 <i>H</i> -chromene-2-carboxamide (Compound A) within the active site of AChE.	16
Figure 14. Structure design of chromone derivatives in this research.	17
Figure 15. Structure design of 7, 4'- <i>O</i> -modified genistein derivatives.	18
Figure 16. The structure of compound B(b) within the active site of AChE.	19
Figure 17. The structure of compound C within the active site of AChE.	22
Figure 18. Structure design of scutellarein- <i>O</i> -acetamidoalkylbenzylamines derivatives (compound D).	23
Figure 19. Structure of chromone derivatives (compound D).	23
Figure 20. The structure of compound D within the active site.	24
Figure 21. The general procedure of synthesis of chromone derivatives (7-18): (i) NaH/THF, room temp (4-6); (ii) amine/CH ₂ Cl ₂ /reflux, then CH ₃ COOH, 70 °C.	28
Figure 22. The mechanism of Claisen condensation.	49
Figure 23. The mechanism of aminolysis reaction.	50

LIST OF FIGURES (continued)

Figure	Page
Figure 24. The reaction of ATCI in the presence of AChE and DTNB.	52
Figure 25. The reaction of BTCl in the presence of BChE.	53
Figure 26. Comparison of %inhibition to AChE and BChE of chromone derivatives.	55
Figure 27. Michaelis-Menten with plotting between velocity (V) and concentration of substrate [S] acetylthiocholine (ATCI).	66
Figure 28. Lineweaver-Burk plot	66
Figure 29. Molecular docking study of compound 14 -TcAChE	68
Figure 30. Molecular docking study of compound 14 -HuBChE	68
Figure 31. Molecular docking study of compound A -TcAChE.	69
Figure 32. Molecular docking study of compound A -HuBChE.	70
Figure 33. Molecular docking study of Tacrine-TcAChE	70
Figure 34. Molecular docking study of Tacrine-HuBChE	71
Figure 35. Molecular docking study of donepezil-TcAChE	71
Figure 36. Molecular docking study of donepezil-HuBChE	72
Figure 37. The IR spectrum of Ethyl-4-oxo-4 <i>H</i> -chromene-2-carboxylate (4)	81
Figure 38. The ¹ H-NMR spectrum of Ethyl-4-oxo-4 <i>H</i> -chromene-2-carboxylate (4) in DMSO- <i>d</i> ₆	82
Figure 39. The ¹ H-NMR spectrum of Ethyl-4-oxo-4 <i>H</i> -chromene-2-carboxylate (4) in DMSO- <i>d</i> ₆ (Enlarged scale)	83
Figure 40. The IR spectrum of Ethyl-7-methoxy-4-oxo-4 <i>H</i> -chromene-2-carboxylate (5)	84
Figure 41. The ¹ H-NMR spectrum of Ethyl-7-methoxy-4-oxo-4 <i>H</i> -chromene-2-carboxylate (5) in DMSO- <i>d</i> ₆	85
Figure 42. The ¹ H-NMR spectrum of Ethyl-7-methoxy-4-oxo-4 <i>H</i> -chromene-2-carboxylate (5) in DMSO- <i>d</i> ₆ (Enlarged scale)	86
Figure 43. The IR spectrum of Ethyl-6, 7-dimethoxy-4-oxo-4 <i>H</i> -chromene-2-carboxylate (6)	87
Figure 44. The ¹ H-NMR spectrum of Ethyl-6, 7-dimethoxy-4-oxo-4 <i>H</i> -chromene-2-carboxylate (6) in DMSO- <i>d</i> ₆	88

LIST OF FIGURES (continued)

Figure	Page
Figure 45. The ^1H -NMR spectrum of Ethyl-6, 7-dimethoxy-4-oxo-4 <i>H</i> -chromene-2-carboxylate (6) in $\text{DMSO-}d_6$ (Enlarged scale)	89
Figure 46. The IR spectrum of <i>N</i> -(2-(dimethylamino)ethyl)-4-oxo-4 <i>H</i> -chromene-2-carboxamide (7)	90
Figure 47. The ^1H -NMR spectrum of <i>N</i> -(2-(dimethylamino)ethyl)-4-oxo-4 <i>H</i> -chromene-2-carboxamide (7) in $\text{DMSO-}d_6$	91
Figure 48. The ^1H -NMR spectrum of <i>N</i> -(2-(dimethylamino)ethyl)-4-oxo-4 <i>H</i> -chromene-2-carboxamide (7) in $\text{DMSO-}d_6$ (Enlarged scale)	92
Figure 49. The ^{13}C -NMR spectrum of <i>N</i> -(2-(dimethylamino)ethyl)-4-oxo-4 <i>H</i> -chromene-2-carboxamide (7) in $\text{DMSO-}d_6$	93
Figure 50. The IR spectrum of 4-oxo- <i>N</i> -(2-(piperidin-1-yl)ethyl)-4 <i>H</i> -chromene-2-carboxamide (8)	94
Figure 51. The ^1H -NMR spectrum of 4-oxo- <i>N</i> -(2-(piperidin-1-yl)ethyl)-4 <i>H</i> -chromene-2-carboxamide (8) in $\text{DMSO-}d_6$	95
Figure 52. The ^1H -NMR spectrum of 4-oxo- <i>N</i> -(2-(piperidin-1-yl)ethyl)-4 <i>H</i> -chromene-2-carboxamide (8) in $\text{DMSO-}d_6$ (Enlarged scale)	96
Figure 53. The ^{13}C -NMR spectrum of 4-oxo- <i>N</i> -(2-(piperidin-1-yl)ethyl)-4 <i>H</i> -chromene-2-carboxamide (8) in $\text{DMSO-}d_6$	97
Figure 54. The IR spectrum of <i>N</i> -(3-(dimethylamino)propyl)-4-oxo-4 <i>H</i> -chromene-2-carboxamide (9)	98
Figure 55. The ^1H -NMR spectrum of <i>N</i> -(3-(dimethylamino)propyl)-4-oxo-4 <i>H</i> -chromene-2-carboxamide (9) in $\text{DMSO-}d_6$	99
Figure 56. The ^1H -NMR spectrum of <i>N</i> -(3-(dimethylamino)propyl)-4-oxo-4 <i>H</i> -chromene-2-carboxamide (9) in $\text{DMSO-}d_6$ (Enlarged scale)	100
Figure 57. The ^1H -NMR spectrum of <i>N</i> -(3-(dimethylamino)propyl)-4-oxo-4 <i>H</i> -chromene-2-carboxamide (9) in $\text{DMSO-}d_6$ (Enlarged scale)	101
Figure 58. The ^{13}C -NMR spectrum of <i>N</i> -(3-(dimethylamino)propyl)-4-oxo-4 <i>H</i> -chromene-2-carboxamide (9) in $\text{DMSO-}d_6$	102

LIST OF FIGURES (continued)

Figure	Page
Figure 59. The IR spectrum of 4-oxo- <i>N</i> -(3-(piperidin-1-yl)propyl)-4 <i>H</i> -chromene-2-carboxamide (10)	103
Figure 60. The ¹ H-NMR spectrum of 4-oxo- <i>N</i> -(3-(piperidin-1-yl)propyl)-4 <i>H</i> -chromene-2-carboxamide (10) in DMSO- <i>d</i> ₆	104
Figure 61. The ¹ H-NMR spectrum of 4-oxo- <i>N</i> -(3-(piperidin-1-yl)propyl)-4 <i>H</i> -chromene-2-carboxamide (10) in DMSO- <i>d</i> ₆ (Enlarged scale)	105
Figure 62. The ¹ H-NMR spectrum of 4-oxo- <i>N</i> -(3-(piperidin-1-yl)propyl)-4 <i>H</i> -chromene-2-carboxamide (10) in DMSO- <i>d</i> ₆ (Enlarged scale)	106
Figure 63. The ¹³ C-NMR spectrum of 4-oxo- <i>N</i> -(3-(piperidin-1-yl)propyl)-4 <i>H</i> -chromene-2-carboxamide (10) in DMSO- <i>d</i> ₆	107
Figure 64. The IR spectrum of <i>N</i> -(2-(dimethylamino)ethyl)-7-methoxy-4-oxo-4 <i>H</i> -chromene-2-carboxamide (11)	108
Figure 65. The ¹ H-NMR spectrum of <i>N</i> -(2-(dimethylamino)ethyl)-7-methoxy-4-oxo-4 <i>H</i> -chromene-2-carboxamide (11) in DMSO- <i>d</i> ₆	109
Figure 66. The ¹ H-NMR spectrum of <i>N</i> -(2-(dimethylamino)ethyl)-7-methoxy-4-oxo-4 <i>H</i> -chromene-2-carboxamide (11) in DMSO- <i>d</i> ₆ (Enlarged scale)	110
Figure 67. The ¹³ C-NMR spectrum of <i>N</i> -(2-(dimethylamino)ethyl)-7-methoxy-4-oxo-4 <i>H</i> -chromene-2-carboxamide (11) in DMSO- <i>d</i> ₆	111
Figure 68. The IR spectrum of 7-methoxy-4-oxo- <i>N</i> -(2-(piperidin-1-yl)ethyl)-4 <i>H</i> -chromene-2-carboxamide (12)	112
Figure 69. The ¹ H-NMR spectrum of 7-methoxy-4-oxo- <i>N</i> -(2-(piperidin-1-yl)ethyl)-4 <i>H</i> -chromene-2-carboxamide (12) in DMSO- <i>d</i> ₆	113
Figure 70. The ¹ H-NMR spectrum of 7-methoxy-4-oxo- <i>N</i> -(2-(piperidin-1-yl)ethyl)-4 <i>H</i> -chromene-2-carboxamide (12) in DMSO- <i>d</i> ₆ (Enlarged scale)	114
Figure 71. The ¹³ C-NMR spectrum of 7-methoxy-4-oxo- <i>N</i> -(2-(piperidin-1-yl)ethyl)-4 <i>H</i> -chromene-2-carboxamide (12) in DMSO- <i>d</i> ₆	115
Figure 72. The IR spectrum of <i>N</i> -(3-(dimethylamino)propyl)-7-methoxy-4-oxo-4 <i>H</i> -chromene-2-carboxamide (13)	116

LIST OF FIGURES (continued)

Figure	Page
Figure 73. The ^1H -NMR spectrum of <i>N</i> -(3-(dimethylamino)propyl)-7-methoxy-4-oxo-4 <i>H</i> -chromene-2-carboxamide (13) in $\text{DMSO-}d_6$	117
Figure 74. The ^1H -NMR spectrum of <i>N</i> -(3-(dimethylamino)propyl)-7-methoxy-4-oxo-4 <i>H</i> -chromene-2-carboxamide (13) in $\text{DMSO-}d_6$ (Enlarged scale)	118
Figure 75. The ^{13}C -NMR spectrum of <i>N</i> -(3-(dimethylamino)propyl)-7-methoxy-4-oxo-4 <i>H</i> -chromene-2-carboxamide (13) in $\text{DMSO-}d_6$	119
Figure 76. The IR spectrum of 7-methoxy-4-oxo- <i>N</i> -(3-(piperidin-1-yl)propyl)-4 <i>H</i> -chromene-2-carboxamide (14)	120
Figure 77. The ^1H -NMR spectrum of 7-methoxy-4-oxo- <i>N</i> -(3-(piperidin-1-yl)propyl)-4 <i>H</i> -chromene-2-carboxamide (14) in $\text{DMSO-}d_6$	121
Figure 78. The ^1H -NMR spectrum of 7-methoxy-4-oxo- <i>N</i> -(3-(piperidin-1-yl)propyl)-4 <i>H</i> -chromene-2-carboxamide (14) in $\text{DMSO-}d_6$ (Enlarged scale)	122
Figure 79. The ^{13}C -NMR spectrum of 7-methoxy-4-oxo- <i>N</i> -(3-(piperidin-1-yl)propyl)-4 <i>H</i> -chromene-2-carboxamide (14) in $\text{DMSO-}d_6$	123
Figure 80. The IR spectrum of <i>N</i> -(2-(dimethylamino)ethyl)-6, 7-dimethoxy-4-oxo-4 <i>H</i> -chromene-2-carboxamide (15)	124
Figure 81. The ^1H -NMR spectrum of <i>N</i> -(2-(dimethylamino)ethyl)-6, 7-dimethoxy-4-oxo-4 <i>H</i> -chromene-2-carboxamide (15) in $\text{DMSO-}d_6$	125
Figure 82. The ^1H -NMR spectrum of <i>N</i> -(2-(dimethylamino)ethyl)-6, 7-dimethoxy-4-oxo-4 <i>H</i> -chromene-2-carboxamide (15) in $\text{DMSO-}d_6$ (Enlarged scale)	126
Figure 83. The ^{13}C -NMR spectrum of <i>N</i> -(2-(dimethylamino)ethyl)-6, 7-dimethoxy-4-oxo-4 <i>H</i> -chromene-2-carboxamide (15) in $\text{DMSO-}d_6$	127
Figure 84. The IR spectrum of 6, 7-dimethoxy-4-oxo- <i>N</i> -(2-(piperidin-1-yl)ethyl)-4 <i>H</i> -chromene-2-carboxamide (16)	128
Figure 85. The ^1H -NMR spectrum of 6, 7-dimethoxy-4-oxo- <i>N</i> -(2-(piperidin-1-yl)ethyl)-4 <i>H</i> -chromene-2-carboxamide (16) in $\text{DMSO-}d_6$	129
Figure 86. The ^1H -NMR spectrum of 6, 7-dimethoxy-4-oxo- <i>N</i> -(2-(piperidin-1-yl)ethyl)-4 <i>H</i> -chromene-2-carboxamide (16) in $\text{DMSO-}d_6$ (Enlarged scale)	130

LIST OF FIGURES (continued)

Figure	Page
Figure 87. The ^{13}C -NMR spectrum of 6, 7-dimethoxy-4-oxo- <i>N</i> -(2-(piperidin-1-yl)ethyl)-4 <i>H</i> -chromene-2-carboxamide (16) in $\text{DMSO-}d_6$	131
Figure 88. The IR spectrum of <i>N</i> -(3-(dimethylamino)propyl)-6, 7-dimethoxy-4-oxo-4 <i>H</i> -chromene-2-carboxamide (17)	132
Figure 89. The ^1H -NMR spectrum of <i>N</i> -(3-(dimethylamino)propyl)-6, 7-dimethoxy-4-oxo-4 <i>H</i> -chromene-2-carboxamide (17) in $\text{DMSO-}d_6$	133
Figure 90. The ^1H -NMR spectrum of <i>N</i> -(3-(dimethylamino)propyl)-6, 7-dimethoxy-4-oxo-4 <i>H</i> -chromene-2-carboxamide (17) in $\text{DMSO-}d_6$ (Enlarged scale)	134
Figure 91. The ^{13}C -NMR spectrum of <i>N</i> -(3-(dimethylamino)propyl)-6, 7-dimethoxy-4-oxo-4 <i>H</i> -chromene-2-carboxamide (17) in $\text{DMSO-}d_6$	135
Figure 92. The IR spectrum of 6, 7-dimethoxy-4-oxo- <i>N</i> -(3-(piperidin-1-yl)propyl)-4 <i>H</i> -chromene-2-carboxamide (18)	136
Figure 93. The ^1H -NMR spectrum of 6, 7-dimethoxy-4-oxo- <i>N</i> -(3-(piperidin-1-yl)propyl)-4 <i>H</i> -chromene-2-carboxamide (18) in $\text{DMSO-}d_6$	137
Figure 94. The ^1H -NMR spectrum of 6, 7-dimethoxy-4-oxo- <i>N</i> -(3-(piperidin-1-yl)propyl)-4 <i>H</i> -chromene-2-carboxamide (18) in $\text{DMSO-}d_6$ (Enlarged scale)	138
Figure 95. The ^{13}C -NMR spectrum of 6, 7-dimethoxy-4-oxo- <i>N</i> -(3-(piperidin-1-yl)propyl)-4 <i>H</i> -chromene-2-carboxamide (18) in $\text{DMSO-}d_6$	139

LIST OF ABBREVIATIONS AND SYBOLS

A β	Amyloid-beta
Acetyl CoA	Acetyl Coenzyme A
ACh	Acetylcholine
AChE	Acetylcholinesterase
AChEI	Acetylcholinesterase inhibitor
ATCI	Acetylthiocholine iodide
AD	Alzheimer's disease
APP	Amyloid precursor protein
Asp	Aspartic acid
BChE	Butyrylcholinesterase
BTCI	Butyrylthiocholine iodide
CAS	Catalytic anionic site
CDCl ₃	Deuterated chloroform
CH ₂ Cl ₂	Dichloromethane
¹³ C-NMR	¹³ C-Nuclear magnetic resonance spectroscopy
CNS	Central nervous system
DMSO	Dimethyl sulfoxide
DTNB	5, 5'-Disthiobis(2-nitrobenzoic acid)
<i>d</i>	Doublet (for NMR signal)
<i>dd</i>	Doublet of Doublet (for NMR signal)
EI-MS	Electron impact-Mass spectrometry
EtOAc	Ethyl acetate
EtOH	Ethanol
FTIR	Fourier Transform Infrared Spectroscopy
Glu	Glutamic acid
Gly	Glycine
HCl	Hydrochloric acid
His	Histidine
¹ H-NMR	¹ H Nuclear magnetic resonance spectroscopy
<i>Hu</i> AChE	Human acetylcholinesterase
<i>Hu</i> BChE	Human butyrylcholinesterase

LIST OF ABBREVIATIONS AND SYBOLS (continued)

<i>Hz</i>	Hertz
<i>J</i>	Coupling constant
KBr	Potassium bromide
Leu	Leucine
MeOH	Methanol
m.p.	Melting point
m/z	Mass-over-charge ratio
NaOH	Sodium hydroxide
PAS	Peripheral anionic site
Phe	Phenylalanine
PNS	Peripheral nervous system
q	Quartet (for NMR signal)
quin	Quintet (for NMR signal)
Ser	Serine
s	Singlet (for NMR signal)
<i>TcAChE</i>	<i>Torpedo californica</i> acetylcholinesterase
THF	Tetrahydrofuran
Trp	Tryptophan
Tyr	Tyrosine
t	Triplet (for NMR signal)
v	Wave number

CHAPTER 1

INTRODUCTION

1. Background, Rationale and Objectives

1.1 Alzheimer's disease

Alzheimer's disease (AD) is the most common form of dementia. It is a progressive and fatal neurodegenerative disorder characterized by memory loss and personality change. AD is not a normal part of aging (Korabecny J. et al. 2015). The greatest known risk factor is increasing age, and the majority of people with disease are 65 and older. AD is also considered as one of the biggest global public burden, currently affecting more than 46 million people worldwide, a number estimated to increase up to 150 million people by 2050. In 2016, six hundred thousand of Thai people were suffered from this disease (นพ.บุญชัย พิพัฒน์วิชิตกุล. 2556).

1.1.1 Symptoms

AD can affect different people in different ways, but the most common symptom pattern begins with gradually worsening difficulty in remembering new information. This is because of disruption of brain cells usually begins in regions involved in forming new memories. As damage spreads, individuals also experience confusion, disorganized thinking, impaired judgment, trouble in expressing themselves and disorientation with regard to time, space and location, which may lead to unsafe wandering and socially inappropriate behavior. In advanced AD, people need help using the bathroom, bathing, eating and other daily activities. Those in the final stages of the disease lose their ability to communicate and others. AD is ultimately fatal (Mebane-Sims I, 2009).

1.1.2 Causes

The histological hallmarks of AD are neuritis plaques of beta-amyloid ($A\beta$) peptide and neurofibrillary tangles of tau protein in brain tissue. There are significant loss of neurons, shrinkage of neuronal volume and loss of synaptic connections. The

areas associated with the loss of neurons involve the cerebral cortex and hippocampus, which are thought to be responsible for the clinical symptoms of AD (Burns A. et al. 2009).

The focus of research over the past decade has concentrated on the “amyloid cascade hypothesis” as a result of the neuritis amyloid plaques. Evidence for this hypothesis in humans includes the observation that early-onset AD results from mutation in the amyloid precursor protein (APP) and the ApoE ϵ 4 allele results in accumulation of amyloid protein leading to the neuropathological characteristics of AD. Therapies arising from this hypothesis have concentrated on preventing A β peptide formation (e.g., gamma secretase inhibitors) and increasing its solubility (e. q., A β aggregation inhibitors) or increasing its clearance (vaccines) (Cummings JL. et al. 2004). While several agents and vaccines have made it to clinical development, failure to show clinical improvement and unacceptable adverse effect in phase III studies have prevented several new AD therapies from reaching the market (Holmes C. et al. 2008).

The “tau hypothesis” represents the other major hypothesis of AD etiology. This hypothesis states that hyperphosphorylation of intraneuronal microtubule-associated protein tau leads to the neurofibrillary tangles observed in AD (Fischer PM. et al. 2008). The result is inflammation and cellular death, which have been implicated in the causal pathway of A β production. As the hypothesized causative pathway for A β production, therapies aimed at A β would only treat the downstream event and may explain why limited clinical benefits have been observed for anti-A β therapy. Several agents are currently under clinical investigation; however, the agent furthest along in clinical development has only reached phase II study (Wischik CM. et al. 2008).

The “cholinergic hypothesis” is an older hypothesis. It is a useful hypothesis for the treatment of AD. According to the cholinergic hypothesis, a progressive loss of presynaptic cholinergic function in the central nervous system (CNS) significantly contributes to the memory and cognitive symptoms of AD (Terry AV. et al. 2003). ChE inhibitors were the first therapies approved in the U.S. for AD and currently, the first-line agents for the treatment of AD are ChE inhibitors. They inhibit the breakdown of the neurotransmitter acetylcholine (ACh) to increase the amount of cholinergic transmission. The ChE inhibitors can be used in any stage of AD (mild to severe).

1.1.3 Acetylcholine (ACh)

Acetylcholine (ACh) was the first discovered neurotransmitter molecule. Its chemical structure is shown in Figure 1 and is composed by an ester of acetic acid and choline.

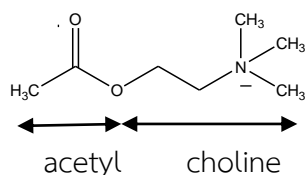


Figure 1. The chemical structure of acetylcholine

In presynaptic nerve terminal, ACh is made from choline and acetyl CoA (Figure 2). Choline is brought into the cell by a transporter. Synthesized ACh is stored in the vesicles. Vesicles release ACh during neurotransmission into the synaptic cleft to bind with ACh receptors in the postsynaptic nerve terminal. ACh is rapidly broken down by the enzyme acetylcholinesterase (AChE) to give acetate and choline. Choline is then transported back into the axon terminal and used to produce more ACh.

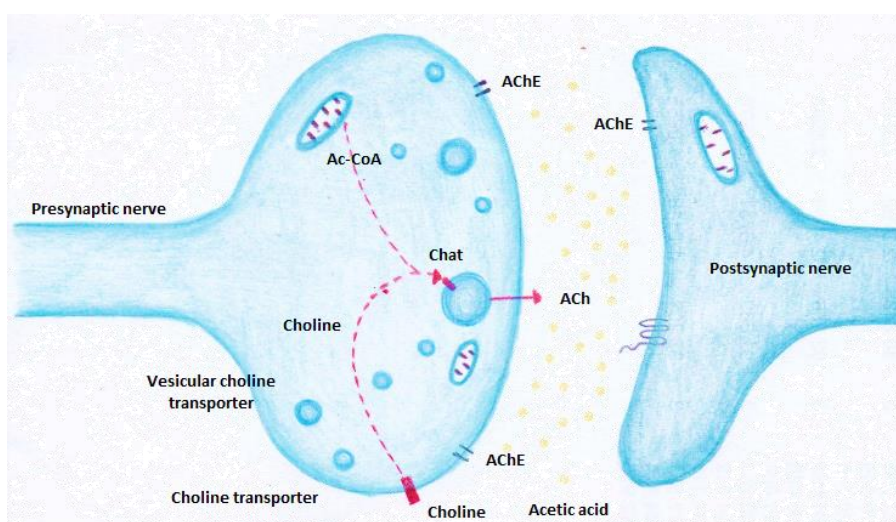


Figure 2. Acetylcholine in cholinergic synapse.

The role of the AChE and butyrylcholinesterase (BChE) at the cholinergic synapses is to terminate neurotransmission by rapid hydrolysis of the substrate. In healthy brains, AChE hydrolyzes the major ACh, while BChE only play a secondary role. In temporal cortex of normal human brain, AChE accounts for approximately 90% of ChE activity and BChE the remaining 10%. There is growing evidence that both AChE and BChE may be important in the development and progression of AD. Up to 45% of AChE may be lost in certain brain regions during progression of this disease while levels of BChE activity conversely increase by up to 90% as shown in Figure 3. Thus both enzymes have been identified as potential targets in the treatment of AD (Greig NH. et al. 2002)

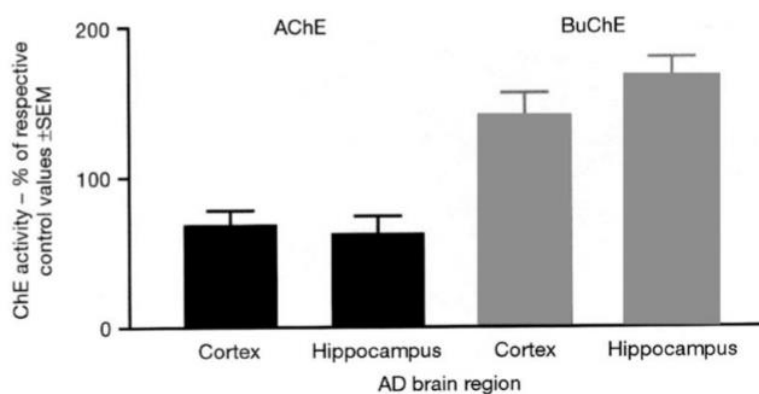


Figure 3. Cholinesterase activity in the cortex and hippocampus of human AD brain.

1.1.4 Acetylcholinesterase (AChE)

AChE is found in many types of conducting tissue: nerve and muscle, central and peripheral tissue and others. AChE is a fold protein containing 534 amino acids. Active site of the enzyme is a deep and narrow gorge which is about 20 Å deep. X-ray crystallographic structure of AChE from *Torpedo californica* (*TcAChE*) (PDB ID: 1EVE) revealed four main binding sites, i.e., esteratic subsite at the bottom of the active site gorge (Ser200, Glu327 and His440). This area is where ACh is hydrolyzed to acetate and choline.; an anionic substrate (AS) binding site having Trp84, Glu199 and Phe330 amino acid; and acyl pocket (Phe288 and Phe299) and peripheral anionic site (PAS) with Tyr70,

Asp72, Tyr121, Trp279 and Phe290 amino acid As shown in Figure 4. Mechanism of ACh hydrolysis catalyzed by AChE is shown in Figure 5.

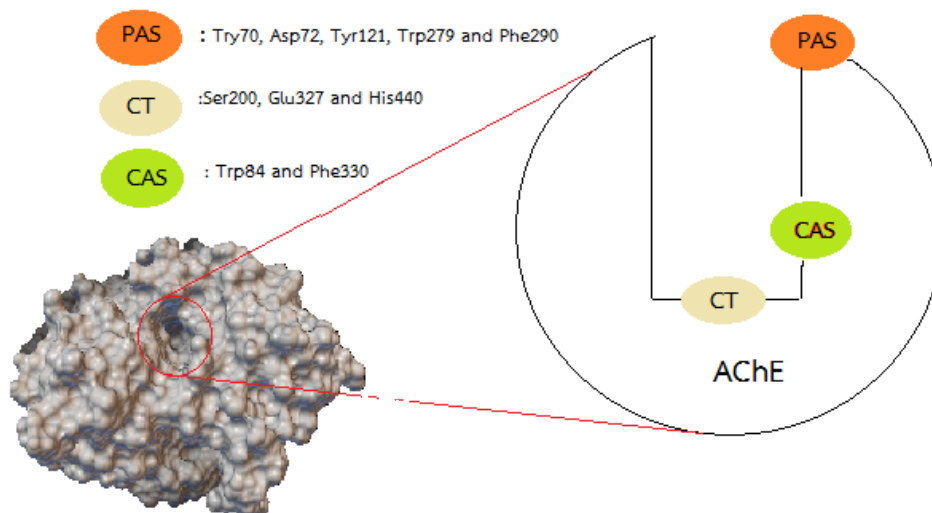


Figure 4. Structure of active site of TcAChE

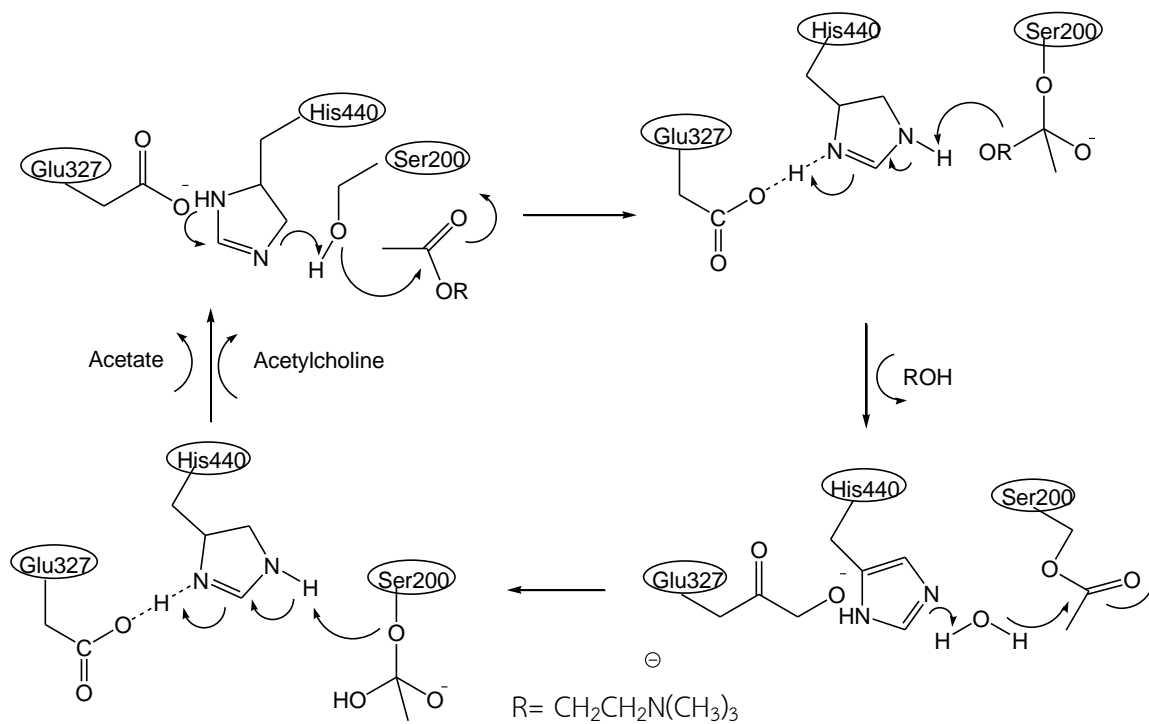


Figure 5. Mechanism of ACh hydrolysis catalyzed by AChE

The hydrolysis reaction of the carboxyl ester leads to the formation of an acyl-enzyme and free choline. Then, the acyl-enzyme undergoes nucleophilic attack by a water molecule, assisted by the His440 group, liberating acetic acid and regenerate the free enzyme.

1.1.5 Butyrylcholinesterase (BChE)

BChE is also known as plasma cholinesterase or pseudocholinesterase. This enzyme is found primary in the liver, intestine, heart, lung and the brain. BChE is a fold protein containing 524 amino acids. Active site of BChE is also a deep and narrow gorge but larger than that of AChE. There are five main binding sites, i.e., Peripheral anionic site (PAS) that located at the mouth of the gorge (Asp70 and Tyr332), choline binding site or cation- π site (Trp82), oxyanion hole that found near the choline binding site (Gly116, Gly117 and Ala199), acyl binding site (Leu286 and Val288) and catalytic triad that composed of Ser198, His438 and Glu325 (Figure 6) (Cokugras AN. 2003).

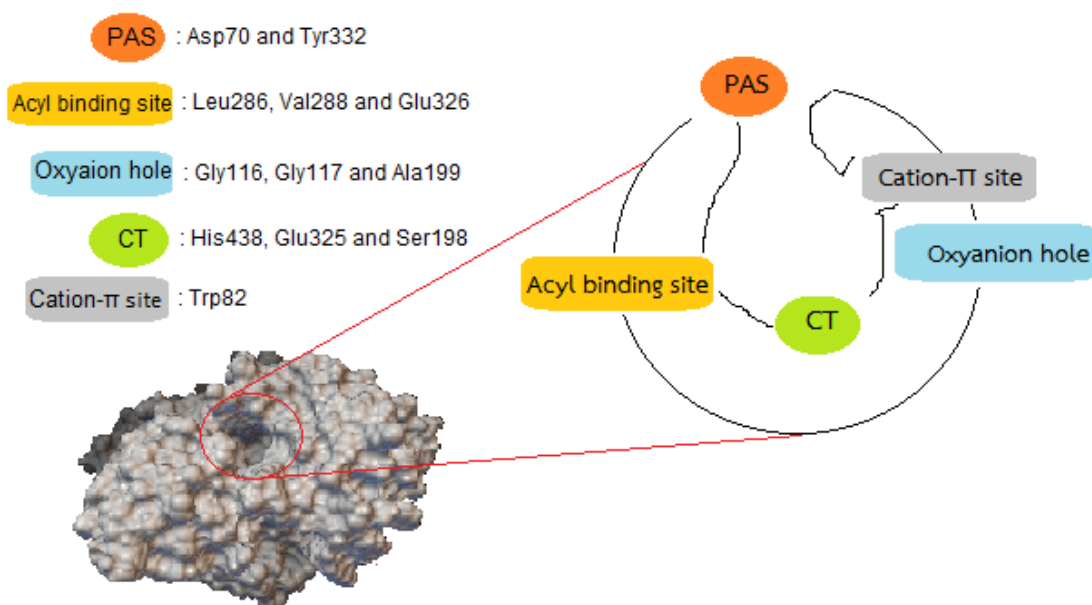


Figure 6. Structure of active site of *HuBChE*.

The kinetic of AChE and BChE can be evaluated by the Michaelis-Menten model. The common reaction for this model is shown in equation 1.



Where:

- E = Enzyme
- S = Substrate
- ES = Enzyme-Substrate complex
- P = Product
- K_m = Equilibrium dissociation constant
- V_{max} = Maximum degradation rate

From the Michaelis-Menten equation showed the relation of V with [S] as follows in equation 2.

$$V = \frac{V_{max} \times [S]}{K_m + [S]} \quad (\text{Equation 2})$$

The enzyme and substrate binds to form an enzyme-substrate complex. K_m is the equilibrium dissociation constant for this binding and characterizes the binding affinity. The substrate is then changed to the product while invigorating the enzyme. V_{max} is the maximum rate the enzymes are able to demote the substrate to the product. Moreover, K_m is the concentration at half the maximal rate. High affinity binding is distinguished by a low K_m and low affinity binding is distinguished by a high K_m . Extremely efficient enzymes or high concentrations of enzyme results in a high V_{max} (Figure 7).

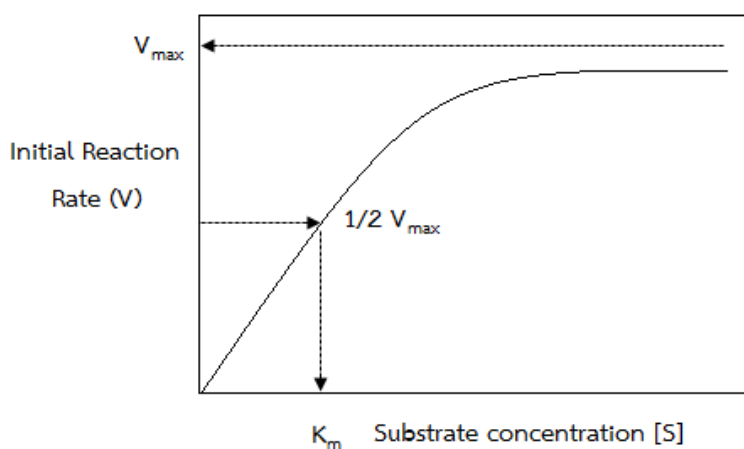


Figure 7. The kinetic enzyme of Michaelis-Menten between concentration of substrate [S] and reaction velocity (V)

From the Michaelis-Menten equation, It can be derived to Lineweaver-Burk equation as follows in equation 3.

$$\frac{1}{V} = \frac{K_m}{V_{max}} \times \frac{1}{[S]} + \frac{1}{V_{max}} \quad (\text{Equation 3})$$

Graph of Lineweaver-Burk shown in Figure 8.

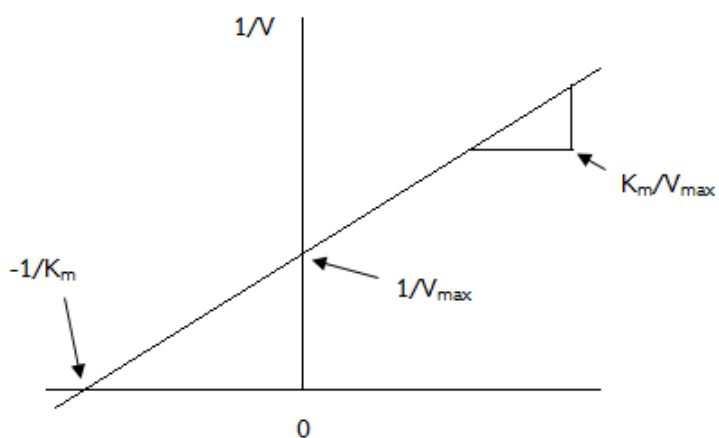


Figure 8. The kinetic enzyme of Lineweaver-Burk between $1/[S]$ and reaction $1/(V)$

1.2 Cholinesterase Inhibitors

1.2.1 Mechanism of cholinesterase Inhibition

There are four modes of inhibition, namely competitive, non-competitive, uncompetitive and mixed-type inhibition as summarized in Table 1.

- Competitive inhibition

Free [E] can be attached to the [S] in catalytic site to give [ES] complex. The inhibitor is structurally similar to the [S]. It is able to bind to [E] give [EI] complex. The general reaction scheme for a competitive inhibition which is observed by an apparent increase in the Michaelis-Menten parameter K_m with increasing inhibitor concentrations.

- Non-competitive inhibition

[I] binds with [E] and [ES] complex give [EI] and [ESI] complex, respectively. [ESI] can not continue to react. Increasing [S] can not overcome [I] inhibition. The general reaction scheme for a noncompetitive inhibition which is observed by an apparent decrease in the Michaelis-Menten parameter v_{max} with increasing inhibitor concentrations.

- Uncompetitive inhibition

[I] binds with [ES] complex only and give [ESI] complex without binding to the free [E]. The general reaction scheme for a uncompetitive inhibition is observed by an apparent decrease in K_m and decrease in v_{max} with increasing inhibitor concentrations.

- Mixed-type inhibition

Mixed type inhibition is similar to non-competitive inhibition. Which has different that binding of the [S] or [I] influence the others enzyme. The general reaction scheme for a mixed-type competitive inhibitor is observed by an apparent increase in K_m and decrease in v_{max} with increasing inhibitor concentrations.

	Competitive Inhibition	Non-competitive Inhibition	Uncompetitive Inhibition	Mix-type Inhibition
Guide				
Equation	$E + S \xrightleftharpoons{K_m} ES \xrightarrow{V_{max}} E + P$ $+ I \xrightleftharpoons{K_i} EI$	$E + S \xrightleftharpoons{K_m} ES \xrightarrow{V_{max}} E + P$ $+ I \xrightleftharpoons{K_i} EI$ $+ I \xrightleftharpoons{K_i} EIS$	$E + S \xrightleftharpoons{K_m} ES \xrightarrow{V_{max}} E + P$ $+ I \xrightleftharpoons{K_i} EIS$	$E + S \xrightleftharpoons{K_m} ES \xrightarrow{V_{max}} E + P$ $+ I \xrightleftharpoons{K_i} EI$ $+ I \xrightleftharpoons{K_i} EIS$

Table 1. Modes of inhibition (competitive, non-competitive, uncompetitive and mixed-type inhibition)

	Competitive Inhibition	Non-competitive Inhibition	Uncompetitive Inhibition	Mix-type Inhibition
Michaelis-Menten				
	V_{max} unchanged K_m increased	V_{max} decreased K_m unchanged	V_{max} decreased K_m decreased	V_{max} decreased K_m increased
Lineweaver-Burk				

Table 1. Modes of inhibition (competitive, non-competitive, uncompetitive and mixed-type inhibition) (continued)

1.2.2 Clinical Pharmacology of the cholinesterase Inhibition

Donepezil, tacrine, rivastigmine and galanthamine all prevent ACh from breaking down by AChE in the brain. As a result, an increased concentration of ACh leads to increased communication between nerve cells.

- Tacrine (Cognex[®])

Tacrine (9-amino-1,2,3,4-tetrahydroacridine) is a reversible inhibitor of AChE and BChE and the first drug approved by the Food and Drug Administration of United States of America for the palliative treatment of AD. Unfortunately, the clinical effects of tacrine were found to be short-lived and further compounded by hepatotoxicity which resulted in its withdrawal from clinical use. X-ray structure of tacrine binding with *TcAChE* (PDB ID: 1ACJ) showed that tacrine has stacked interaction with Trp84 and Phe330 at anionic subsite of the active site. Ring nitrogen showed hydrogen bond with carbonyl oxygen of His440 (3.1 Å) and amino nitrogen formed a hydrogen bond to a water molecule. ($IC_{50} = 184.1$ nM (AChE), 6.7 nM (BChE)). (Figure 9). (Jin H. et al. 2014)

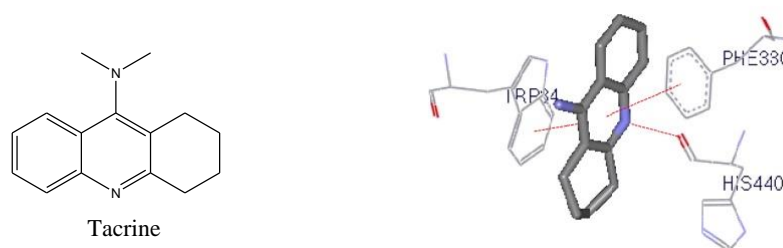


Figure 9. Structure and molecular docking study of tacrine-*TcAChE*.

- Galanthamine (Razadyne[®])

Galanthamine is an alkaloid isolated from the plant *Galanthus nivalis* (snowdrop) being applied for the treatment of mild to moderate AD. It is a selective, competitive, rapidly reversible inhibitor. For x-ray structure of galanthamine binding with *TcAChE* (PDB ID: 1DX6), cyclohexene ring interacted with both the choline-binding site (Trp84) and the acyl-binding pocket (Phe288, Phe290). The tertiary amine

interacted with Asp72 show hydrogen bond and the hydroxyl group showed strong hydrogen bond (2.7 Å) with Glu199. (IC_{50} = 0.35 μ M (AChE), 18.6 mM (BChE)) (Figure 10). (Greenblatt HM. et al. 1999).

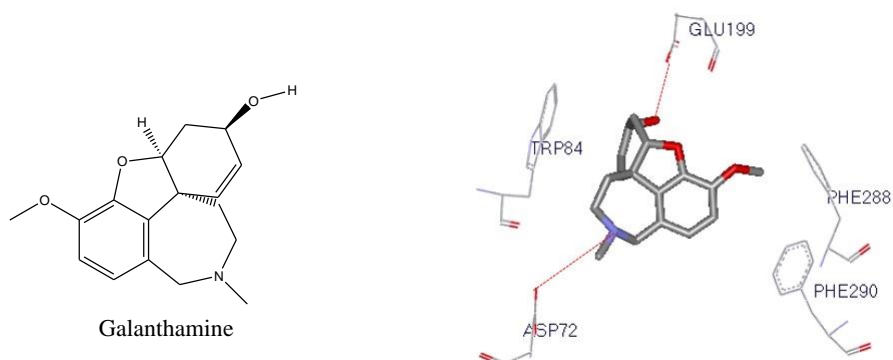


Figure 10. Structure and molecular docking study of galanthamine-*TcAChE*.

- Rivastigmine (Exelon[®])

Rivastigmine is a carbamate inhibitor of AChE which was approved for the treatment of mild to moderate AD. This drug is extensively metabolized to (-)-S-3-[(1-dimethylamino)ethyl]phenol (NAP), by cholinesterase-mediated decarbamylation (Ser200). This is the key step required for cholinesterase inhibition (Chen TH. et al.2017). X-ray structure of NAP binding with *TcAChE* (PDB ID: 1GQR) showed π - π interactions of NAP with Trp84 and Phe330. The hydroxyl oxygen of NAP showed H-bond with Glu199 and the tertiary ammonium side chain is oriented toward the acyl binding pocket and the oxyanion hole. (IC_{50} = 4.15 μ M (AChE), 37 nM (BChE)) (Figure 11). (Bar-on P. et al. 2002).

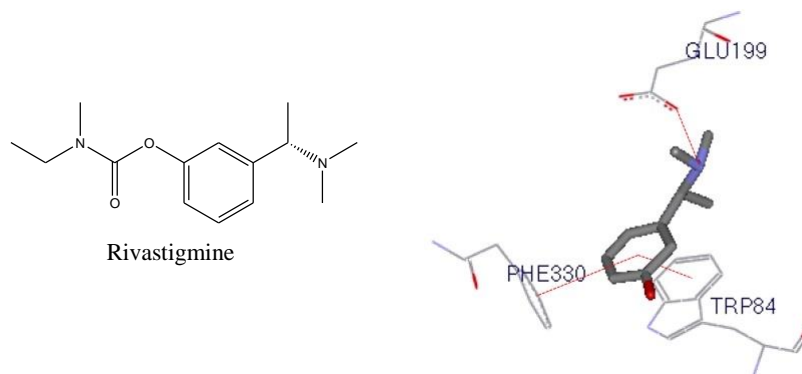


Figure 11. Structure and molecular docking study of NAP-*TcAChE*.

- Donepezil (Aricept®)

Donepezil was approved in 1996 for the treatment of mild to moderate AD. It has 570 to 1250 – fold selectivity for AChE than for BChE and inhibits AChE in dual binding site manner. X-ray structure of the complex between *TcAChE* and donepezil (PDB ID: 1EVE) showed that the elongated structure of donepezil spans the entire length of the enzyme active site gorge forming a variety of interactions with specific residues, such as dimethoxyindanone moiety could interact with PAS of enzyme and showed π - π interaction with Trp279, the tertiary amino group or piperidine ring interacted by cation- π interaction with the phenol ring of Phe330, and the benzyl group interacted by π - π interaction with Trp84. (IC_{50} = 0.006 μ M (AChE), 5.38 μ M (BChE)) as shown in Figure 12. (Camps P. et al. 2001).

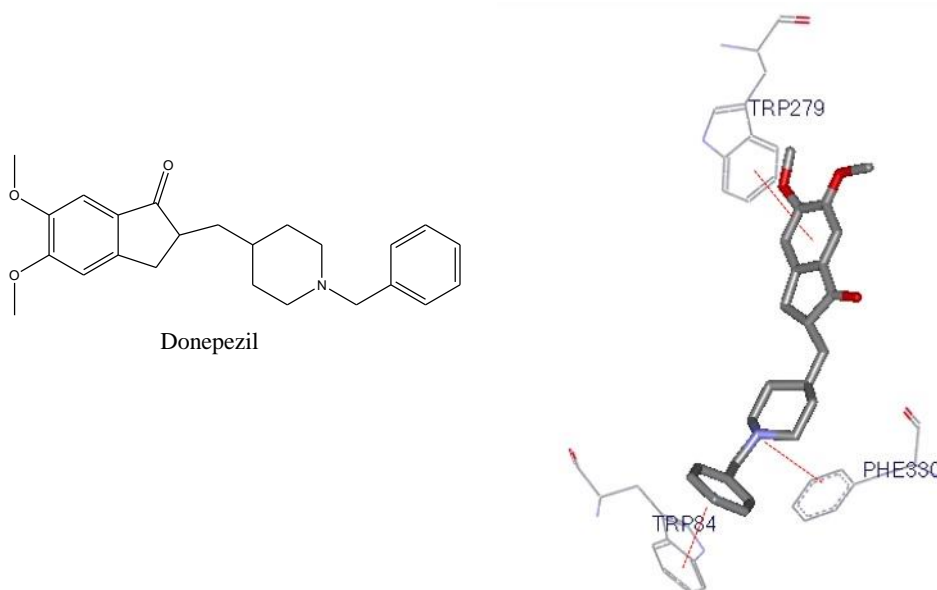


Figure 12. Structure and molecular docking study of donepezil.

The most usual side effects of galanthamine, rivastigmine, donepezil are nausea, vomiting, diarrhea and others. This might be the result of inhibition of peripheral AChE.

1.3 Rationale

The main objective of this study is to design and synthesize innovative active chromone derivatives displaying anti-AD activity through inhibition of AChE and BChE based on structural alteration of donepezil. The x-ray crystallography and docking studies proved that donepezil has a dual-binding mode of action. It was found that piperidine ring conduces its inhibitory activity by interacting with the CAS, while the indanone ring of the molecule binds the PAS of enzyme.

In many reports, chromone derivatives have attracted much attention in recent years because of their diverse pharmacological properties such as anti-inflammatory effect, metal chelating ability and neuroprotective effect. Previous study of chromone derivatives demonstrated that *N*-(4-((2-methoxybenzyl)ethyl)amino)butyl)-5-hydroxy-4-oxo-4*H*-chromene-2-carboxamide (Compound **A**) had a dual-binding mode with AChEI ($IC_{50}=0.55\pm 0.03 \mu M$) and BChEI ($IC_{50}=51.50\pm 1.87 \mu M$) activities. Molecular docking study showed that the chromone ring of the compound bound to the PAS of enzyme via

π - π interaction with the Trp278. At the mid-gorge, the methylene chain interacted with Phe329 and Phe330 via hydrophobic interaction. At the CAS, benzyl group of compound **A** showed π - π interaction with Trp83 (Figure 13.). (Liu Q. et al. 2015)

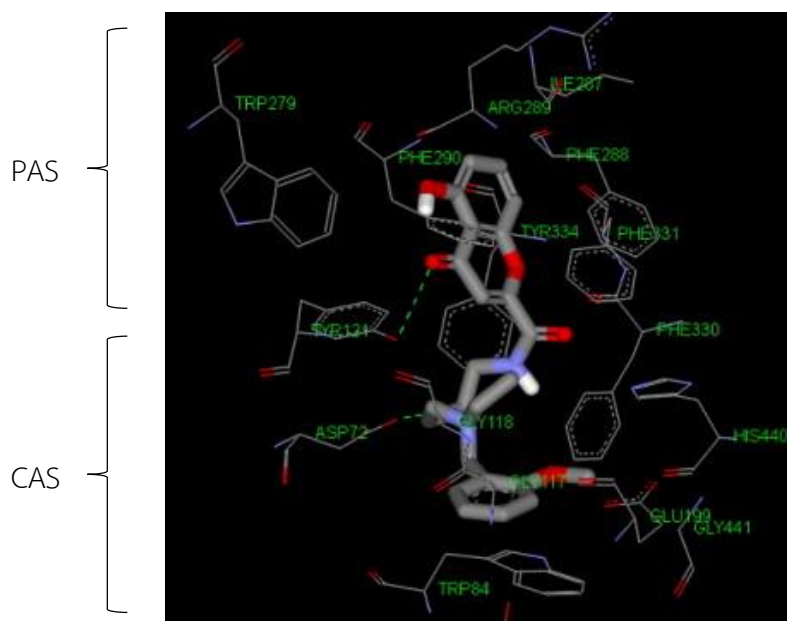


Figure 13. The structure of *N*-(4-((2-methoxybenzyl)ethyl)amino)butyl)-5-hydroxy-4-oxo-4*H*-chromene-2-carboxamide (Compound **A**) within the active site of AChE.

These findings inspired us to design new dual inhibitors of both AChE and BChE with increased potency for the treatment AD.

In this research, chromone ring is used for the inhibition of ChE through its binding to the PAS of enzyme, while the tertiary amino group having piperidine ring or dimethylamine moiety are used for its ability for interaction with the CAS of enzyme. The chromone ring and tertiary amino group are connected via a methylene linker ($n=2, 3$ carbon). Furthermore, position 6 and 7 of the chromone ring system will be replaced with monomethoxy and dimethoxy groups to survey structure-activity relationships as shown in Figure 14.

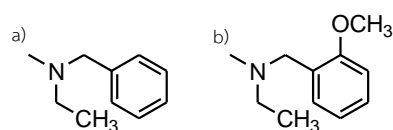
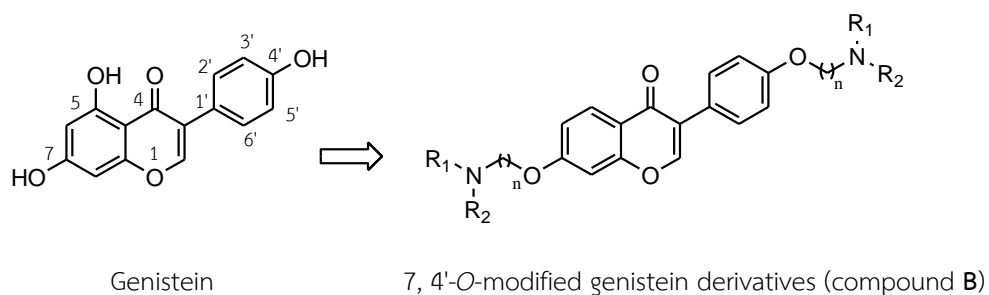


Figure 15. Structure design of 7, 4'-O-modified genistein derivatives.

The designed compounds displayed potent inhibitory activities at the micromolar range (IC_{50} = 0.09-0.90 μ M). Donepezil was used as reference compound. (Table 2). Compound **B(b)** exhibited potent AChE inhibitory activities (IC_{50} = 0.09 \pm 0.02 μ M) but it was still less active than donepezil.

Compounds	n	IC_{50} of AChE (μ M \pm SD)
B(a)	4	0.90 \pm 0.06
B(b)	4	0.09 \pm 0.02
Donepezil	-	0.015 \pm 0.002

AChE from *Rat cortex homogenate*

Table 2. Acetylcholinesterase inhibitory activity of 7, 4'-O-modified genistein derivatives.

Furthermore, kinetic study of AChE inhibition was also performed. It can be characterized by the Michaelis-Menten model that compound **B(b)** showed mixed type inhibition (K_i = 0.14 μ M). This propounded that this compound was able to bind both PAS and CAS of the active site of AChE. This can be confirmed by results of molecular docking study. The complex of compound **B(b)** – TcAChE showed the dual

binding mode. At the CAS, *N*-(2-methoxybenzyl)-ethylamine moiety at position 7 on the genistein bound with Trp84 showing π - π interaction and showed the hydrophobic interaction with Tyr130 and His440. At the PAS, *N*-(2-methoxybenzyl)-ethylamine moiety at position 4' on the genistein bound with Trp279 and Leu282 showing hydrophobic interaction. In the mid-gorge of enzyme, methylene chain interacted with Gly335, Phe290, Tyr334, Tyr70, Asp72, Tyr121 and Phe330 via a hydrophobic interaction (Figure 16).

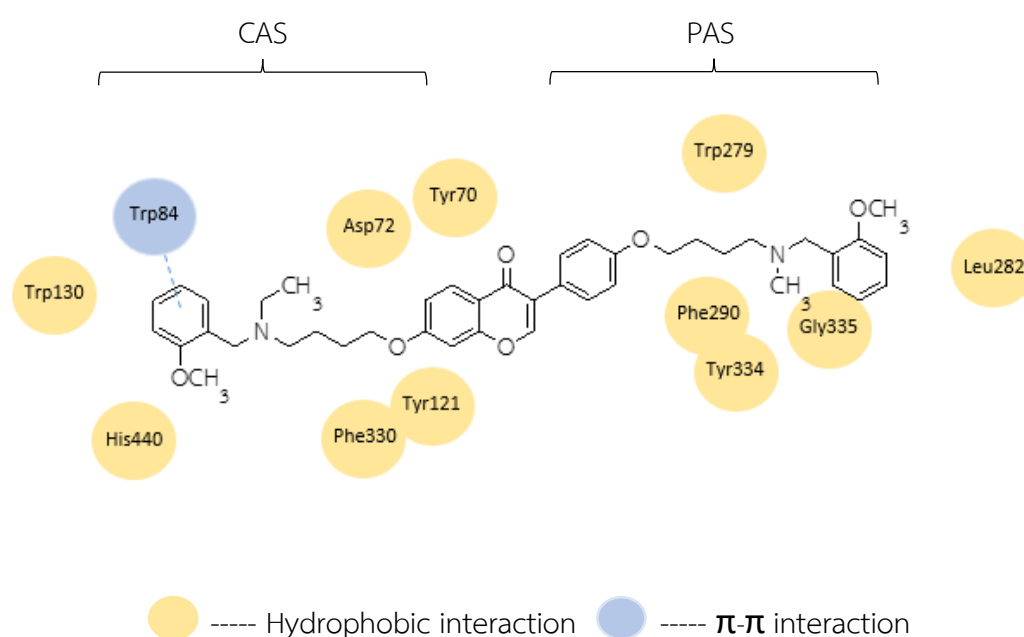
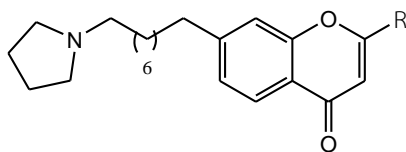


Figure 16. The structure of compound **B(b)** within the active site of AChE.

Luo W et al. (2016) design and synthesized AChEI from 7-aminoalkyl-substituted flavonoid derivatives. Rivastigmine was used as reference compound.

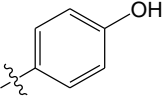
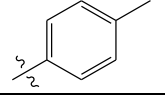
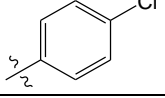
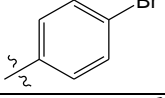
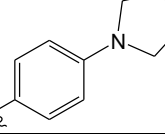
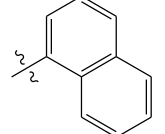
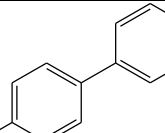
AChEI and BChEI activities were studied in vitro. It can be seen from IC_{50} values that the synthesized compounds displayed potent cholinesterase inhibitory activities at the micromolar range (IC_{50} = 0.64 – 4.80 μ M). All of the compounds showed greater activity than the standard drug rivastigmine (IC_{50} = 6.35 \pm 1.50 μ M) as summarized in Table 3. Substituents on the phenyl group seemed to influence the activity.



7-aminoalkyl-substituted flavonoid derivatives

Compounds	R	IC ₅₀ of AChE ^a (μM , IC ₅₀ \pm SEM)	IC ₅₀ of BChE ^b (μM , IC ₅₀ \pm SEM)
a		1.09 \pm 0.03	2.24 \pm 0.01
b		0.64 \pm 0.04	0.76 \pm 0.02
c		0.67 \pm 0.05	2.29 \pm 0.04
d		1.70 \pm 0.05	5.42 \pm 0.13
e		0.83 \pm 0.01	3.43 \pm 0.22
f		1.08 \pm 0.02	2.20 \pm 0.06
g		2.01 \pm 0.03	5.26 \pm 0.21
h		3.07 \pm 0.21	1.26 \pm 0.01
i		1.58 \pm 0.12	>25
j		1.12 \pm 0.05	4.92 \pm 0.67
k		1.90 \pm 0.13	>25

Table 3. Activity of AChEI and BChEI of 7-aminoalkyl-substituted flavonoid derivatives.

Compounds	R	IC ₅₀ of AChE ^a (μM , IC ₅₀ \pm SEM)	IC ₅₀ of BChE ^b (μM , IC ₅₀ \pm SEM)
l		1.21 \pm 0.08	4.58 \pm 0.08
m		1.25 \pm 0.01	1.92 \pm 0.003
n		1.12 \pm 0.02	3.46 \pm 0.23
o		2.15 \pm 0.12	10.25 \pm 0.27
p		1.38 \pm 0.11	4.10 \pm 0.43
q		0.72 \pm 0.03	0.42 \pm 0.01
r		4.80 \pm 0.21	>25
Rivastigmine	-	6.35 \pm 1.50	1.70 \pm 0.09

a= AChE from *electric eel*

b= BChE from *equine serum*

Table 3. Activity of AChEI and BChEI of 7-aminoalkyl-substituted flavonoid derivatives (continued).

The compounds that was seen to be the most successful as ChEI was 2-(naphthalene-1-yl)-7-(6-(pyrrolidin-1-yl)hexyl)-4*H*-chromen-4-one (compound **C**) with 1-naphtyl (**q**) substituent (IC₅₀ = 0.72 \pm 0.03 μM for AChE and 0.42 \pm 0.01 μM for BChE). For kinetic studies to the inhibition of AChE and BChE showed mixed type inhibition (decrease V_{max} , higher K_{m}) show that K_{i} = 0.206 μM . This propounded that compound **C** was able to bind both PAS and CAS of active site. From molecular docking study, the complex of compound **C**-TcAChE showed dual-binding mode. At the CAS, nitrogen on

piperidine ring interacted with Trp84 and Phe330 via a cation- π interaction and hydrogen bond with His440. At the PAS, naphthalene ring interacted with Trp279 by π - π stacking interaction (Figure 17).

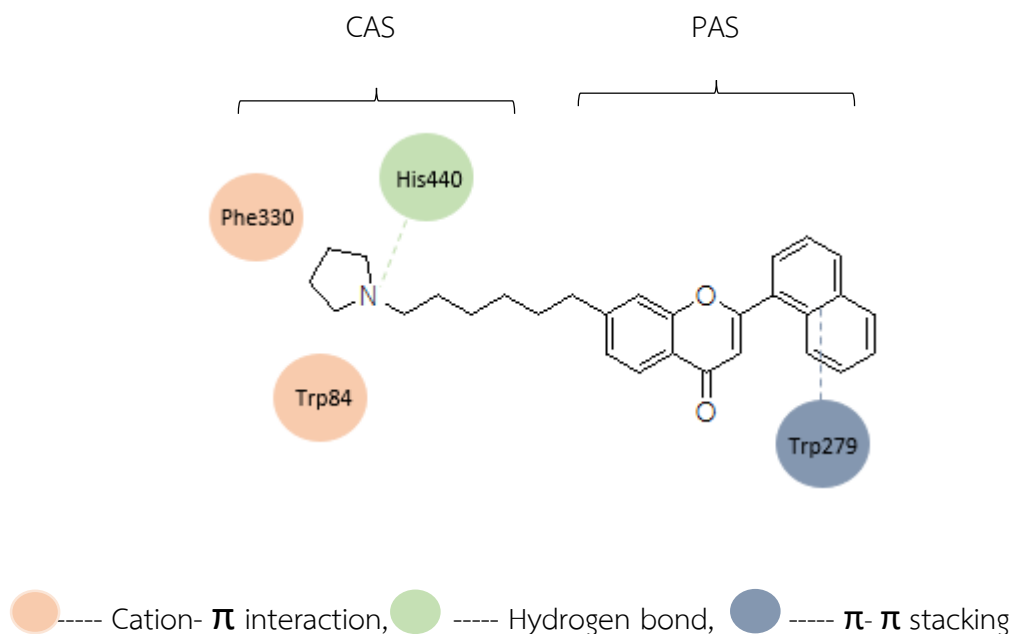


Figure 17. The structure of compound C within the active site of AChE.

Sang Z et al. (2017) designed and evaluated AChEI and BChEI activity of scutellarein-*O*-acetamidoalkylbenzylamines derivatives (compound D) which has 5, 4'-dihydroxy-6, 7-dimethoxyflavone with suitable benzylamine fragments connected by amide linker ($n = 2, 3, 4$ and 6 carbon) as shown in Figure 18.

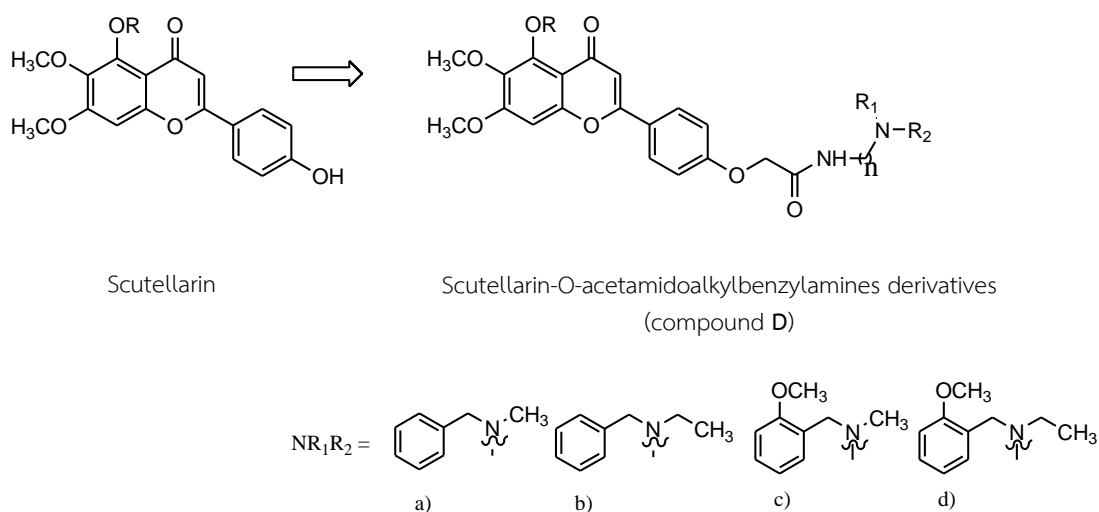


Figure 18. Structure design of scutellarein-*O*-acetamidoalkylbenzylamines derivatives (compound D).

The results showed that *N*-2-methoxybenzyl groups indicated stronger inhibitory potency than *N*-benzyl groups. The compound that was seen to be the most successful as ChEI was *N*-(4-((2-methoxybenzyl)(ethyl)amino)butyl)-2-(4-(5-hydroxy-6,7-dimethoxy-4-oxo-4*H*-chromene-2-yl)phenoxy)acetamide (compound D, Figure 19) that had IC₅₀ values of 0.051 ± 0.001 μM (AChE) but showed weak activity against BChE (IC₅₀ = >500 μM).

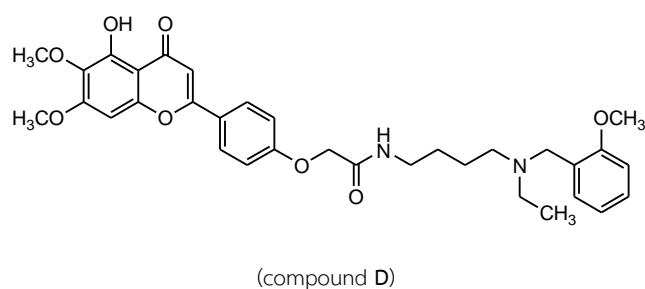


Figure 19. Structure of chromone derivatives (compound D).

For kinetic studies to the inhibition of AChE showed mixed type inhibition (decreased V_{max} , higher K_m). For the molecular docking study, the complex of compound **D**-TcAChE showed dual-binding mode. At the PAS, the benzene ring of 4*H*-chromen-4-one was observed to bind with Trp279 via a π - π interaction and ability hydrophobic interaction with Leu282, Phe288 and Phe331 residues. The 5-hydroxy group at flavonoid ring interact with Ser286 via a hydrogen bond. The benzene ring could bind with Tyr334 via a π - π interaction. The amide group could bind with Tyr121 via a hydrogen bond and *N*-(2-methoxybenzyl)ethanamine moiety occupied the CAS of enzyme show hydrophobic interaction with Ser124, Tyr130, Trp84, Gly123 and Ser122 (Figure 20.)

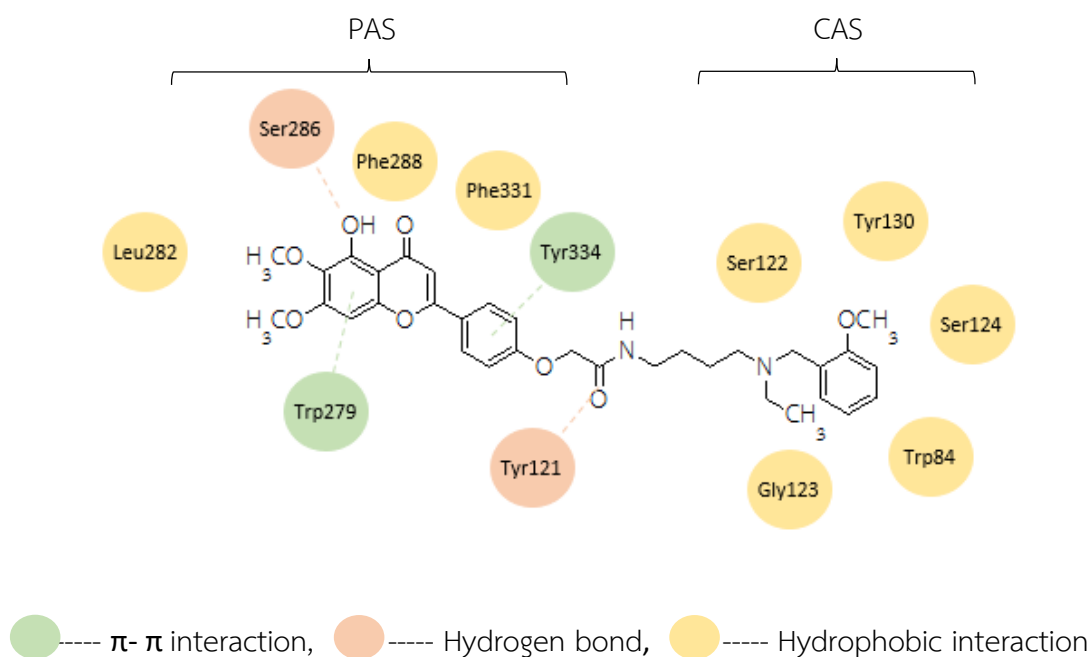


Figure 20. The structure of compound **D** within the active site.

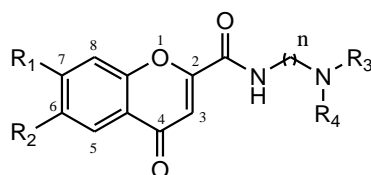
3. Objectives

3.1 To design and synthesize novel chromone-2-carboxamido-alkylamine derivatives as acetylcholinesterase inhibitor.

3.2 To evaluate the *in vitro* acetylcholinesterase and butyrylcholinesterase inhibitory activities of synthesized compounds.

3.3 To evaluate the mode of the inhibitor against AChE.

3.4 To evaluate interaction between chromone derivatives with AChE by using molecular docking study.



Compounds	R ₁	R ₂	NR ₃ R ₄	n
7	H	H		2
8	H	H		2
9	H	H		3
10	H	H		3
11	OCH ₃	H		2
12	OCH ₃	H		2
13	OCH ₃	H		3
14	OCH ₃	H		3
15	OCH ₃	OCH ₃		2
16	OCH ₃	OCH ₃		2
17	OCH ₃	OCH ₃		3
18	OCH ₃	OCH ₃		3

Table 4. Structure of the chromone-2-carboxamido-alkylamine derivatives.

CHAPTER 2

EXPERIMENT

1. Instruments

1.1 Infrared Spectrophotometer

: Perkin Elmer precisely

1.2 Fourier Transform Nuclear Magnetic Resonance Spectrometer

: Varian Unity Inova 500 MHz

1.3 Melting Point Apparatus

: Mel-TEMP II LABORATORY DEVICES.USA

1.4 Mass Spectrophotometer

: Thermo Finnigan MAT 95XL

1.5 Microplate reader

: PowerWave_x, Biotek

2. Chemicals

- | | |
|---|--|
| - Acetone ^c | - Acetylthiocholine iodide ^e |
| - Albumin from bovin serum ^a | - 1-(2-Aminoethyl)piperidine ^e |
| - <i>N</i> -(3-Aminopropyl)piperidine ^e | - Butyrylthiocholine iodide ^e |
| - Dichloromethane ^c | - Diethyloxalate ^e |
| - 3-(Dimethylamino)-1-propyl-amine ^e | - <i>N,N</i> -Dimethylenediamine ^e |
| - 5,5'-Disthiobis(2-nitrobenzoic acid) ^e | - Donepezil ^e |
| - Ethanol ^c | - Ethylacetate ^c |
| - Galanthamine ^b | - Glacial acetic acid ^c |
| - Hexane ^d | - Hydrochloric acid ^c |
| - 2'-Hydroxyacetophenone ^e | - 2'-Hydroxy-4',5'-dimethoxy-acetophenone ^e |
| - 2'-Hydroxy-4'-dimethoxy-acetophenone ^e | - Methanol ^c |
| - Potassium bromide ^f | - Sodium hydroxide ^c |
| - Tacrine ^e | - Tetrahydrofuran ^c |
| - Trizma [®] base ^e | |

Enzymes

Acetylcholinesterase from *Electrophorus electricus* (electric eel)

Acetylcholinesterase from *Human*

Butyrylcholinesterase from *Horse serum*

Program for molecular docking

AutoDock Vina 1.1.2

Discovery Studio 2.5.

^a= Fluka

^c= LAB-SCAN Analytical sciences

^e= Sigma Aldrich

^b= JANSSEN-CILAG

^d= P.S. Science chemical

^f= UNIVER Ajax Finechem

3. Methods

3.1 Synthesis and characterization

Twelve chromone derivatives (**7-18**) were designed and synthesized as shown in Figure 21. Ethyl-4-oxo-4*H*-chromene-2-carboxylate derivatives (**4-6**) were prepared from Claisen condensation between substituted 2-hydroxyacetophenone (**1-3**) and diethyloxalate. Chromone-2-carboxamido-alkylamine derivatives (**7-18**) were prepared by aminolysis of Ethyl-4-oxo-4*H*-chromene-2-carboxylate derivatives (**4-6**) with *N*-alkyl dimethylamines and *N*-alkyl piperidine to give chromone derivatives (**7-18**). Structure of compounds was characterized with IR, ¹H-NMR, ¹³C-NMR and Mass spectrometry.

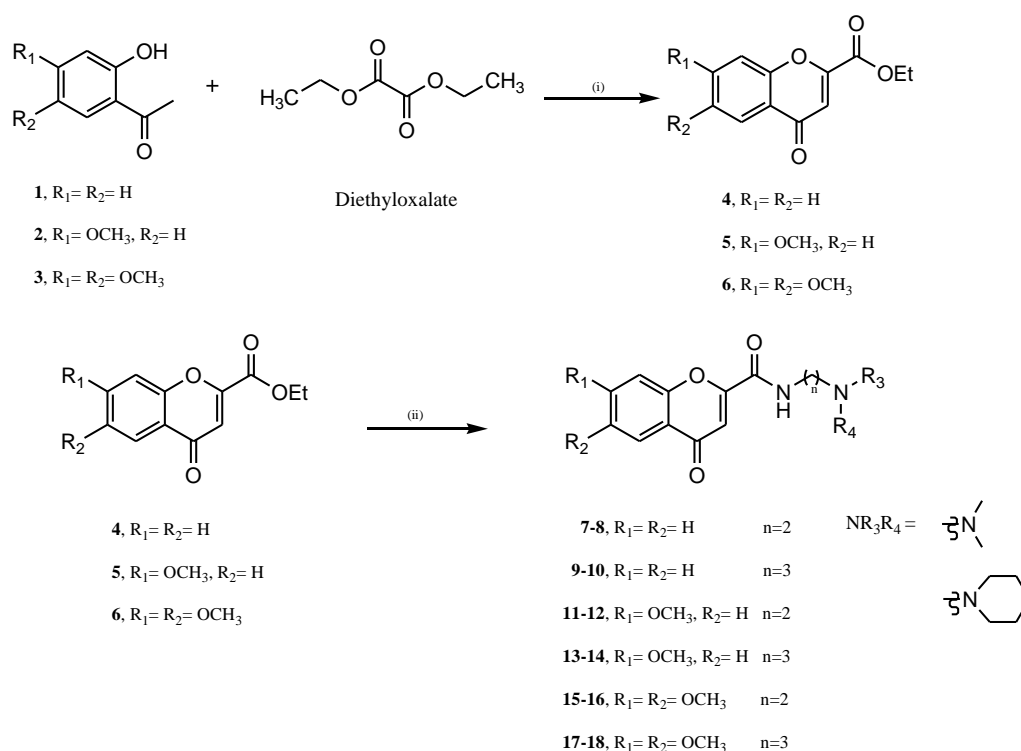
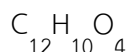
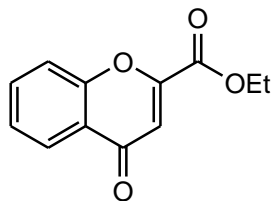


Figure 21. The general procedure of synthesis of chromone derivatives (**7-18**): (i) NaH/THF, room temp (**4-6**); (ii) amine/CH₂Cl₂/reflux, then CH₃COOH, 70 °C.

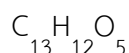
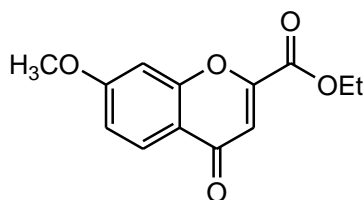
Ethyl-4-oxo-4*H*-chromene-2-carboxylate (**4**, Walenzyk T et al., 2005)



To a slurry of sodium hydride (2.70 g, 65 mmol) stirred in THF (10 ml), a mixture of 2'-hydroxyacetophenone (2.04 g, 15 mmol) and diethyloxalate (5.12 g, 35 mmol) in THF (20 ml) were added and the reaction mixture was stirred overnight at room temperature under nitrogen. It was then poured into ice-water (70 ml), HCl (6N, 20 ml) and extracted with ether (3x80 ml). The organic layer was dried by rotary evaporator to give a yellow solid. The product was purified by column chromatography technique by using EtOAc: Hexane (40: 60) as mobile phase and then recrystallized in EtOAc to give pale yellow solid. The yield was 82% and m.p. 100-102 °C.

IR: (cm⁻¹) 3448 (v, Aromatic), 2984 (v, C-H, Aliphatic), 1740 (v, C=O), 1658 (KBr) (v, C=O), 1465 (v, C=C, Aromatic), 1258 (v, C-O), 772 (v, Aromatic) (Figure 37.)

¹H-NMR: (ppm) 1.32 (t, *J*=7.11 Hz, 3H, CH₃), 4.37 (q, *J*=7.11 Hz, 2H, CH₂), 6.92 (s, (DMSO-*d*₆) 1H, H-3), 7.51 (ddd, *J*=1.04, 7.15, 8.11 Hz, 1H, H-6), 7.71 (m, 1H, H-8), 7.85 (ddd, *J*=1.72, 7.15, 8.57 Hz, 1H, H-7), 8.02 (dd, *J*=1.59, 8.11 Hz, 1H, H-5)

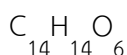
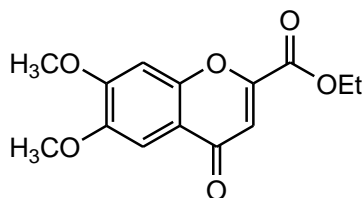
Ethyl-7-methoxy-4-oxo-4*H*-chromene-2-carboxylate (5, Walenzyk T et al., 2005)

To a slurry of sodium hydride (2.70 g, 65 mmol) stirred in THF (10 ml), a mixture of 2'-hydroxy-4'-methoxyacetophenone (2.49 g, 15 mmol) and diethyloxalate (5.12 g, 35 mmol) in THF (20 ml) were added and the reaction mixture was stirred overnight at room temperature under nitrogen. It was then poured into ice-water (70 ml), HCl (6N, 20 ml) and extracted with ether (3x80 ml). The organic layer was dried by rotary evaporator to give a yellow solid. The product was purified by column chromatography technique by using EtOAc: Hexane (40:60) as mobile phase and then recrystallized in EtOAc to give pale yellow solid. The yield was 78% and m.p. 113- 115 °C.

IR: (cm⁻¹) 3462 (v, Aromatic), 2919 (v, C-H, Aliphatic), 1743 (v, C=O), 1663 (KBr) (v, C=O), 1439 (v, C=C, Aromatic), 1257 (v, C-O), 778 (v, Aromatic) (Figure 40.)

¹H-NMR: (ppm) 1.34 (t, *J*= 7.11 Hz, 3H, CH₃), 3.92 (s, 3H, OCH₃), 4.39 (quin, *J*= 7.11 Hz, 2H, CH₂), 6.88 (s, 1H, H-3), 7.10 (dd, *J*= 2.40, 8.88 Hz, 1H, H-6), 7.23 (d, *J*= 2.39 Hz, 1H, H-8), 7.94 (d, *J*= 8.88 Hz, 1H, H-5) (DMSO-*d*₆) (Figure 41-42.)

Ethyl-6, 7-dimethoxy-4-oxo-4*H*-chromene-2-carboxylate (**6**, Walenzyk T et al., 2005)

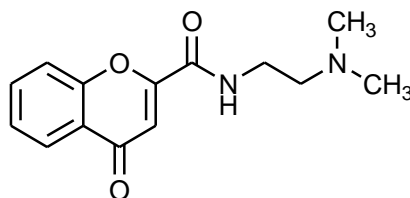


To a slurry of sodium hydride (2.70 g, 65 mmol) stirred in THF (10 ml), a mixture of 2'-hydroxy-4', 5'-dimethoxyacetophenone (2.94 g, 15 mmol) and diethyloxalate (5.12 g, 35 mmol) in THF (20 ml) were added and the reaction mixture was stirred overnight at room temperature under nitrogen. It was then poured into ice-water (70 ml), HCl (6N, 20 ml) and extracted with ether (3x80 ml). The organic layer was dried by rotary evaporator to give a yellow solid. The product was purified by column chromatography technique by using EtOAc: Hexane (40: 60) as mobile phase and then recrystallized in EtOAc to give pale yellow solid. The yield was 86% and m.p. 116-117°C.

IR: (cm⁻¹) 3606 (**v**, Aromatic), 2983 (**v**, C-H, Aliphatic), 1742 (**v**, C=O), 1632 (KBr) (**v**, C=O), 1510 (**v**, C=C, Aromatic), 1255 (**v**, C-O), 865 (**v**, Aromatic) (Figure **43**.)

¹H-NMR: (ppm) 1.34 (t, *J*= 7.11 Hz, 3H, CH₃), 3.86 (s, 3H, OCH₃), 3.94 (s, 3H, OCH₃), (DMSO-*d*₆) 4.39 (quin, *J*= 7.11 Hz, 2H, CH₂), 6.89 (s, 1H, H-8), 7.29 (s, 1H, H-5), 7.35 (s, 1H, H-3). (Figure **44-45**.)

N-(2-(dimethylamino)ethyl)-4-oxo-4*H*-chromene-2-carboxamide (**7**, Sarkar D et al., 2011)



Ethyl-4-oxo-4*H*-chromene-2-carboxylate (**4**), (0.10 g, 0.46 mmol) and *N,N*-dimethylenediamine (0.12 g, 1.38 mmol) were dissolved in dichloromethane (5 ml) and allowed to reflux for 20 minutes, glacial acetic acid (5 ml) was added and the solution was stirred at 75 °C under nitrogen for 24 hours. The mixture was extracted with ethylacetate (3x80 ml). The organic layer was dried by rotary evaporator to give yellow solution. The product was purified by column chromatography technique by using CH₂Cl₂: MeOH (80: 20) as mobile phase and then recrystallized in EtOAc to obtain pale yellow solid. The yield was 64% and m. p. 97-100 °C.

IR: (cm⁻¹) 3851 (v, N-H), 3311 (v, C-H Aromatic), 2947 (v, Aliphatic), 1652 (v, C=O), 1532 (v, Amide), 1464 (v, C=C Aromatic), 1387 (v, C-N Aliphatic), 1018 (v, C-O), 758 (v, Aromatic) (Figure 46.)

¹H-NMR: (ppm) 2.21 (s, 6H, 2xCH₃), 2.48 (m, 2H, CH₂), 3.39 (m, 2H, CH₂), 6.81 (s, 1H, H-3), 7.53 (m, 1H, H-6), 7.72 (m, 1H, H-8), 7.88 (ddd, *J*=1.72, 7.11, 8.50 Hz 1H, H-7), 8.04 (dd, *J*= 1.89, 7.83 Hz, 1H, H-5), 9.03 (t, *J*= 5.51 Hz, 1H, N-H) (Figure 47-48.)

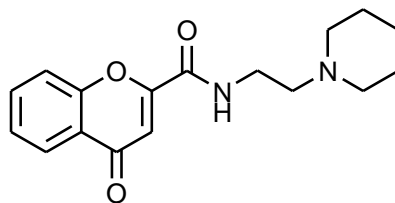
¹³C-NMR: (ppm) 34.40 (2'-CH₂), 45.20 (2xCH₃), 57.79 (3'-CH₂), 110.57 (3-CH), 118.89 (8-CH), 123.70 (8a-C), 124.98 (5-CH), 126.14 (6-CH), 135.03 (7-CH), 155.20 (2-C), 155.76 (4a-C), 159.06 (4-C=O), 177.42 (1'-C=O) (Figure 49.)

ESI-MS: [M+H]⁺ 261.1234

Calcd for 261.1236

C₁₄H₁₆N₂O₃

4-oxo-*N*-(2-(piperidin-1-yl)ethyl)-4*H*-chromene-2-carboxamide (**8**, Sarkar D et al., 2011)



Ethyl-4-oxo-4*H*-chromene-2-carboxylate (**4**), (0.10 g, 0.46 mmol) and 1-(2-Aminoethyl)piperidine (0.18 g, 1.37 mmol) were dissolved in dichloromethane (5 ml) and allowed to reflux for 20 minutes, glacial acetic acid (5 ml) was added and the solution was stirred at 75 °C under nitrogen for 24 hours. The mixture was extracted with ethylacetate (3x80 ml). The organic layer was dried by rotary evaporator to give yellow solution. The product was purified by column chromatography technique by using CH₂Cl₂: MeOH (80: 20) as mobile phase and then recrystallized in EtOAc to obtain pale yellow solid. The yield was 62% and m. p. 110-113 °C.

IR: (cm⁻¹) 3518 (v, N-H), 3303 (v, C=H Aromatic), 2936 (v, Aliphatic), 1654 (KBr) (v, C=O), 1606 (v, Amide), 1464 (v, C=C Aromatic), 1385 (v, C-N Aliphatic), 1130 (v, C-O), 757 (v, Aromatic) (Figure 50.)

¹H-NMR: (ppm) 1.51 (m, 6H, 3xCH₂), 2.68 (m, 6H, 3xCH₂), 3.50 (m, 2H, CH₂), 6.83 (s, 1H, H-3), 7.53 (ddd, *J*= 1.06, 7.16, 8.07 Hz, 1H, H-6), 7.74 (dd, *J*= 0.60, 8.62 Hz, 1H, H-8), 7.88 (ddd, *J*= 1.71, 7.16, 8.62 Hz, 1H, H-7), 8.04 (dd, *J*= 1.54, 8.07 Hz, 1H, H-5), 9.21 (s, 1H, N-H) (Figure 51-52.)

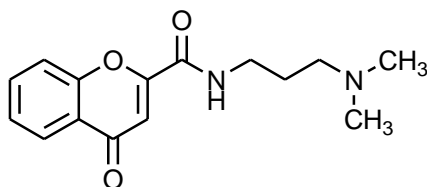
¹³C-NMR: (ppm) 24.27 (3"-CH₂), 25.82 (2", 4"-2xCH₂), 37.18 (2'-CH₂), 54.36 (1", 5"-2xCH₂), 57.45 (3'-CH₂), 110.90 (3-CH), 119.19 (8-CH), 124.11 (8a-C), 125.43 (5-CH), 126.50 (6-CH), 135.48 (7-CH), 155.52 (2-C), 156.09 (4a-C), 159.42 (4-C=O), 177.75 (1'-C=O) (Figure 53.)

ESI-MS: [M+H]⁺ 301.1547

Calcd for 301.1549

C₁₇H₂₀N₂O₃

N-(3-(dimethylamino)propyl)-4-oxo-4*H*-chromene-2-carboxamide (**9**, Sarkar D et al., 2011)



Ethyl-4-oxo-4*H*-chromene-2-carboxylate (**4**), (0.10 g, 0.46 mmol) and 3-(dimethylamino)-1-propyl-amine (0.14 g, 1.37 mmol) were dissolved in dichloromethane (5 ml) and allowed to reflux for 20 minutes, glacial acetic acid (5 ml) was added and the solution was stirred at 75 °C under nitrogen for 24 hours. The mixture was extracted with ethylacetate (3x80 ml). The organic layer was dried by rotary evaporator to give yellow solution. The product was purified by column chromatography technique by using CH₂Cl₂: MeOH (80: 20) as mobile phase and then recrystallized in EtOAc to obtain pale yellow solid. The yield was 68% and m. p. 99-112 °C.

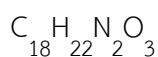
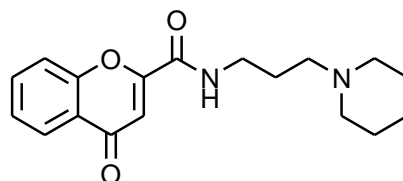
IR: (cm⁻¹) 3867 (v, N-H), 3400 (v, C-H, Aromatic), 2943 (v, Aliphatic), 1654 (v, C=O), 1532 (v, Amide), 1464 (v, C=C Aromatic), 1386 (v, C-N Aliphatic), 1019 (v, C-O), 758 (v, Aromatic) (Figure 54.)

¹H-NMR: (ppm) 1.69 (quin, *J*= 6.95 Hz, 2H, CH₂), 2.16 (s, 6H, 2xCH₃), 2.30 (t, *J*= 6.90 Hz, 2H, CH₂), 3.30 (m, 2H, CH₂), 6.81 (s, 1H, H-3), 7.53 (m, 1H, H-6), 7.71 (ddd, *J*= 0.45, 1.04, 8.48 Hz, 1H, H-8), 7.89 (ddd, *J*= 1.73, 7.12, 8.48 Hz, 1H, H-7), 8.05 (dd, *J*=1.70, 7.94 Hz, 1H, H-5), 9.22 (t, *J*=5.55 Hz, 1H, N-H) (Figure 55-57.)

¹³C-NMR: (ppm) 26.92 (3'-CH₂), 38.50 (2'-CH₂), 45.54 (2xCH₃), 57.35 (4'-CH₂), 110.79 (3-CH), 119.16 (8-CH), 124.08 (8a-C), 125.40 (5-CH), 126.46 (6-CH), 135.46 (7-CH), 155.52 (2-C), 156.20 (4a-C), 159.25 (4- C=O), 177.76 (1'-C=O) (Figure 58.)

ESI-MS: [M+H]⁺ 275.1383
 Calcd for 275.1398
 C₁₅H₁₈N₂O₃

4-oxo-*N*-(3-(piperidin-1-yl)propyl)-4*H*-chromene-2-carboxamide (**10**, Sarkar D et al., 2011)



Ethyl-4-oxo-4*H*-chromene-2-carboxylate (**4**), (0.10 g, 0.46 mmol) and *N*-(3-Aminopropyl)piperidine (0.19 g, 1.38 mmol) were dissolved in dichloromethane (5 ml) and allowed to reflux for 20 minutes, glacial acetic acid (5 ml) was added and the solution was stirred at 75 °C under nitrogen for 24 hours. The mixture was extracted with ethylacetate (3x80 ml). The organic layer was dried by rotary evaporator to give yellow solution. The product was purified by column chromatography technique by using CH₂Cl₂: MeOH (80: 20) as mobile phase and then recrystallized in EtOAc to obtain pale yellow solid. The yield was 63% and m. p. 108-112 °C

IR: (cm⁻¹) 3748 (v, N-H), 3429 (v, C-H, Aromatic), 2947 (v, Aliphatic), 1652 (KBr) (v, C=O), 1606 (v, Amide), 1464 (v, C=C Aromatic), 1388 (v, C-N Aliphatic), 1019 (v, C-O), 758 (v, Aromatic) (Figure 59.)

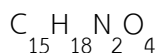
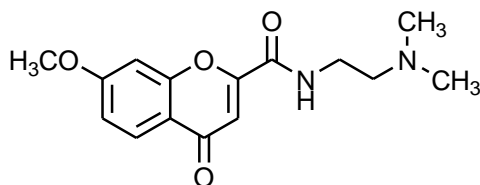
¹H-NMR: (ppm) 1.67 (m, 6H, 3xCH₂), 1.99 (m, 2H, CH₂), 2.99 (m, 4H, 2xCH₂), 3.30 (DMSO-*d*₆) (m, 4H, 2xCH₂), 6.84 (s, 1H, H-3), 7.54 (ddd, *J*= 1.04, 7.20, 8.01 Hz, 1H, H-6), 7.75 (dd, *J*= 0.49, 8.60 Hz, 1H, H-8), 7.90 (ddd, *J*= 1.71, 7.20, 8.60 Hz, 1H, H-7), 8.05 (dd, *J*=1.67, 8.01 Hz, 1H, H-5), 9.34 (t, *J*= 6.06 Hz, 1H, N-H) (Figure 60-62.)

¹³C-NMR: (ppm) 21.57 (3''-CH₂), 22.52 (2'', 4''-2xCH₂), 23.48 (3'-CH₂), 36.82 (4'-CH₂), (DMSO-*d*₆) 52.11 (1'', 5''-2xCH₂), 53.77 (2'-CH₂), 110.62 (3-CH), 118.99 (8-CH), (Figure 63.)

123.77 (8a-C), 125.08 (5-CH), 126.22 (6-CH), 135.17 (7-CH), 155.25 (2-C), 155.69 (4a-C), 159.39 (4-C=O), 177.50 (1'-C=O)

ESI-MS: [M+H]⁺ 315.1558
 Calcd for 315.1560
 C₁₈H₂₂N₂O₃

N-**(2-(dimethylamino)ethyl)-7-methoxy-4-oxo-4*H*-chromene-2-carboxamide (11,**
 Sarkar D et al., 2011)



Ethyl-7-methoxy-4-oxo-4*H*-chromene-2-carboxylate (5), (0.10 g, 0.40 mmol) and *N,N*-Dimethylenediamine (0.11 g, 1.21 mmol) were dissolved in dichloromethane (5 ml) and allowed to reflux for 20 minutes, glacial acetic acid (5 ml) was added and the solution permitted to stir at 75 °C under nitrogen for 24 hours. The mixture was extracted with ethylacetate (3x80 ml). The organic layer was dried by rotary evaporator to give yellow solution. The product was purified by column chromatography technique by using CH₂Cl₂: MeOH (80: 20) as mobile phase and then recrystallized in EtOAc to obtain pale yellow solid. The yield was 74% and m. p. 117-119 °C.

IR: (cm⁻¹) 3315 (v, N-H), 2947 (v, C-H, Aromatic), 2823 (v, Aliphatic), 1649 (KBr) (v, C=O), 1609 (v, Amide), 1439 (v, C=C Aromatic), 1386 (v, C-N Aliphatic), 1022 (v, C-O), 833 (v, Aromatic) (Figure 64.)

¹H-NMR: (ppm) 2.25 (s, 6H, 2xCH₃), 2.52 (m, 2H, CH₂), 3.41 (m, 2H, CH₂), 3.91 (s, (DMSO-*d*₆) 3H, OCH₃), 6.74 (s, 1H, H-3), 7.10 (dd, *J*= 2.43, 8.88 Hz, 1H, H-6), (Figure 65-66.) 7.17 (d, *J*= 2.43 Hz, 1H, H-8), 7.94 (d, *J*= 8.88 Hz, 1H, H-5), 9.01 (t, *J*= 5.47 Hz, 1H, N-H)

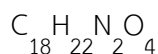
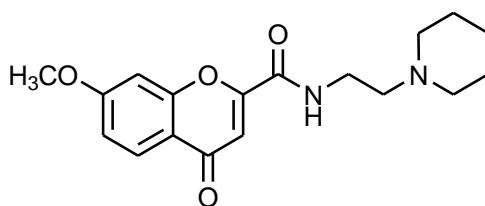
¹³C-NMR: (ppm) 36.71 (2'-CH₂), 44.61 (2xCH₃), 56.58 (7a-OCH₃), 57.38 (3'-CH₂), (DMSO-*d*₆) 101.38 (8-CH), 111.01 (6-CH), 115.82 (4a-C), 117.86 (3-CH), 126.91 (5-CH), 155.62 (8a-C), 157.36 (2-C), 159.77 (7-C), 164.81 (4-C=O), 177.04 (1'-C=O)

ESI-MS: [M+H]⁺ 291.1338

Calcd for 291.1351

C₁₅H₁₈N₂O₄

7-methoxy-4-oxo-*N*-(2-(piperidin-1-yl)ethyl)-4*H*-chromene-2-carboxamide (12, Sarkar D et al., 2011)

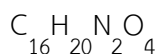
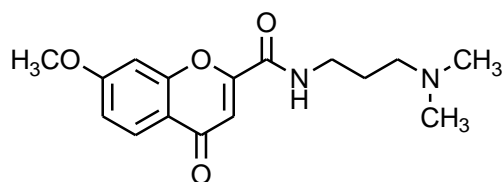


Ethyl-7-methoxy-4-oxo-4*H*-chromene-2-carboxylate (5), (0.10 g, 0.41 mmol) and 1-(2-Aminoethyl)piperidine (0.16 g, 1.22 mmol) were dissolved in dichloromethane (5 ml) and allowed to reflux for 20 minutes, glacial acetic acid (5 ml) was added and the solution was stirred at 75 °C under nitrogen for 24 hours. The mixture was extracted with ethylacetate (3x80 ml). The organic layer was dried by rotary evaporator to give yellow solution. The product was purified by column chromatography technique by using CH₂Cl₂: MeOH (80: 20) as mobile phase and then recrystallized in EtOAc to obtain pale yellow solid. The yield was 66% and m. p. 119-121 °C.

IR: (cm⁻¹) 3323 (v, N-H), 2936 (v, C-H, Aromatic), 2839 (v, Aliphatic), 1649 (KBr) (v, C=O), 1609 (v, Amide), 1439 (v, C=C Aromatic), 1386 (v, C-N Aliphatic), 1024 (v, C-O), 835 (v, Aromatic)

¹ H-NMR: (ppm) (DMSO- <i>d</i> ₆) (Figure 69-70.)	1.45 (m, 6H, 3xCH ₂), 2.53 (m, 6H, 3xCH ₂), 3.43 (m, 2H, CH ₂), 3.91 (s, 3H, OCH ₃), 6.74 (s, 1H, H-3), 7.11 (dd, <i>J</i> = 2.41, 8.87 Hz, 1H, H-6), 7.16 (d, <i>J</i> = 2.41 Hz, 1H, H-8), 7.94 (d, <i>J</i> = 8.87 Hz, 1H, H-5), 9.01 (t, <i>J</i> = 5.60 Hz, 1H, N-H)
¹³ C-NMR: (ppm) (DMSO- <i>d</i> ₆) (Figure 71.)	23.97 (3''-CH ₂), 25.43 (2'', 4''-2xCH ₂), 36.85 (2'-CH ₂), 54.17 (1'', 5''-2xCH ₂), 56.54 (7a-OCH ₃), 57.29 (3'-CH ₂), 101.34 (8-CH), 110.95 (6-CH), 115.71 (4a-C), 117.94 (3-CH), 126.86 (5-CH), 155.69 (8a-C), 157.35 (2-C), 159.47 (7-C), 172.48 (4-C=O), 176.87 (1'-C=O)
ESI-MS: [M+H] ⁺	331.1644
Calcd for	331.1666
C ₁₈ H ₂₂ N ₂ O ₄	

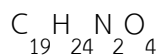
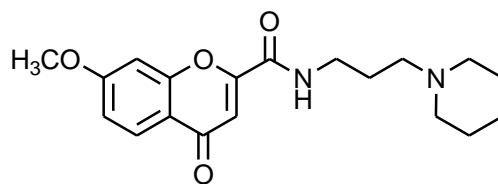
N-(3-(dimethylamino)propyl)-7-methoxy-4-oxo-4*H*-chromene-2-carboxamide (13, Sarkar D et al., 2011)



Ethyl-7-methoxy-4-oxo-4*H*-chromene-2-carboxylate (5), (0.10 g, 0.40 mmol) and 3-(Dimethylamino)-1-propyl-amine (0.12 g, 1.21 mmol) were dissolved in dichloromethane (5 ml) and allowed to reflux for 20 minutes, glacial acetic acid (5 ml) was added and the solution was stirred at 75 °C under nitrogen for 24 hours. The mixture was extracted with ethylacetate (3x80 ml). The organic layer was dried by rotary evaporator to give yellow solution. The product was purified by column chromatography technique by using CH₂Cl₂: MeOH (80: 20) as mobile phase and then recrystallized in EtOAc to obtain pale yellow solid. The yield was 72% and m. p. 120-123 °C.

IR: (cm ⁻¹) (KBr) (Figure 72.)	3447 (v, N-H), 2943 (v, C-H, Aromatic), 2863 (v, Aliphatic), 1649 (v, C=O), 1613 (v, Amide), 1440 (v, C=C Aromatic), 1388 (v, C-N Aliphatic), 1021 (v, C-O), 836 (v, Aromatic)
¹ H-NMR: (ppm) (DMSO- <i>d</i> ₆) (Figure 73-74.)	1.68 (m, 2H, CH ₂), 2.14 (s, 6H, 2xCH ₃), 2.27 (t, <i>J</i> = 6.95 Hz, 2H, CH ₂), 2.49 (m, 2H, CH ₂), 3.92 (s, 3H, OCH ₃), 6.73 (s, 1H, H-3), 7.11 (dd, <i>J</i> = 2.41, 8.86 Hz, 1H, H-6), 7.15 (d, <i>J</i> = 2.41 Hz, 1H, H-8), 7.94 (d, <i>J</i> = 8.86 Hz, 1H, H-5), 9.13 (t, <i>J</i> = 4.51 Hz, 1H, N-H)
¹³ C-NMR: (ppm) (DMSO- <i>d</i> ₆) (Figure 75.)	26.80 (3'-CH ₂), 38.05 (2'-CH ₂), 45.28 (2xCH ₃), 56.23 (7a-OCH ₃), 56.96 (4'-CH ₂), 100.98 (8-CH), 110.53 (6-CH), 115.41 (4a-C), 117.63 (3-CH), 126.56 (5-CH), 155.55 (8a-C), 157.06 (2-C), 158.95 (7-C), 164.38 (4-C=O), 176.55 (1'-C=O)
ESI-MS: [M+H] ⁺	305.1496
Calcd for	305.1509
C ₁₆ H ₂₀ N ₂ O ₄	

7-methoxy-4-oxo-*N*-(3-(piperidin-1-yl)propyl)-4*H*-chromene-2-carboxamide (14, Sarkar D et al., 2011)



Ethyl-7-methoxy-4-oxo-4*H*-chromene-2-carboxylate (5), (0.10 g, 0.40 mmol) and *N*-(3-Aminopropyl)piperidine (0.17 g, 1.21 mmol) were dissolved in dichloromethane (5 ml) and allowed to reflux for 20 minutes, glacial acetic acid (5 ml) was added and the solution was stirred at 75 °C under nitrogen for 24 hours. The mixture was extracted with ethylacetate (3x80 ml). The organic layer was dried by rotary evaporator to give yellow solution. The product was purified by column chromatography technique by using CH₂Cl₂: MeOH (80: 20) as mobile phase and then

recrystallized in EtOAc to obtain pale yellow solid. The yield was 71% and m. p. 123-126 °C.

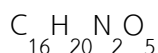
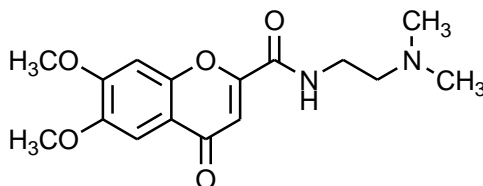
IR: (cm⁻¹) 3421 (v, N-H), 2945 (v, C-H, Aromatic), 2686 (v, Aliphatic), 1650 (v, C=O), 1609 (v, Amide), 1439 (v, C=C Aromatic), 1386 (v, C-N Aliphatic), 1022 (v, C-O), 839 (v, Aromatic)
(KBr)
(Figure 76.)

¹H-NMR: (ppm) 1.89 (m, 8H, 4xCH₂), 2.66 (m, 6H, 3xCH₂), 3.35 (m, 2H, CH₂), 3.91 (s, 3H, OCH₃), 6.76 (s, 1H, H-3), 7.11 (dd, *J*= 2.42, 8.88 Hz, 1H, H-6), 7.20 (d, *J*= 2.42 Hz, 1H, H-8), 7.95 (d, *J*= 8.88 Hz, 1H, H-5), 9.25 (t, *J*= 5.77 Hz, 1H, N-H)
(DMSO-*d*₆)
(Figure 77-78.)

¹³C-NMR: (ppm) 21.83 (3''-CH₂), 22.83 (2'', 4''-2xCH₂), 23.75 (3'-CH₂), 36.97 (4'-CH₂), 52.31 (7a-OCH₃), 54.07 (2'-CH₂), 56.27 (1'', 5''-2xCH₂), 101.18 (8-CH), 110.65 (6-CH), 115.41 (4a-C), 117.64 (3-CH), 126.55 (5-CH), 155.35 (8a-C), 157.09 (2-C), 159.34 (7-C), 164.41 (4-C=O), 176.60 (1'-C=O)
(DMSO-*d*₆)
(Figure 79.)

ESI-MS: [M+H]⁺ 345.1804
Calcd for 345.1823
C₁₉H₂₄N₂O₄

N-(2-(dimethylamino)ethyl)-6, 7-dimethoxy-4-oxo-4*H*-chromene-2-carboxamide
(15, Sarkar D et al., 2011)



Ethyl-6, 7-dimethoxy-4-oxo-4*H*-chromene-2-carboxylate (**6**), (0.10 g, 0.36 mmol) and *N,N*-dimethylethylenediamine (0.09 g, 1.08 mmol) were dissolved in dichloromethane (5 ml) and allowed to reflux for 20 minutes, glacial acetic acid (5 ml) was added and the solution was stirred at temp 75 °C under nitrogen for 24 hours. The mixture was extracted with ethylacetate (3x80 ml). The organic layer was dried by rotary evaporator to give yellow solution. The product was purified by column chromatography technique by using CH₂Cl₂: MeOH (80: 20) as mobile phase and then recrystallized in EtOAc to obtain pale yellow solid. The yield was 64% and m. p. 115-118 °C.

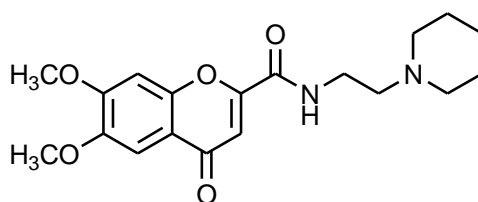
IR: (cm⁻¹) 3446 (v, N-H), 2923 (v, C-H, Aromatic), 2863 (v, Aliphatic), 1642 (v, C=O), 1598 (v, Amide), 1536 (v, C=C Aromatic), 1273 (v, C-N Aliphatic), 1021 (v, C-O), 863 (v, Aromatic)
(KBr) (Figure **80**.)

¹H-NMR: (ppm) 2.22 (s, 6H, CH₃), 2.50 (m, 2H, CH₂), 3.41 (m, 2H, CH₂), 3.86 (s, 3H, OCH₃), 3.93 (s, 3H, OCH₃), 6.75 (s, 1H, H-8), 7.23 (s, 1H, H-5), 7.34 (s, 1H, H-3), 9.00 (t, *J*= 5.68 Hz, 1H, N-H)
(DMSO-*d*₆) (Figure **81-82**.)

¹³C-NMR: (ppm) 37.70 (2'-CH₂), 45.55 (1'', 2''-2xCH₃), 56.27-56.75 (6a, 7a-2xOCH₃), 58.22 (3'-CH₂), 100.95 (8-CH), 103.96 (5-CH), 110.37 (4a-C), 117.40 (3-CH), 148.24 (6-CH), 151.51 (8a-C), 155.21 (7-C), 155.32 (2-C), 159.46 (4-C=O), 176.52 (1'-C=O)
(DMSO-*d*₆) (Figure **83**.)

ESI-MS: [M+H]⁺ 321.1450
 Calcd for 321.1456
 C₁₆H₂₀N₂O₅

6, 7-dimethoxy-4-oxo-N-(2-(piperidin-1-yl)ethyl)-4H-chromene-2-carboxamide
 (16, Sarkar D et al., 2011)



Ethyl-6, 7-dimethoxy-4-oxo-4H-chromene-2-carboxylate (**6**), (0.10 g, 0.40 mmol) and 1-(2-Aminoethyl)piperidine (0.14 g, 1.08 mmol) were dissolved in dichloromethane (5 ml) and allowed to reflux for 20 minutes, glacial acetic acid (5 ml) was added and the solution was stirred at 75 °C under nitrogen for 24 hours. The mixture was extracted with ethylacetate (3x80 ml). The organic layer was dried by rotary evaporator to give yellow solution. The product was purified by column chromatography technique by using CH₂Cl₂: MeOH (80: 20) as mobile phase and then recrystallized in EtOAc to obtain pale yellow solid. The yield was 78% and m. p. 121-123 °C

IR: (cm⁻¹) 3422 (v, N-H), 2935 (v, C-H, Aromatic), 2863 (v, Aliphatic), 1643 (KBr) (v, C=O), 1608 (v, Amide), 1506 (v, C=C Aromatic), 1270 (v, C-N Aliphatic), 1019 (v, C-O), 828 (v, Aromatic)

¹H-NMR: (ppm) 1.49 (m, 6H, 3xCH₂), 2.58 (m, 6H, 3xCH₂), 3.46 (m, 2H, CH₂), 3.86 (DMSO-*d*₆) (s, 3H, OCH₃), 3.93 (s, 3H, OCH₃), 6.76 (s, 1H, H-8), 7.23 (s, 1H, H-5), 7.34 (s, 1H, H-3), 9.09 (s, 1H, N-H)

¹³C-NMR: (ppm) 23.65 (3''-CH₂), 25.03 (2'', 4''-2xCH₂), 36.46 (2'-CH₂), 53.97 (6a, 7a-2xOCH₃), 56.74 (1'', 5''-2xCH₂), 57.09 (3'-CH₂), 100.95 (8-CH),

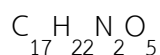
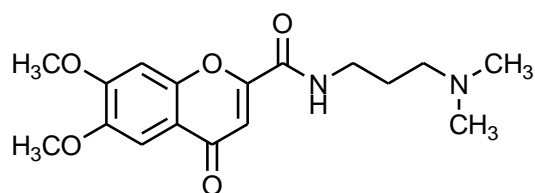
(Figure 87.) 103.94 (5-CH), 110.34 (4a-C), 117.40 (3-CH), 148.25 (6-C), 151.51 (8a-C), 155.21 (7-C), 159.60 (2-C), 172.51 (4-C=O), 176.52 (1'-C=O)

ESI-MS: [M+H]⁺ 361.1754

Calcd for 361.1763

C₁₉H₂₄N₂O₅

N-(3-(dimethylamino)propyl)-6, 7-dimethoxy-4-oxo-4*H*-chromene-2-carboxamide (17, Sarkar D et al., 2011)



Ethyl-6, 7-dimethoxy-4-oxo-4*H*-chromene-2-carboxylate (6), (0.10 g, 0.36 mmol) and 3-(dimethylamino)-1-propyl-amine (0.11 g, 1.08 mmol) were dissolved in dichloromethane (5 ml) and allowed to reflux for 20 minutes, glacial acetic acid (5 ml) was added and the solution was stirred at 75 °C under nitrogen for 24 hours. The mixture was extracted with ethylacetate (3x80 ml). The organic layer was dried by rotary evaporator to give yellow solution. The product was purified by column chromatography technique by using CH₂Cl₂: MeOH (80: 20) as mobile phase and then recrystallized in EtOAc to obtain pale yellow solid. The yield was 67% and m. p. 119-123 °C.

IR: (cm⁻¹) 3447 (v, N-H), 2955 (v, C-H, Aromatic), 2714 (v, Aliphatic), 1643 (KBr) (v, C=O), 1600 (v, Amide), 1510 (v, C=C Aromatic), 1275 (v, C-N Aliphatic), 1021 (v, C-O), 865 (v, Aromatic)

¹H-NMR: (ppm) 1.90 (m, 2H, CH₂), 2.70 (s, 6H, 2xCH₃), 3.02 (m, 2H, CH₂), 3.35 (m, (DMSO-*d*₆) 2H, CH₂), 3.87 (s, 3H, OCH₃), 3.94 (s, 3H, OCH₃), 6.77 (s, 1H, H-8), (Figure 89-90.) 7.22 (s, 1H, H-5), 7.36 (s, 1H, H-3), 9.20 (t, *J*= 5.84 Hz, 1H, N-H)

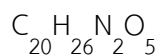
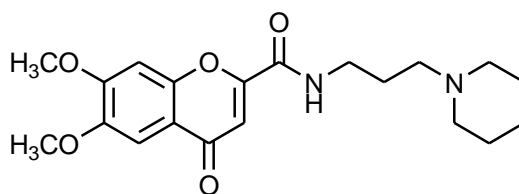
¹³C-NMR: (ppm) 24.67 (3'-CH₂), 36.88 (2'-CH₂), 42.82 (2xCH₃), 55.11 (4'-CH₂), 56.35-56.82 (6a, 7a-2xOCH₃), 100.92 (8-CH), 104.02 (5-CH), 110.44 (4a-C), 117.43 (3-CH), 148.34 (6-C), 151.56 (8a-C), 155.25 (7-C), 155.33 (2-C), 159.89 (4-C=O), 176.58 (1'-C=O)

ESI-MS: [M+H]⁺ 335.1605

Calcd for 335.1615

C₁₇H₂₂N₂O₅

6, 7-dimethoxy-4-oxo-N-(3-(piperidin-1-yl)propyl)-4H-chromene-2-carboxamide (18, Sarkar D et al., 2011)



Ethyl-6, 7-dimethoxy-4-oxo-4H-chromene-2-carboxylate (**6**), (0.10 g, 0.36 mmol) and N-(3-Aminopropyl)piperidine (0.15 g, 1.08 mmol) were dissolved in dichloromethane (5 ml) and allowed to reflux for 20 minutes, glacial acetic acid (5 ml) was added and the solution was stirred at 75 °C under nitrogen for 24 hours. The mixture was extracted with ethylacetate (3x80 ml). The organic layer was dried by rotary evaporator to give yellow solution. The product was purified by column chromatography technique by using CH₂Cl₂: MeOH (80: 20) as mobile phase and then recrystallized in EtOAc to obtain pale yellow solid. The yield was 70% and m. p 122-125 °C.

IR: (cm⁻¹) 3423 (v, N-H), 2939 (v, C-H, Aromatic), 2871(v, Aliphatic), 1643 (KBr) (v, C=O), 1606 (v, Amide), 1474 (v, C=C Aromatic), 1276(v, C-N Aliphatic), 1013 (v, C-O), 826 (v, Aromatic)

¹ H-NMR: (ppm) (DMSO- <i>d</i> ₆) (Figure 93-94.)	1.80 (m, 8H, 4xCH ₂), 2.94 (m, 6H, 3xCH ₂), 3.35 (m, 2H, CH ₂), 3.12 (s, 3H, OCH ₃), 3.93 (s, 3H, OCH ₃), 6.77 (s, 1H, H-8), 7.23 (s, 1H, H-5), 7.35 (s, 1H, H-3), 9.20 (s, 1H, N-H)
¹³ C-NMR: (ppm) (DMSO- <i>d</i> ₆) (Figure 95.)	21.55 (3"-CH ₂), 22.95 (2", 4"-2xCH ₂), 23.97 (3'-CH ₂), 36.92 (4'-CH ₂), 52.60 (1", 5"-2xCH ₂), 54.18 (2'-CH ₂), 56.26- 56.75 (6a, 7a- 2xOCH ₃), 100.82 (8-CH), 103.89 (5-CH), 110.36 (4a-C), 117.30 (3-CH), 148.27 (6-C), 151.51 (8a-C), 155.15 (7-C), 155.30 (2-C), 159.88 (4-C=O), 176.64 (1'-C=O)
ESI-MS: [M+H] ⁺	375.1915
Calcd for C ₂₀ H ₂₆ N ₂ O ₅	375.1934

3.2 Acetylcholinesterase inhibitory activity

In vitro, the AChE inhibitory activity of the synthesized compounds was evaluated with a method modified from Ellman's method (Ellman's et al.1961) by using AChE from *Electrophorus electricus* (electric eel). Donepezil and tacrine were used as positive controls.

This assay was carried out on a 96-well plate, 25 µl of 100 µM sample dissolved in ethanol, 125 µl of 3 mM 5, 5'-dithiobis(2-nitrobenzoic acid) (DTNB), 25 µl of 1.5 mM of substrate (Acetylthiocholine iodide, ATCI), 50 µl of 50 mM Tris/HCl (pH= 8) and followed by 25 µl of enzyme (*EeAChE*). The microplate was then read at 405 nm every 11s for 2 minutes. Each experiment was repeated in triplicate. The result of the measurements showed mean velocity value which was obtained from graph plotted between times and absorbance. The percentage inhibition of all compounds (7-18) for the AChE inhibitory activity were calculated using the following formula:

$$\% \text{inhibition} = \frac{(\text{Mean velocity of blank} - \text{Mean velocity of sample}) \times 100}{\text{Mean velocity of blank}}$$

Determination of 50% inhibition of the AChE activity (IC₅₀) values was performed graphically from inhibition curve (log inhibitor concentration VS percent of inhibition)

and done under the same protocol of inhibitory activity test using AChE from electric eel and human. Eight different concentrations of the inhibitor ($50 \mu\text{M} - 1.6 \times 10^{-3} \mu\text{M}$) were used. The response curve was created using GraphPad Prism 2.01.

3.3 Butyrylcholinesterase inhibitory activity

Evaluation of BChE inhibitory activity of the synthesized compounds was also performed with modified Ellman's method using BChE from *Horse serum*. Butyrylthiocholine iodide (BTCI) was used as substrate. Donepezil and tacrine were used as positive controls.

3.4 The kinetic study for characterization of AChE inhibition

The kinetic study for characterization of AChE inhibition was evaluated with same protocol of inhibitory activity by using AChE from electric eel.

In this study, compound with the highest inhibitory activity was chosen and tested at three different concentrations (2.5, 7.5 and 15 μM). The kinetic of AChE can be evaluated by the Michaelis-Menten model were constructed by plotting velocity (V) opposite to concentration of substrate $[S]$ at varying concentrations of the substrate acetylthiocholine that 5, 10, 25, 50, 125 and 250 μM . Michaelis-Menten model was converted to Lineweaver-Burk model into a straight line by plotting $1/\text{velocity}$ opposite to $1/[S]$ by Prism5 program. Type of inhibition (competitive, noncompetitive, uncompetitive and mixed type inhibition) can be determined from the variation of K_m and V_{max} .

3.5 Molecular docking studies

In molecular docking studies, interactions between enzyme and ligand were evaluated by using computer program which calculates three dimensional structure and properties of the molecule. In this study, AutoDock Vina 1.1.2 (Trott O. and Olson AJ. 2010) and Discovery Studio 2.5 programs were used for molecular docking and

visualization. The protocol included three main steps: optimization, minimization and molecular docking study.

The best compound from results of inhibitory activity was selected for this experiment. The structure of the compound was optimized using density functional theory at B3LYP/6-311G (d, p) level while the enzymes were minimized using by AMBER software. It was prepared under the protein preparation protocol achieved in Discovery Studio 2.5. PROKA was used to assign protonation state at neutral pH (pH= 7). This assay can be used enzyme structure from *Torpedo californica* acetylcholinesterase (*TcAChE*, PDB ID: 1EVE) and Human butyrylcholinesterase (*HuBChE*, PDB ID: 4BDS) were achieved from protein data bank (PDB) and the molecular docking studies were carried out on AutoDock Vina 1.1.2 where the binding site was covered the PAS and CAS of the enzyme. It can be able to determine grid box at the center of active site of enzyme; for *TcAChE*, the center of the grid box was placed at the bottom of the active site gorge (x= 2.023, y= 63.295, z= 67.062) and the dimensions of the active site box were set at 50 Å x 50 Å x 50 Å and *HuBChE*, the center of the grid box determined at x= 135.117, y= 119.222, z= 40.667 and the dimensions of the active site box were set at 34 Å x 46 Å x 34 Å. After that, ligands are put in the grid box for calculate free energy of binding (ΔG). Ligands are arranged by the calculated ΔG value; lower ΔG values correspond to more desirable ligand binding, while higher ΔG values are less desirable (Jacob RB. et al. 2012). The docking score is the predicted binding affinity in kcal/mol. Finally, the resultant structure files were evaluated using Discovery Studio 2.5 program.

CHAPTER 3

Results and Discussion

In this research, 12 novel chromone-2-carboxamido-alkylamine derivatives were designed and synthesized, then evaluated for *in vitro* AChE and BChE inhibitory activities. Kinetic study was performed in order to characterize AChE inhibition mode. Molecular docking was done to determine interactions between the enzymes and the compound.

1. Synthesis of chromone derivatives

The final products were obtained via two steps synthesis which included the synthesis of Ethyl-4-oxo-4*H*-chromene-2-carboxylate derivatives (**4-6**) and synthesis of Chromone-2-carboxamido-alkylamine derivatives (**7-18**). These compounds were purified by extraction, column chromatography technique and recrystallization. Structures of the target compounds were characterized with IR, ¹H-NMR, ¹³C-NMR spectroscopy and Mass spectrometry and melting points were measured.

Ethyl-4-oxo-4*H*-chromene-2-carboxylate derivatives (**4-6**)

Ethyl-4-oxo-4*H*-chromene-2-carboxylate derivatives were prepared by Claisen condensation from substitute 2-hydroxyacetophenone (**1-3**) and diethyloxalate. The reaction mixture was stirred overnight at room temperature under nitrogen. The reaction mechanism of Claisen reaction is provided in Figure **22**. Compounds (**4-6**) were obtained as yellow solid and in high percent yield (more than 70%).

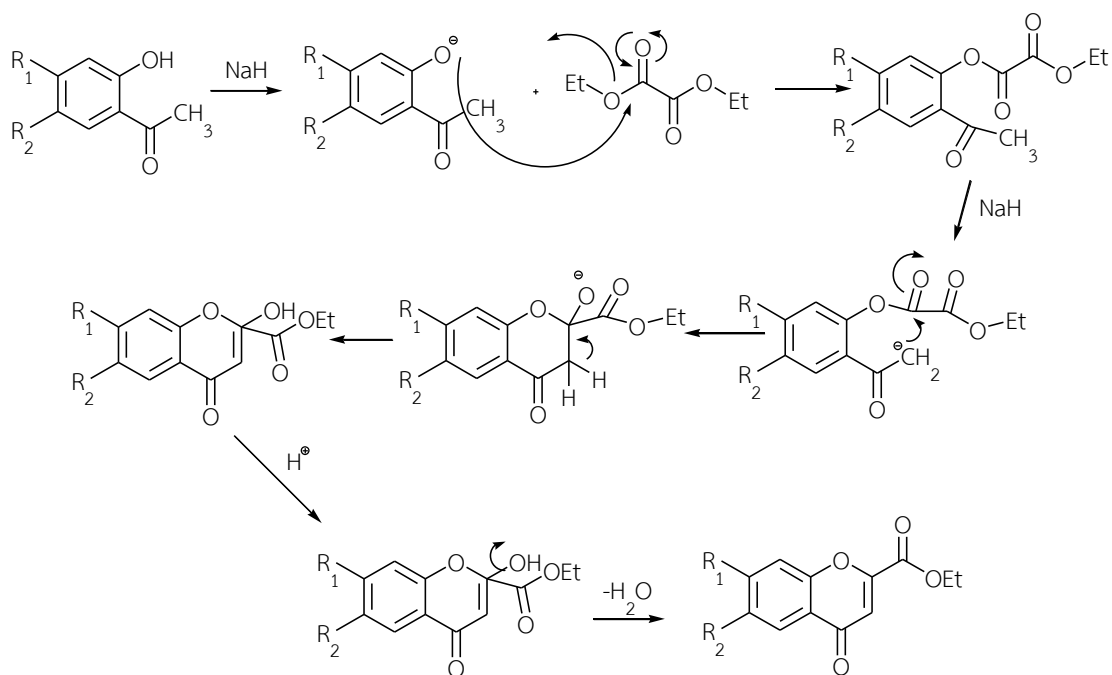


Figure 22. The mechanism of Chaisen condensation.

Chromone-2-carboxamido-alkylamine derivatives (7-18)

Chromone-2-carboxamido-alkylamine derivatives (7-18) were prepared from aminolysis of Ethyl-4-oxo-4*H*-chromene-2-carboxylate derivatives (4-6) with the corresponding amine to give chromone derivatives (7-18). The reaction mixture was heated overnight at 75 °C under nitrogen for 24 hours. Mechanism of aminolysis reaction is proposed in Figure 23. Compounds 7-18 were obtained as yellow solid and percent yield were higher than 60%.

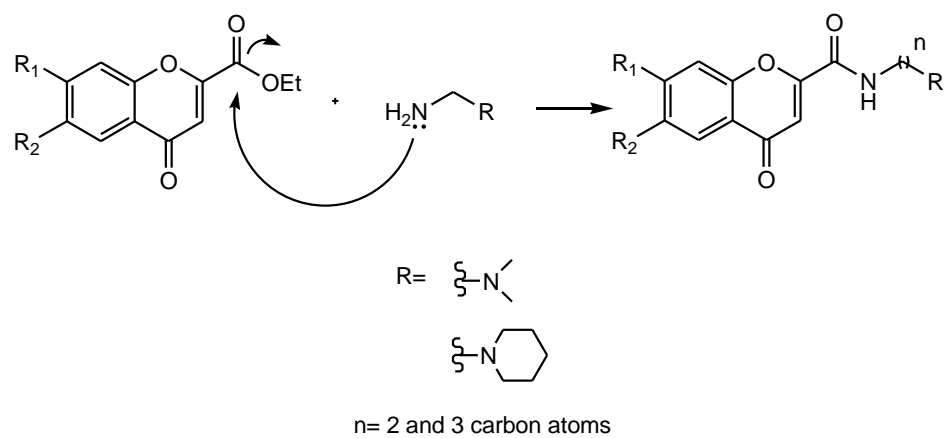
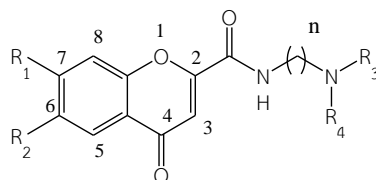


Figure 23. The mechanism of aminolysis reaction.

2. Evaluation for *in vitro* inhibitory activities AChE and BChE

Cholinesterase activities of the 12 synthesized compounds (7-18) were determined as summarized in Table 5.



Compounds	R1	R2	NR ₃ R ₄	n
7	H	H	a	2
8	H	H	b	2
9	H	H	a	3
10	H	H	b	3
11	OCH ₃	H	a	2
12	OCH ₃	H	b	2
13	OCH ₃	H	a	3
14	OCH ₃	H	b	3
15	OCH ₃	OCH ₃	a	2
16	OCH ₃	OCH ₃	b	2
17	OCH ₃	OCH ₃	a	3
18	OCH ₃	OCH ₃	b	3

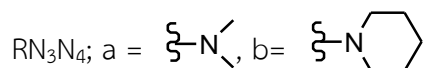


Table 5. The synthesized of chromone derivatives (7-18)

The compounds can be divided into three series according to the structure; series 1 (compounds **7-10**) with non-substituted chromone system, series 2 (compounds **11-14**), with 7-methoxy chromone moiety ($R_1 = \text{OCH}_3$) and series 3 (compounds **15-18**) with dimethoxy groups on position 6 (R_2) and 7 (R_1) of the chromone system. All of the synthesized compounds (**7-18**), R_3 and R_4 positions are

replaced with dimethylamine and piperidine ring and vary lengths of linker (n=2 and 3 carbon).

In this thesis, chromone-2-carboxamido-alkylamine derivatives (**7-18**) were evaluated by Ellman's method. This assay determined of activity of cholinesterase enzyme.

In this method, AChE hydrolyzes acetylthiocholine iodide (ATCI), an analog substrate of ACh, to form thiocholine and acetate. Ellman's reagent, 5, 5'-dithiobis(2-nitrobenzoic acid), also known as DTNB, rapidly reacts with thiocholine to form a yellow product of 5-thio-2-nitrobenzoate that can be measured spectrophotometrically at 405 nm every 11s for 2 minutes as shown in Figure 24. The increasing of yellow color shows no inhibition of acetylcholinesterase because substrate can be hydrolyzed by the enzyme.

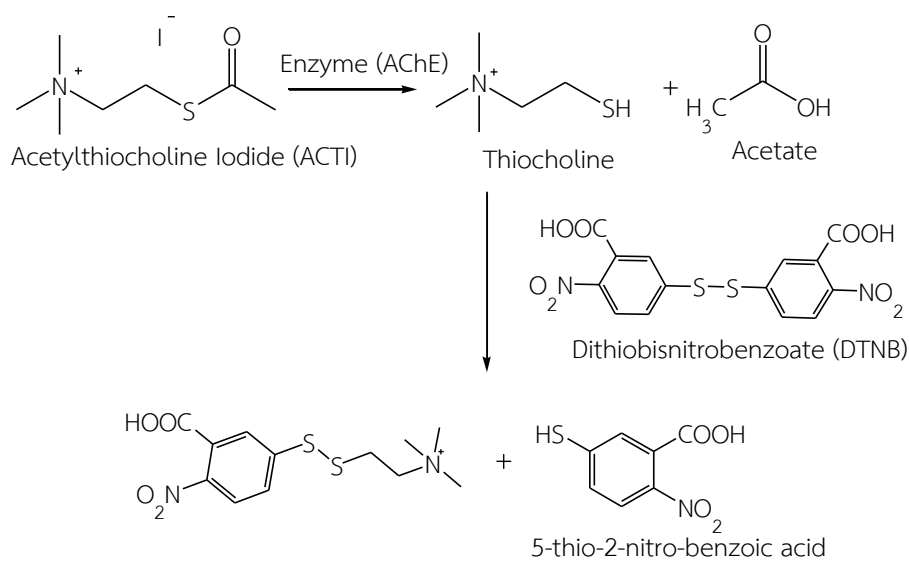


Figure 24. The reaction of ATCI in the presence of AChE and DTNB.

The activity of BChE can be measured in the same manner: in this case, an alternative substrate (selective for BChE), such as butyrylthiocholine iodide (BTCI), is used to form the products thiocholine and butyrate as shown in Figure 25. The thiocholine rapidly reacts with the DTNB to form the same yellow product that can be measured at 405 nm every 11s for 2 minutes.

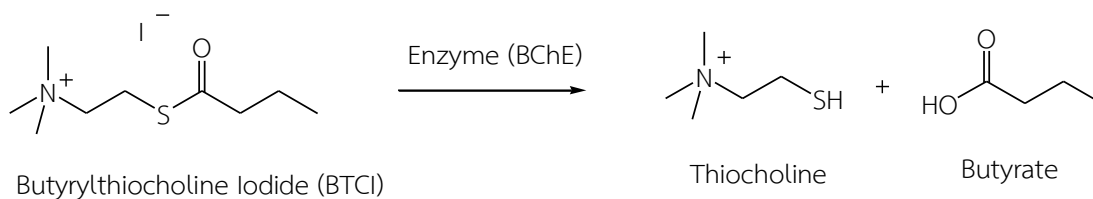
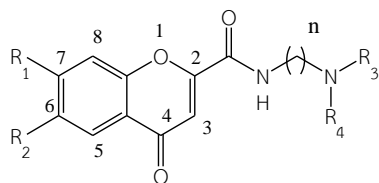


Figure 25. The reaction of BTCl in the presence of BChE.

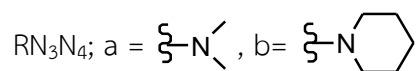
In this research, donepezil and tacrine were used as the positive controls. For the evaluation of AChE inhibitory activity, acetylcholinesterase enzyme from *Electrophorus electricus* (electric eel) and the evaluation of BChE inhibitory activity, butyrylcholinesterase enzyme from horse serum. Before the assay was performed, mean velocity value was limited to be in the range of 80-120. The absorbance as the assay progress were plotted against time to obtain Michaelis-Menten plot. Mean velocity values were calculated from the slope of the plot. The percentage inhibition of all compounds (**7-18**) for the AChE and BChE inhibitory activity were calculated using the following formula.

$$\% \text{inhibition} = \frac{(\text{Mean velocity of blank} - \text{Mean velocity of sample}) \times 100}{\text{Mean velocity of blank}}$$

All the synthesized chromone derivatives (**7-18**) (at 100 μM) were evaluated for the *in vitro* AChE and BChE inhibitory activity by using the Ellman's method in triplicate. Donepezil and tacrine were used as the reference compounds. The results can be summarized in Table **6** and can be presented as bar graph in Figure **26**. All compounds (**7-18**) exhibited more than 50% inhibition at 100 μM concentration for AChE and BChE inhibitions.



Compounds	R ₁	R ₂	NR ₃ R ₄	n	%inhibition of AChE ^a ± SD	%inhibition of BChE ^b ± SD
7	H	H	a	2	71.27±1.28	92.55±2.22
8	H	H	b	2	96.63±0.09	86.85±0.40
9	H	H	a	3	73.28±3.14	90.93±1.41
10	H	H	b	3	78.62±0.76	83.75±0.45
11	OCH ₃	H	a	2	79.13±0.91	83.70±0.75
12	OCH ₃	H	b	2	97.64±0.75	88.95±0.71
13	OCH ₃	H	a	3	74.25±1.64	97.20±0.17
14	OCH ₃	H	b	3	96.70±0.93	83.03±0.42
15	OCH ₃	OCH ₃	a	2	72.90±1.76	50.91±0.77
16	OCH ₃	OCH ₃	b	2	88.16±1.19	90.41±1.17
17	OCH ₃	OCH ₃	a	3	66.90±1.01	66.11±0.14
18	OCH ₃	OCH ₃	b	3	69.48±0.85	84.19±0.98
Tacrine	-	-	-	-	98.01±0.42	97.56±0.57
Donepezil	-	-	-	-	98.70±0.32	97.44±1.40



a= AChE from electric eel

b= BChE from horse serum

Table 6. % Inhibition of AChE and BChE of chromone derivatives.

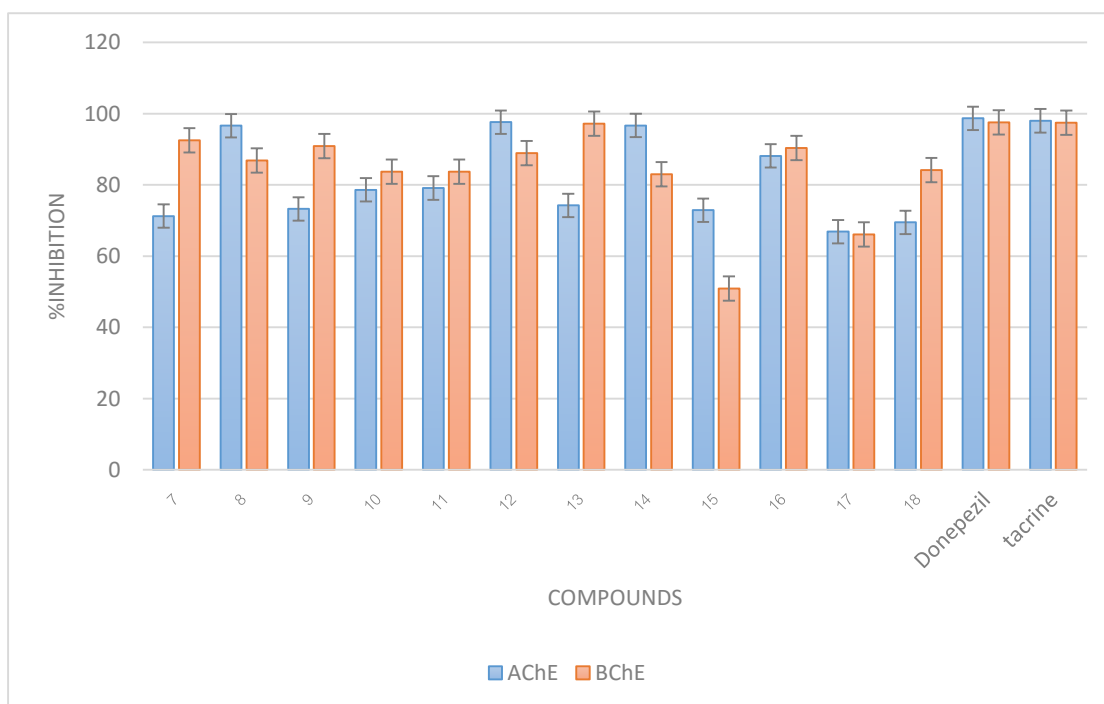


Figure 26. Comparison of %inhibition to AChE and BChE of chromone derivatives.

Then all compounds (**7-18**) were further evaluated for 50% inhibition of the AChE and BChE inhibitory activity (IC_{50}), Ellman's method was used and then the data was analyzed using the Software Prism.

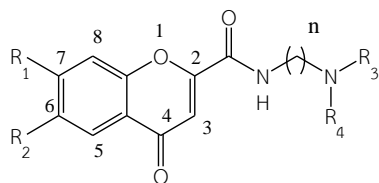
Determination of 50% of the AChE and BChE inhibitory activity (IC_{50})

Inhibitory activities of AChE and BChE of the synthesized compounds **7-18** were primarily assayed *in vitro* on AChE from electric eel and BChE from horse serum. Furthermore, the synthesized compounds were evaluated using human AChE (*HuAChE*). Donepezil and tacrine were used as the positive controls.

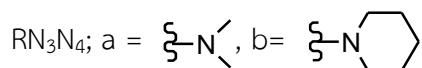
The results of IC_{50} showed that most of the synthesized compound exhibited potent AChE inhibitory activities at the nanomolar to micromolar range (IC_{50} 0.09-9.16 μ M) as shown in Table 7.

When compared among three series of synthesized compounds, the trend of AChE inhibitory activities was observed as series 2 > series 3 > series 1. In series 1, compounds **7-10** (non-substituted chromone moiety) showed activities with IC_{50} values ranging from 1.75-2.55 μM . Compound **8** was the most potent with IC_{50} value 1.75 ± 0.19 μM . While position structure of this compound in replacing by piperidine ring at R_3 and R_4 position and the length of linker $n=2$. In series 3, compound **15-18** have 6,7-dimethoxy chromone moiety. This series showed activities with IC_{50} values ranging from 0.14-2.56 μM . Compound **15** was the most potent AChEI with IC_{50} value 0.14 ± 0.03 μM . In this compound, dimethylamine was replaced at R_3 and R_4 positions and the length of linker $n=2$. The compounds in series 2 exhibited the best inhibitory potency for AChE with IC_{50} value ranging from 0.09-9.16 μM . When compared with series 1 and series 3, compound **14** showed significant AChE inhibitory activities with IC_{50} values in nanomolar range of 0.09 ± 0.0003 μM . Position R_3 and R_4 of this compound are replaced with piperidine ring and the length of linker $n=3$.

The result of AChEI activity test of compound in three series, showed that substitution on the chromone moiety at position 6(R_2) and 7(R_1) with 7-monomethoxy and 6,7-dimethoxy groups (series 2 and 3) tended to give higher potency of AChE inhibitory activity than compounds in series 1 which are non-substituted. Similarly, the comparison of substituents at position NR_3R_4 , it was found that substitution of piperidine ring tends to give higher potent than dimethylamine and the result of compound **14** showed greater inhibitory activity with IC_{50} values of 0.09 ± 0.0003 μM which was better than tacrine (IC_{50} value 0.13 ± 0.02 μM) but it was 15 times less potent than donepezil (IC_{50} value 0.006 ± 0.001 μM).



Compounds	R ₁	R ₂	NR ₃ R ₄	n	IC ₅₀ of AChE ^a (μM)			
					1	2	3	Average ± SD
7	H	H	a	2	7.52	8.52	6.70	7.58±0.91
8	H	H	b	2	1.53	1.84	1.89	1.75±0.19
9	H	H	a	3	3.66	3.55	3.06	3.42±0.32
10	H	H	b	3	2.62	2.52	2.51	2.55±0.06
11	OCH ₃	H	a	2	0.87	0.99	1.29	1.05±0.22
12	OCH ₃	H	b	2	0.79	0.94	0.92	0.88±0.08
13	OCH ₃	H	a	3	9.18	9.40	8.91	9.16±0.24
14	OCH ₃	H	b	3	0.09	0.09	0.09	0.09±0.0003
15	OCH ₃	OCH ₃	a	2	0.18	0.11	0.14	0.14±0.03
16	OCH ₃	OCH ₃	b	2	0.37	0.46	0.41	0.41±0.04
17	OCH ₃	OCH ₃	a	3	2.50	2.60	2.59	2.56±0.06
18	OCH ₃	OCH ₃	b	3	0.83	0.74	0.78	0.78±0.04
Tacrine	-	-	-	-	0.15	0.13	0.11	0.13±0.02
Donepezil	-	-	-	-	0.006	0.005	0.007	0.006±0.001



a = 50% inhibitory concentration of AChE from electric eel

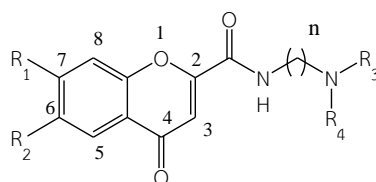
Table 7. Inhibition concentration at 50% to AChE (electric eel) of chromone derivatives.

The result of IC_{50} demonstrated moderate BChE inhibitory activities at the micromolar range (12.09-44.56 μM) as shown in Table 8.

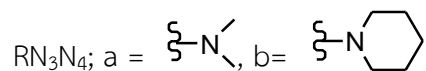
From the table, the synthesized compounds can be divided into three series. When compared BChE inhibitory activity of the synthesized compounds, it can be observed that the trend was series 3 > series 2 > series 1. This might be due to different substituents on chromone moiety and tertiary amino group. In series 1, compound **7-10** contains non-substituted chromone moiety. They showed activities with IC_{50} values ranging from 13.74-28.32 μM . Compound **10** exhibited BChE inhibitory activities with IC_{50} value $13.74 \pm 0.96 \mu\text{M}$, while this compound has a piperidine ring at R_3 and R_4 position and the length of linker $n=3$. In series 2, compounds **11-14** are monomethoxy that replaced on position 7 (R_1). This series showed activities with IC_{50} values ranging from 12.23-27.91 μM . Compound **12** exhibited BChE inhibitory activities with IC_{50} value $12.23 \pm 0.76 \mu\text{M}$, which has a length of linker $n=2$. In series 3, compounds **15-18** are 7, 8-dimethoxy analogs that showed activities with IC_{50} values ranging from 12.09-44.56 μM . Compound **17** exhibited BChE inhibitory activities with IC_{50} value $12.09 \pm 1.23 \mu\text{M}$, which has a length of linker $n=3$.

The result of BChEI activity test of compounds in three series, showed that 7-monomethoxy and 7, 8-dimethoxy analogs (series 2 and 3) tended to give high potency of BChE activity than compounds in series 1. This trend was also observed in AChE inhibitory activity. This suggested that the methoxy group might play a role in binding with the active site of the enzyme.

Similarly, in the comparison of substituents at position NR_3R_4 , it was found that the dimethylamine moiety tended to give higher potency than the piperidine ring and the result of compound **17** showed higher BChE inhibitory activity with IC_{50} values of $12.09 \pm 1.23 \mu\text{M}$, which was less than tacrine ($0.01 \pm 0.001 \mu\text{M}$) and donepezil ($1.06 \pm 0.02 \mu\text{M}$).



Compounds	R ₁	R ₂	NR ₃ R ₄	n	IC ₅₀ of BChE ^c (μM)			
					1	2	3	Average ± SD
7	H	H	a	2	20.16	33.06	15.63	22.95±0.04
8	H	H	b	2	28.78	26.54	29.64	28.32±1.60
9	H	H	a	3	11.73	16.37	15.44	14.51±0.45
10	H	H	b	3	12.65	14.45	14.13	13.74±0.96
11	OCH ₃	H	a	2	18.76	15.61	19.09	17.82±0.92
12	OCH ₃	H	b	2	10.96	11.48	14.24	12.23±0.76
13	OCH ₃	H	a	3	10.89	17.61	12.66	13.72±0.48
14	OCH ₃	H	b	3	25.86	27.40	30.47	27.91±0.34
15	OCH ₃	OCH ₃	a	2	34.23	51.04	48.43	44.56±0.46
16	OCH ₃	OCH ₃	b	2	40.75	44.03	34.09	39.62±0.06
17	OCH ₃	OCH ₃	a	3	10.96	14.67	10.65	12.09±1.23
18	OCH ₃	OCH ₃	b	3	32.49	33.33	31.08	32.3±1.13
Tacrine	-	-	-	-	0.02	0.01	0.01	0.01±0.001
Donepezil	-	-	-	-	1.07	1.08	1.04	1.06±0.02



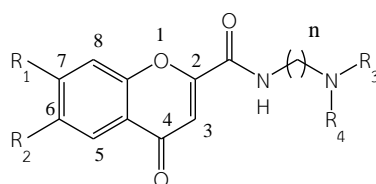
c = 50% inhibitory concentration of BChE from horse serum

Table 8. Inhibition concentration at 50% to BChE (horse serum) of chromone derivatives.

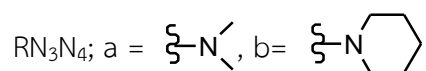
Moreover, the compounds were evaluated using human AChE (*HuAChE*). The result of IC_{50} demonstrated potent AChE inhibitory activities at the nanomolar to micromolar range (0.09-6.38 μM) as shown in Table 9.

From three series of synthesized compound the trend for AChE inhibitory activity was series 2 > series 3 > series 1. In series 2 and 3 (compound **11-18**) exhibited high activity more than series 1 (compound **7-10**). When compared between series 2 and series 3, it was found that series 2 showed higher activity. It showed activities with IC_{50} value ranging from 0.09-3.14 μM . Compound **14** exhibited AChE inhibitory activities with IC_{50} value $0.09 \pm 0.02 \mu\text{M}$. Which has length of linker $n=3$.

Similarly, the comparison of substituents at position NR_3R_4 , it was found that substitution with piperidine ring tended to give higher potency than dimethylamine group. Compound **14**, which was better than tacrine (IC_{50} value $0.31 \pm 0.002 \mu\text{M}$) but this compound showed less potency, as compared donepezil (IC_{50} value $0.004 \pm 0.001 \mu\text{M}$)



Compounds	R ₁	R ₂	NR ₃ R ₄	n	IC ₅₀ of AChE ^b (μM)			
					1	2	3	Average ± SD
7	H	H	a	2	4.04	4.79	3.47	4.10±0.66
8	H	H	b	2	7.11	5.81	6.20	6.38±0.67
9	H	H	a	3	5.35	5.77	4.90	5.34±0.43
10	H	H	b	3	1.55	1.76	1.54	1.61±0.12
11	OCH ₃	H	a	2	2.29	2.17	1.98	2.15±0.16
12	OCH ₃	H	b	2	1.65	1.79	1.75	1.73±0.07
13	OCH ₃	H	a	3	3.19	3.18	3.09	3.16±0.06
14	OCH ₃	H	b	3	0.11	0.08	0.08	0.09±0.02
15	OCH ₃	OCH ₃	a	2	2.43	2.61	3.29	2.78±0.46
16	OCH ₃	OCH ₃	b	2	1.33	1.29	1.43	1.35±0.07
17	OCH ₃	OCH ₃	a	3	3.38	3.48	2.58	3.15±0.49
18	OCH ₃	OCH ₃	b	3	0.20	0.22	0.23	0.22±0.02
Tacrine	-	-	-	-	0.32	0.29	0.31	0.31±0.02
Donepezil	-	-	-	-	0.004	0.005	0.004	0.004±0.001

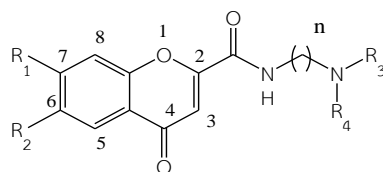


b = 50% inhibitory concentration of AChE from *human*

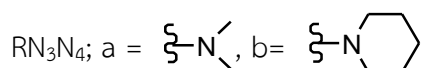
Table 9. Inhibition concentration at 50% to AChE (human) of chromone derivatives.

From the AChEI and BChEI activity evaluation of chromone derivatives (7-18) the IC₅₀ values and selectivity index of AChEI and BChEI were summarized in Table 10.

All the compounds exhibited significant AChEI activities with IC₅₀ values ranging from nanomolar to micromolar and showed weak BChEI activities (IC₅₀ of AChE ranging from 0.09-9.16 μM, *Ee*AChE and IC₅₀ of BChE ranging from 12.09-44.56 μM, BChE from Horse serum).



Compounds	R ₁	R ₂	NR ₃ R ₄	R	IC ₅₀ ±SD (μM)		SI*
					<i>Ee</i> AChE	Horse BChE	
7	H	H	a	2	7.58±0.91	22.95±0.04	3.03
8	H	H	b	2	1.75±0.19	28.32±1.60	16.18
9	H	H	a	3	3.42±0.32	14.51±0.45	4.24
10	H	H	b	3	2.55±0.06	13.74±0.96	5.38
11	OCH ₃	H	a	2	1.05±0.22	17.82±0.92	16.97
12	OCH ₃	H	b	2	0.88±0.08	12.23±0.76	13.89
13	OCH ₃	H	a	3	9.16±0.24	13.72±0.48	1.49
14	OCH ₃	H	b	3	0.09±0.0003	27.91±0.34	310.11
15	OCH ₃	OCH ₃	a	2	0.14±0.03	44.56±0.46	318.29
16	OCH ₃	OCH ₃	b	2	0.41±0.04	39.62±0.06	96.63
17	OCH ₃	OCH ₃	a	3	2.56±0.06	12.09±1.23	4.72
18	OCH ₃	OCH ₃	b	3	0.78±0.04	32.3±1.13	41.41
Tacrine	-	-	-	-	0.13±0.02	0.01±0.001	0.86
Donepezil	-	-	-	-	0.006±0.001	1.06±0.02	176.67



$$\text{SI}^* = \text{Selectivity index for AChE} = \text{IC}_{50}(\text{BChE}) / \text{IC}_{50}(\text{AChE})$$

Table 10. AChE and BChE inhibitory activity and selectivity index of chromone derivatives.

Compound **14** with 7-monomethoxy chromone moiety, R₃ and R₄ positions replaced with piperidine ring (b) and the length of linker n=3 showed the best AChE inhibitory activity (IC₅₀= 0.09±0.0003 μM). And compound **17** with 6, 7-dimethoxy chromone moiety, R₃ and R₄ positions replaced with dimethylamine (a) and the length of linker n=3 showed the best BChE inhibitory activity (IC₅₀= 12.09±1.23 μM).

Selectivity of cholinesterase inhibitory activity can be assayed by the ratio between IC₅₀ of BChE with IC₅₀ of AChE. If the compound has high selectivity value, this means the compound is selective to acetylcholinesterase. From the experiment, compound **14** exhibited selectivity index with 310.11 while selectivity index of tacrine and donepezil were 0.86 and 176.67, respectively.

In addition, compound **15** with 6, 7-dimethoxy coumarin moiety in series 3 also showed highly potent AChEI with IC₅₀= 0.14±0.03 μM (AChEI) and IC₅₀= 44.56±0.46 μM (BChEI). In this compound, dimethylamine was replaced at R₃ and R₄ position and the length of linker n=2 and selectivity index equals 318.29, this means the compound **15** is selective to acetylcholinesterase.

Therefore, AChE inhibitory activity of compound **14** and **15** were compared with Tacrine by using computer program (Microsoft excel: t-test). (Table 11).

Compounds	mean	S.D.	t	p
14	0.09	1.56×10 ⁻⁷	-2.81	0.01*
Tacrine	0.13	0.0002		

Compounds	mean	S.D.	t	p
15	0.14	0.0004	0.29	0.008*
Tacrine	0.13	0.0002		

*p < 0.05

Table 11. Comparison between compound 14 and 15 by t-test

From Table 11, compound **14** and **15** showed $p < 0.05$, this mean the IC_{50} values of these compounds are significantly different from Tacrine. Compound **14** is considered to be more potent than Tacrine. Result of IC_{50} value and selectivity index suggested that Compound **14** was selective AChE inhibitor. Based on the above assay results, to choose the most potent AChE inhibitor, **14**, for kinetic analysis to inquire the type of inhibition.

3. Kinetic study for the inhibition of AChE

The kinetic study for characterization of AChE inhibition was evaluated with the same protocol of inhibitory activity by using AChE from electric eel.

A kinetic study was carried out on compound **14** and measured at three different concentrations (2.5, 7.5 and 15 μM). Michaelis-Menten Plot (Figure 27.) was created by plotting between velocity (V) and varied concentration of the substrate [S] acetylthiocholine (ATCl: 5, 10, 25, 50, 125 and 250 μM) as summarized in Table 12.

Velocity [ATCI]	0				2.5				7.5				15			
	1	2	3	Average	1	2	3	Average	1	2	3	Average	1	2	3	Average
5	4.69	5.05	6.89	5.55	6.55	6.40	5.55	6.17	8.28	9.87	10.51	9.55	4.02	5.39	7.85	5.75
10	12.19	12.13	13.42	12.58	10.51	10.71	12.94	11.39	9.88	11.16	9.77	10.27	6.64	6.39	7.82	6.95
25	20.73	24.16	24.26	23.05	19.37	20.67	22.41	20.82	15.37	16.71	17.55	16.55	10.35	10.89	12.29	11.18
50	39.90	43.22	41.64	41.59	33.57	37.97	32.83	34.83	22.84	24.29	24.98	24.04	14.46	14.83	16.19	15.16
125	92.43	94.08	94.31	93.61	49.78	51.27	49.95	50.34	30.94	33.03	33.31	32.42	20.93	23.07	22.84	22.28
250	129.31	132.81	126.61	129.58	66.79	64.97	64.83	65.53	41.65	39.98	41.03	40.89	26.81	25.14	26.28	26.08

Table 12. Data of Michaelis-Menten with plotting between velocity (V) and concentration of substrate [S] acetylthiocholine (ATCI)

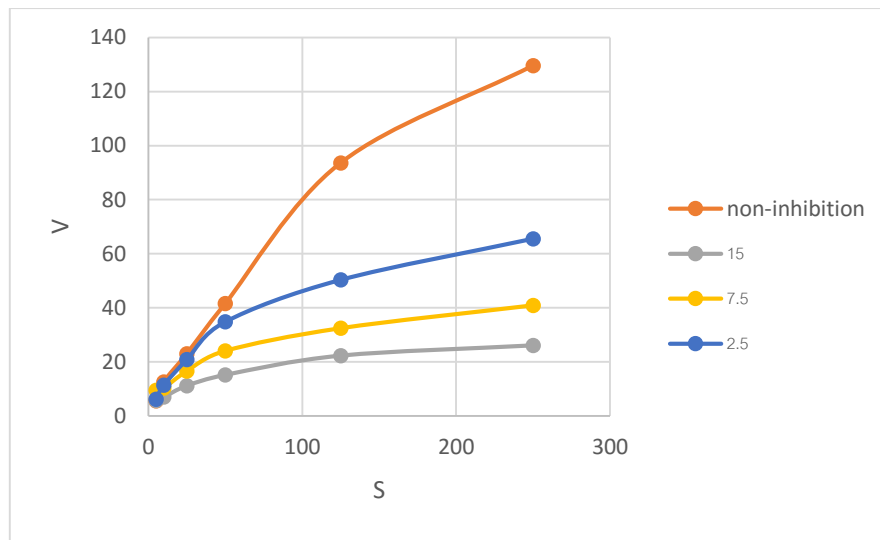


Figure 27. Michaelis-Menten with plotting between velocity (V) and concentration of substrate $[S]$ acetylthiocholine (ATCI).

Michaelis-Menten plot was converted to Lineweaver-Burk plot (Figure 28.) into a straight line by plotting between $1/\text{velocity}$ and $1/[S]$ by Prism5 program. The result showed decreased V_{max} and decreased K_m at increasing concentration of the inhibitor, which showed uncompetitive inhibition. It displayed that inhibitor binding with enzyme-substrate $[ES]$ complex only and give enzyme-substrate-inhibitor $[ESI]$ complex without binding to the free enzyme.

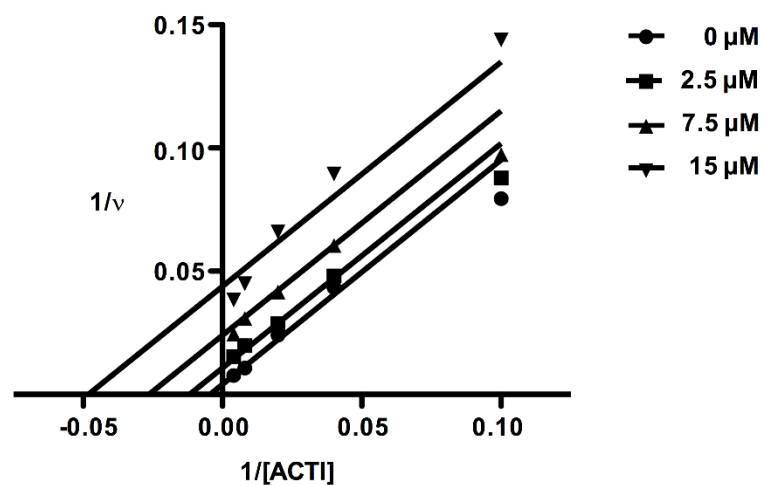


Figure 28. Lineweaver-Burk plot

4. Molecular docking study

The initial structure of *Torpedo californica* acetylcholinesterase (*TcAChE*) and *Human* butyrylcholinesterase (*HuBChE*) were retrieved from protein data bank with PDB ID: 1EVE and 4BDS, respectively. A molecular modeling study was performed using the docking program by AutoDock Vina 1.1.2 and Discovery studio 2.5.

The result showed affinity of binding energy between enzyme and compound as shown in Table 13.

Compounds	IC ₅₀ ±SD (μM)			Binding energy (kcal/mol)	
	<i>EeAChE</i>	<i>Horse BChE</i>	<i>HuAChE</i>	<i>TcAChE</i> (PDB ID: 1EVE)	<i>HuBChE</i> (PDB ID: 4BDS)
14	0.09±0.0003	27.91±0.34	0.09±0.02	-9.5	-7.9
A (Liu Q. et al. 2015.)	0.55±0.03	ND*	ND*	-9.6	-9.5
Tacrine	0.13±0.02	0.01±0.001	0.31±0.02	-8.3	-8.4
Donepezil	0.006±0.001	1.06±0.02	0.004±0.001	-10.9	-9.1

*ND= not determined

Table 13. Affinity of binding energy of compound **14**, **A** (Liu Q. et al. 2015.), tacrine and donepezil.

Compound **14**-*TcAChE* showed affinity of binding energy -9.5 kcal/mol. This compound occupied the entire enzymatic PAS, mid-gorge and CAS (Figure 29.). The chromone showed interaction with PAS of active site of enzyme and showed π - π interaction with Trp278 (distance of 3.53 Å), methylene chain showed hydrophobic interaction with Phe330 in the mid-gorge and piperidine ring of compound showed cation- π interaction with Phe329 (distance of 4.17 Å).

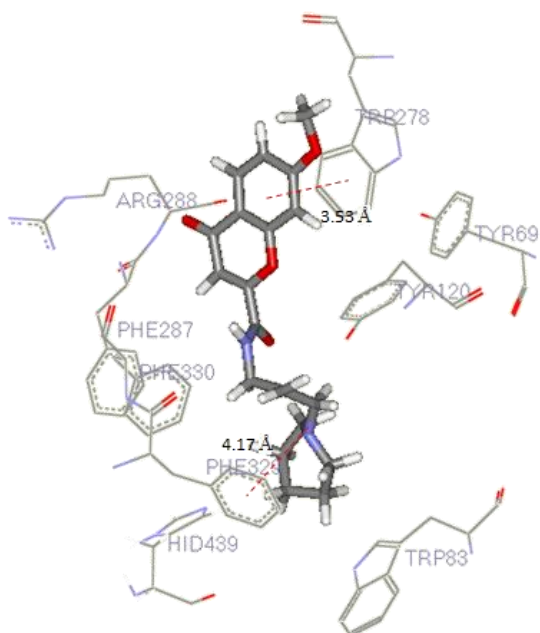


Figure 29. Molecular docking study of compound **14-TcAChE**

Compound **14-HuBChE** showed affinity of binding energy -7.9 kcal/mol demonstrating that the tertiary amino group of compound interacted with Trp279 (distance of 4.20 Å) and cation- π interaction as shown in Figure **30**.

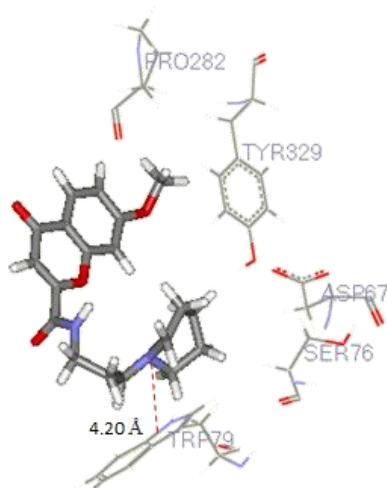


Figure 30. Molecular docking study of compound **14-HuBChE**

Compound **A-TcAChE** could bind to PAS, mid-gorge and CAS of AChE. This complex showed affinity the binding energy -9.6 kcal/mol. From figure **31**, the chromone interacted with PAS of active site of enzyme and showed π - π interaction with Trp278 (distance 3.43 Å). At the mid-gorge, the methylene chain interacted with Phe329 and Phe330 via the hydrophobic interaction. At the CAS, π - π interaction between benzyl group of compound and Trp83 (distance 3.78 Å) was observed as well.

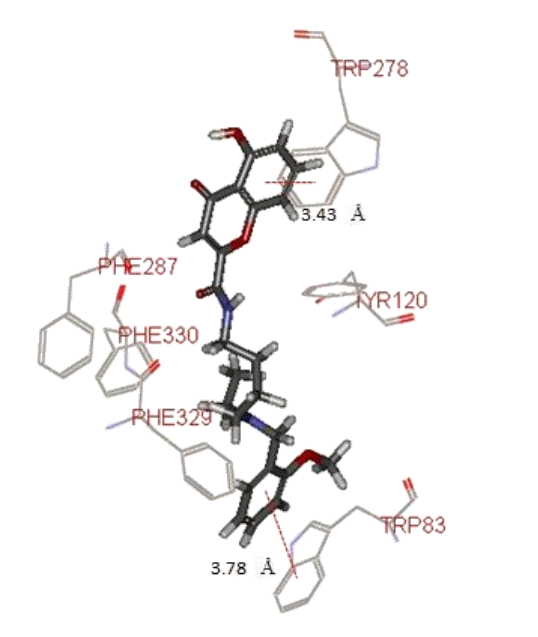


Figure 31. Molecular docking study of compound **A-TcAChE**.

For compound **A-HuBChE**, total interaction energy was -9.5 kcal/mol. From Figure **32**, 4-carbonyl group at the chromone show hydrogen bond with Ser195 (distance 3.02 Å) and benzyl group of compound show π - π interaction with Trp79 (distance 4.18 Å).

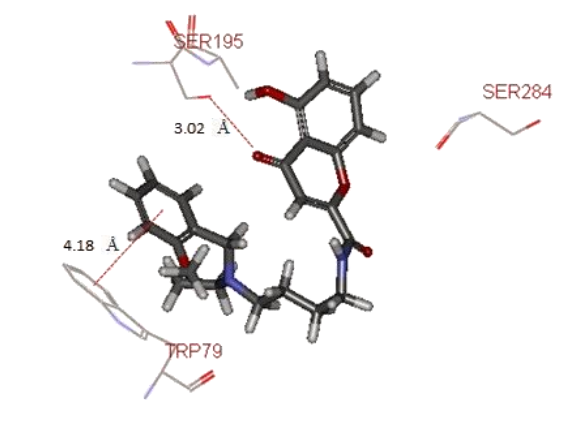


Figure 32. Molecular docking study of compound A-*HuBChE*.

Tacrine-*TcAChE* showed affinity the binding energy -8.3 kcal/mol. This compound bound only with CAS of active site of enzyme. The structure of tacrine showed stacking interaction with Trp83 (distance of 3.89 Å) and Phe329 of active site of *TcAChE*. The nitrogen atom on the tetrahydroacridine ring exhibited hydrogen bond with carbonyl oxygen of Hid439 (distance of 3.1 Å) as shown in Figure 33.

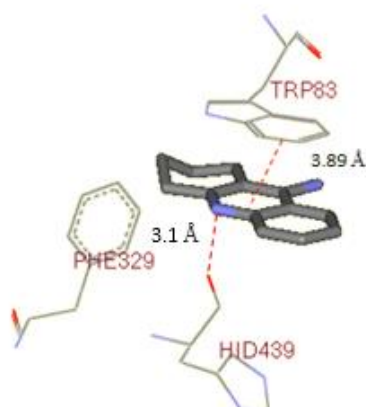


Figure 33. Molecular docking study of Tacrine-*TcAChE*

Tacrine-*HuBChE* showed affinity the binding energy -8.4 kcal/mol. This compound showed π - π interaction with Trp79 (distance of 3.50 Å) as showed in Figure 34.

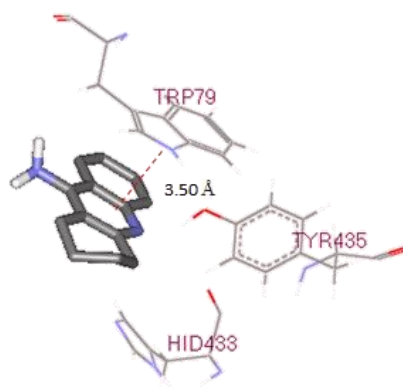


Figure 34. Molecular docking study of Tacrine-*HuBChE*

Affinity the binding energy of Donepezil-*TcAChE* is -10.9 kcal/mol. At the PAS, indanone ring showed π - π interaction with Trp278 (distance of 3.63 Å). At the mid-gorge, the long chain of methylene interacted with Phe330 via the hydrophobic interaction. At the CAS, piperidine ring showed cation- π interaction with Phe329 (distance of 3.96 Å) and benzyl group of compound, it can interact with π - π interaction by Trp83 (distance of 4.15 Å) as shown in Figure 35.

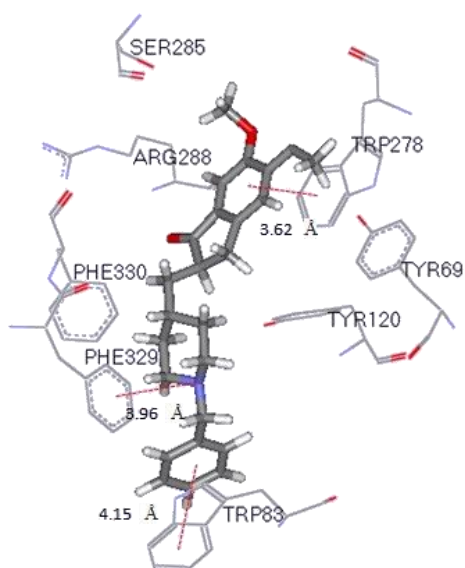


Figure 35. Molecular docking study of donepezil-*TcAChE*

Affinity the binding energy of Donepezil-*Hu*BChE is -9.1 kcal/mol. The hydrophobic interaction with Tyr329 at mid-gorge of active site and π - π interaction between the benzyl group and Trp79 (distance of 3.75 Å) as shown in Figure 36.

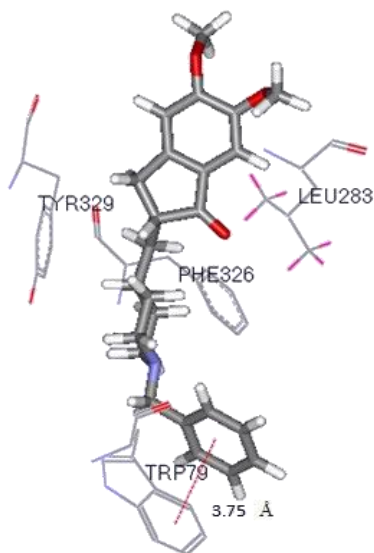


Figure 36. Molecular docking study of donepezil-*Hu*BChE

The molecular docking studies of compound **14**, compound **A** (Liu Q. et al. 2015), tacrine and donepezil resulted in the low negative binding energy which indicated strong favorable binding for both enzymes (*Tc*AChE and *Hu*BChE). The lowest binding energy conformer of each ligand was picked to investigate the residue interaction. Furthermore, distance values which were measured of the distance between amino acid residues in active site of enzyme and functional groups on the ligands were calculated.

Binding energy and key interaction residues between the ligands and the enzymes and distance (Å) are summarized in Table **14**.

Ligands	Enzyme	Binding energy (kcal/mol)	Type of interaction	Distance (Å)	Ligand interaction moiety
14	<i>TcAChE</i>	-9.5	π - π (Trp278) cation- π (Phe329) hydrophobic (Phe330)	3.53 4.17	Chromone ring Piperidine ring Methylene chain
	<i>HuBChE</i>	-7.9	cation- π (Trp79)	4.20	Tertiary amino group
A (Liu Q. et al. 2015.)	<i>TcAChE</i>	-9.6	π - π (Trp83) π - π (Trp278) hydrophobic (Phe329, 330)	3.78 3.43	Benzyl group Chromone ring Methylene chain
	<i>HuBChE</i>	-9.5	π - π (Trp79) hydrogen bond (Ser195)	4.18 3.02	Benzyl group 4-carbonyl group
Tacine	<i>TcAChE</i>	-8.3	Stacking (Trp83, Phe329) hydrogen bond (His439)	3.89 3.10	Benzene ring Nitrogen atom
	<i>HuBChE</i>	-8.4	π - π (Trp79)	3.50	Benzene ring
Donepezil	<i>TcAChE</i>	-10.9	π - π (Trp83) π - π (Trp278) cation- π (Phe329) hydrophobic (Phe330)	4.15 3.63 3.96	Benzyl group Indanone ring Piperidine ring Methylene chain
	<i>HuBChE</i>	-9.1	π - π (Trp79) hydrophobic (Phe329)	3.75	Benzyl group Methylene chain

Table 14. Binding energy, key enzyme-ligand interactions and distance of compound 14, A (Liu Q. et al. 2015.), tacrine and donepezil.

In this research, 12 novel chromone derivatives were designed, synthesized and evaluated for *in vitro* AChE and BChE inhibitory activities (%inhibition and IC_{50}), kinetic study and molecular docking. It can be summarized as follow:

The products of 12 novel chromone derivatives (**7-18**) were obtained as yellow solid with percent yield higher than 60%. *In vitro* AChE and BChE inhibitory activities were evaluated by using Ellman's method. All synthesized compounds showed more than 50% inhibition at 100 μ M concentration for *Ee*AChE and BChE from horse serum and then all compounds were further evaluated for 50% inhibition of the AChE and BChE inhibitory activity (IC_{50}). Tacrine and donepezil was used as the reference compounds.

Compound **14** showed significant AChE inhibitory activity with IC_{50} value of 0.09 ± 0.003 μ M. (selectivity index= 310.11) this means the compound is selective to acetylcholinesterase more than butyrylcholinesterase. Compound **14** showed higher potency than tacrine but less potent than donepezil. Therefore, based on the above assay results, the most potent AChE inhibitor, **14**, was chosen for kinetic analysis to inquire the type of inhibition.

The result of enzyme kinetic showed uncompetitive inhibition It exhibited that compound **14** or inhibitor binding with enzyme-substrate [ES] complex only.

In the last part of the molecular docking studies, the results revealed that compound **14**, **A** and donepezil acted as dual binding site inhibitors which had interactions with various amino acid residues both in the catalytic anionic site (CAS) and peripheral anionic site (PAS) of the enzymes but tacrine bound only with CAS of active site of enzyme. Therefore, compound **A** showed higher binding energy than compound **14** but both compounds has better binding energy than tacrine but all compounds had less binding energy than donepezil. These results were consistent with the IC_{50} values.

CHAPTER 4

CONCLUSION

Cholinergic hypothesis is the major hypothesis in the pathogenesis of Alzheimer's Disease. Acetylcholinesterase inhibitors have been widely used for the treatment of AD in the clinic. These drugs can block function of acetylcholinesterase and butyrylcholinesterase and subsequently increased neurotransmitter (ACh) in the brain and improve cognition and learning.

In this research, chromone derivatives were designed, synthesized and evaluated as cholinesterase inhibitor. Target compounds have been successfully synthesized in 2 steps; synthesis of Ethyl-4-oxo-4*H*-chromene-2-carboxylate derivatives (**4-6**) and synthesis of Chromone-2-carboxamido-alkylamine derivatives (**7-18**). The desired products were obtained in high yields. Structure of all compounds was confirmed by IR, ¹H-NMR, ¹³C-NMR and Mass spectrometry. The cholinesterase inhibitory activity of all compounds was evaluated by Ellman's method. Chromone derivatives (**7-18**) showed higher than 50% AChE and BChE inhibition at 100 μM. Most of the synthesized compound exhibited potent AChE inhibitory activities at the nanomolar to micromolar range (IC₅₀ 0.09-9.16 μM) and demonstrated weak BChE inhibitory activities at the micromolar range (IC₅₀ 12.09-44.56 μM). Compound with the best activity is **14** (R₁ = OCH₃, R₂ = H, NR₃R₄ = piperidine ring, n=3) showed higher potency than the drug tacrine but it was still less active than the currently most potent drug donepezil.

Based on the above assay results, compound **14** was then subjected for kinetic analysis to inquire the type of inhibition. The kinetic analysis showed uncompetitive inhibition with both of decreased V_{max} and K_m at increasing concentration of the inhibitor. This result is in good agreement with the results of molecular docking studies that compared between compound **14**, tacrine and donepezil. Compound **14** showed higher affinity than tacrine but less affinity than donepezil. This compound occupied the entire enzymatic PAS, mid-gorge and CAS. At the PAS, chromone showed π-π interaction with Trp278. At the mid-gorge, the long chain of methylene interacted with Phe330 via the hydrophobic interaction. At the CAS, piperidine ring showed cation-π interaction with Phe329.

In summary, chromone-2-carboxamido-alkylamine derivatives were designed, synthesized, and evaluated for cholinesterase activity. Compound **14** was the most potent AChEI in this series; it exerted IC_{50} in nanomolar range, higher activity than the clinical used drug tacrine. Enzyme kinetic study and molecular docking revealed that compound **14** was uncompetitive inhibitor and dual-binding site inhibitor. Compound **14** is promising molecule for further evaluation for development as AChEI for the treatment of Alzheimer's disease.

BIBLIOGRAPHY

- นพ.บุญชัย พิพัฒน์วชิชกุล และคณะ (2556) รายงาน “ดูแลอย่างไรกับผู้สูงวัยสมองเสื่อม”
Available:<http://www.mcot.net/site/>. สืบค้นวันที่ 16 มกราคม 2559.
- Bar-On P, Millard CB, Harel M, et al. Kinetic and structural studies on the interaction of cholinesterases with the anti-Alzheimer drug rivastigmine. *Biochemistry* 2002; 41: 3555-3564.
- Burns A, Iliffe S. Alzheimer's disease. *BMJ* 2009; 5: 338-349.
- Camps P and Muñoz-Torrero D. Tacrine-huperzine A hybrids (Huprines): A new class of highly potent and selective acetylcholinesterase inhibitors of interest for the treatment of Alzheimer's disease. *Mini Rev Med Chem* 2001; 1: 163-174.
- Chen TH, Chou MC, Lai CL, et al. Factors affecting therapeutic response to Rivastigmine in Alzheimer's disease patients in Taiwan. *J Med Sci* 2017; 33: 277-283.
- Cokugras AN. Butyrylcholinesterase: Structure and Physiological Importance. *J Biochem* 2003; 28: 54-61.
- Cummings JL. Alzheimer's Disease. *N Engl J Med* 2004; 351: 56-67.
- Ellman G, Courtney K, Andres V, et al. A new and rapid colorimetric determination of acetylcholinesterase activity. *Biochem Pharm* 1961;7:88-95.
- Fischer PM. Turning down tau phosphorylation. *Nat Rev Drug Discov* 2008; 4: 448-449.
- Greenblatt HM, Kryger G, Lewis T, et al. Structure of acetylcholinesterase complexed with (-)-galanthamine at 2.3 Å resolution. *FEBS Letters* 1999; 463: 321-326.
- Greig NH, Lahiri DK and Sambamurti K, Butyrylcholinesterase: An important new target in Alzheimer's disease therapy. *Int Psychogeriatr* 2002; 14: 77-91.
- Holmes C, Boche D, Wilkinson D, et al. Long-term effects of A[beta]42 immunisation in Alzheimer's disease: follow-up of a randomised, placebocontrolled phase I trial. *The Lancet* 2008; 372: 216-223.

BIBLIOGRAPHY (continued)

- Jacob RB, Andersen T and McDougal OM, Accessible High-Throughput Virtual Screening Molecular Docking Software for Students and Educators. *PLoS Comput Biol* 2012, 8(5).
- Jin H, Nguyen T and Go ML. Acetylcholinesterase and Butyrylcholinesterase Inhibitory Properties of Functionalized Tetrahydroacridines and Related Anaogs. *Med Chem* 2014; 4: 10.
- Korabecny J, Spilovska K, Horova A, et al. Design, synthesis and in vitro testing of 7-methoxytacrineamantadine analogues: a novel cholinesterase inhibitors of the treatment of Alzheimer's disease. *Med Chem Res* 2015; 24: 2645-2655.
- Liu Q, Qiang X, Li Y, et al. Design, synthesis and evaluation of Chromone-2-carboxamido-alkylbenzylamines as multifunctional agents for the treatment of Alzheimer's disease. *Bioorg Med Chem* 2015; 23: 911-923.
- Luo W, Chen Y, Wang T, et al. Design, synthesis and evaluation of novel 7-aminoalkyl-substituted flavonoid derivatives with improved cholinesterase inhibitory activities. *Bioorg Med Chem* 2016;24 :672-680.
- Mebane-Sims I. 2009 Alzheimer's disease facts and figures. *Alzheimer's & Dementia* 2009; 5: 234-270.
- Qiang X, Sang Z, Yuan W, et al. Design, synthesis and evaluation of genistein-o-alkylbenzylamines as potential multifunctional agents for the treatment of Alzheimer's disease. *Eur J Med Chem* 2014; 76: 314-331.
- Sang Z, Qiang X, Li Y, et al. Design, synthesis and evaluation of scutellarein-O-acetamidoalkylbenzylamines as potential multifunctional agents for the treatment of Alzheimer's disease. *Eur J Med Chem* 2017; 28:307-323.
- Terry AV Jr and Buccafusco JJ. The cholinergic hypothesis of age and Alzheimer's disease-related cognitive deficits: recent challenges and their implications for novel drug development. *J Pharmacol Exp Ther* 2003; 306: 821-7.

BIBLIOGRAPHY (continued)

- Trott O. and Olson AJ. AutoDock Vina: improving the speed and accuracy of docking with a new scoring function, efficient optimization, and multithreading. *J Comput. Chem* 2010, 31, 461-455.
- Walenzyk T, Carola C, Buchholz H, et al. Chromone derivatives which bind to human hair, *Tetrahedron Lett* 2005; 7366-7377.
- Wischik CM, Bentham P, Wischik DJ, et al. O3-04-07: Tau aggregation inhibitor (TAI) therapy with rember(TM) arrests disease progression in mild and moderate Alzheimer's disease over 50 weeks. Alzheimer's and Dementia, Alzheimer's Association International Conference on Alzheimer's Disease 2008; 4: T167.

APPENDIX

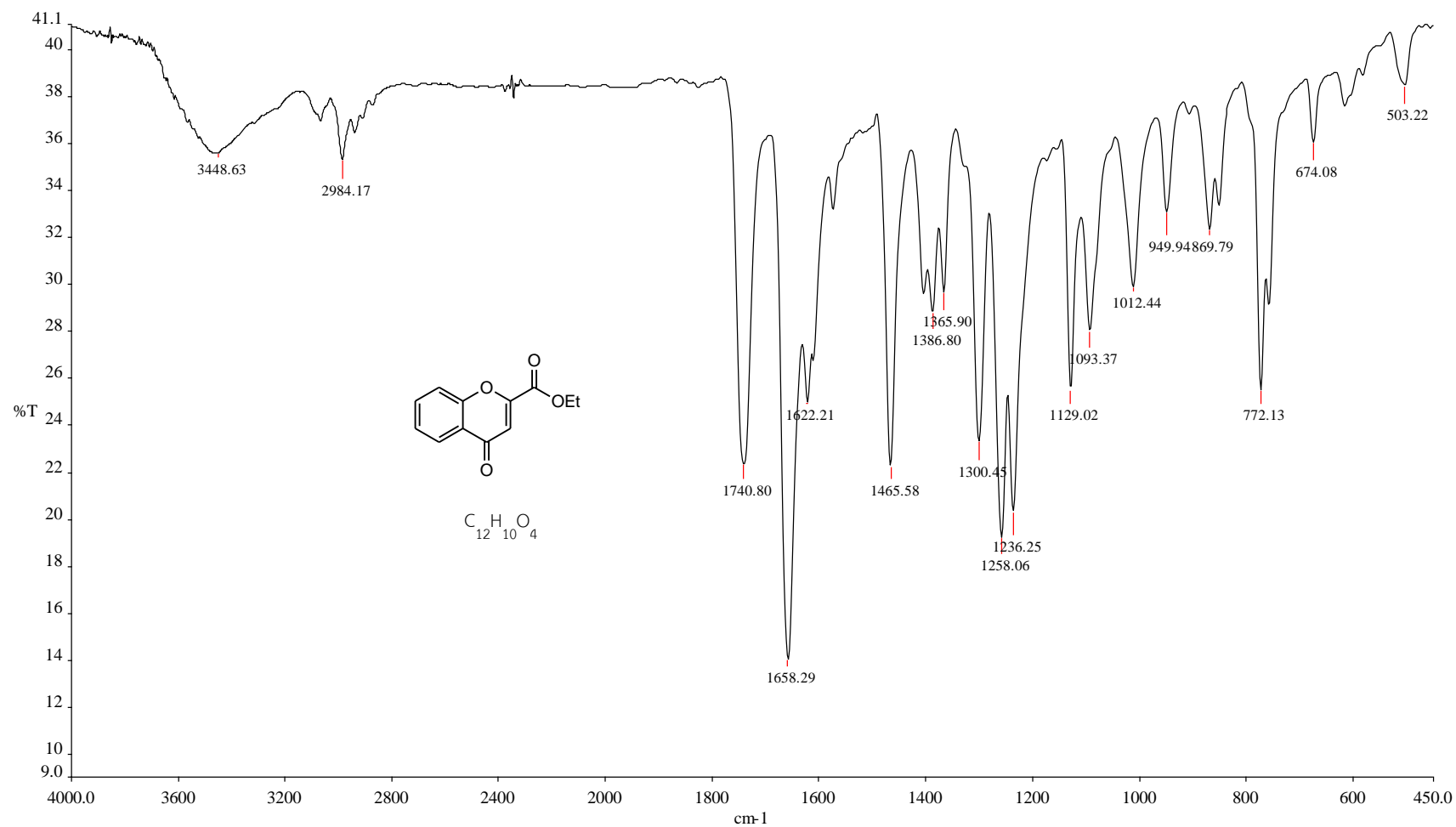


Figure 37. The IR spectrum of Ethyl-4-oxo-4H-chromene-2-carboxylate (4)

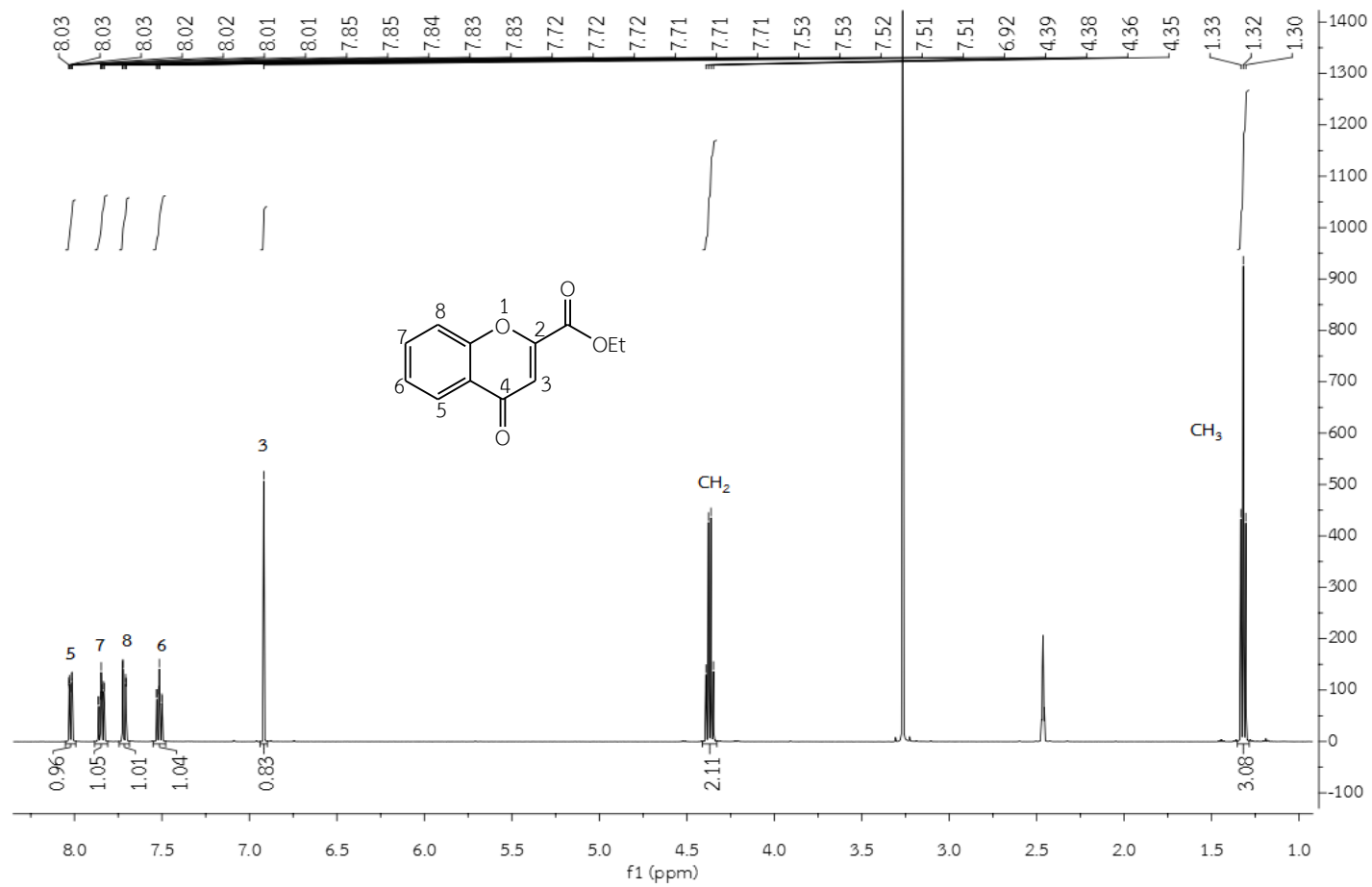


Figure 38. The ¹H-NMR spectrum of Ethyl-4-oxo-4H-chromene-2-carboxylate (**4**) in DMSO-d₆

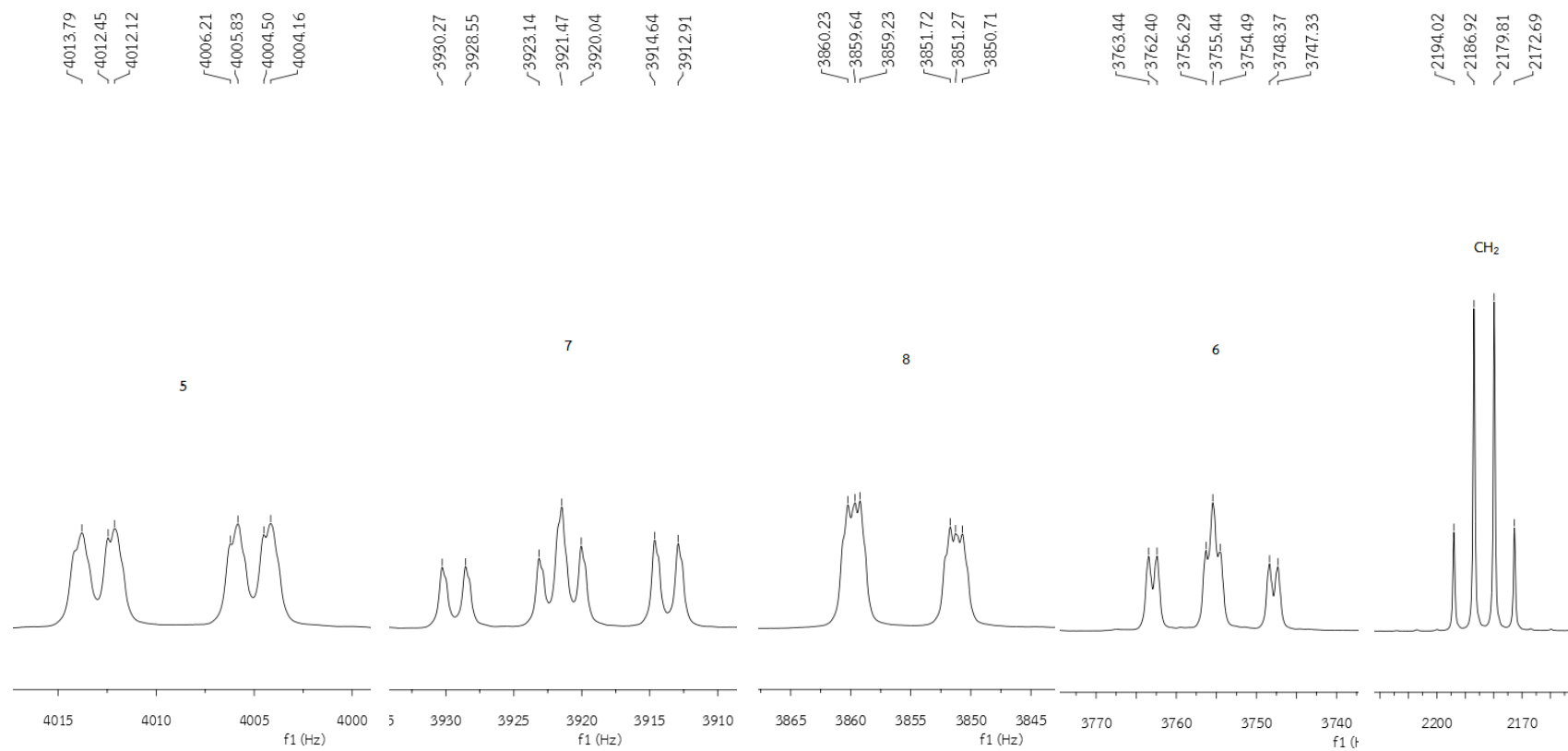


Figure 39. The ¹H-NMR spectrum of Ethyl-4-oxo-4*H*-chromene-2-carboxylate (**4**) in DMSO-*d*₆ (Enlarged scale)

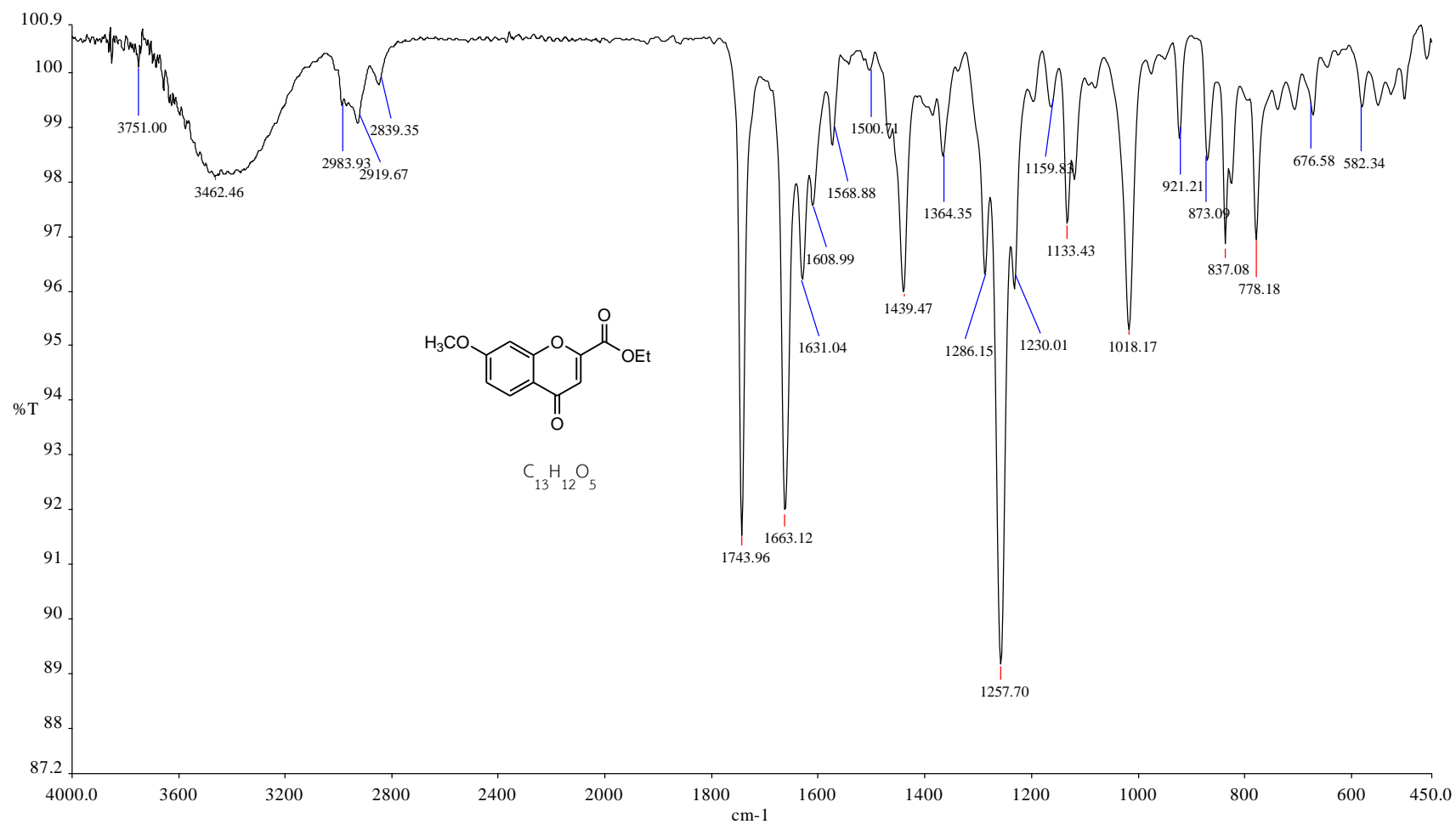


Figure 40. The IR spectrum of Ethyl-7-methoxy-4-oxo-4H-chromene-2-carboxylate (5)

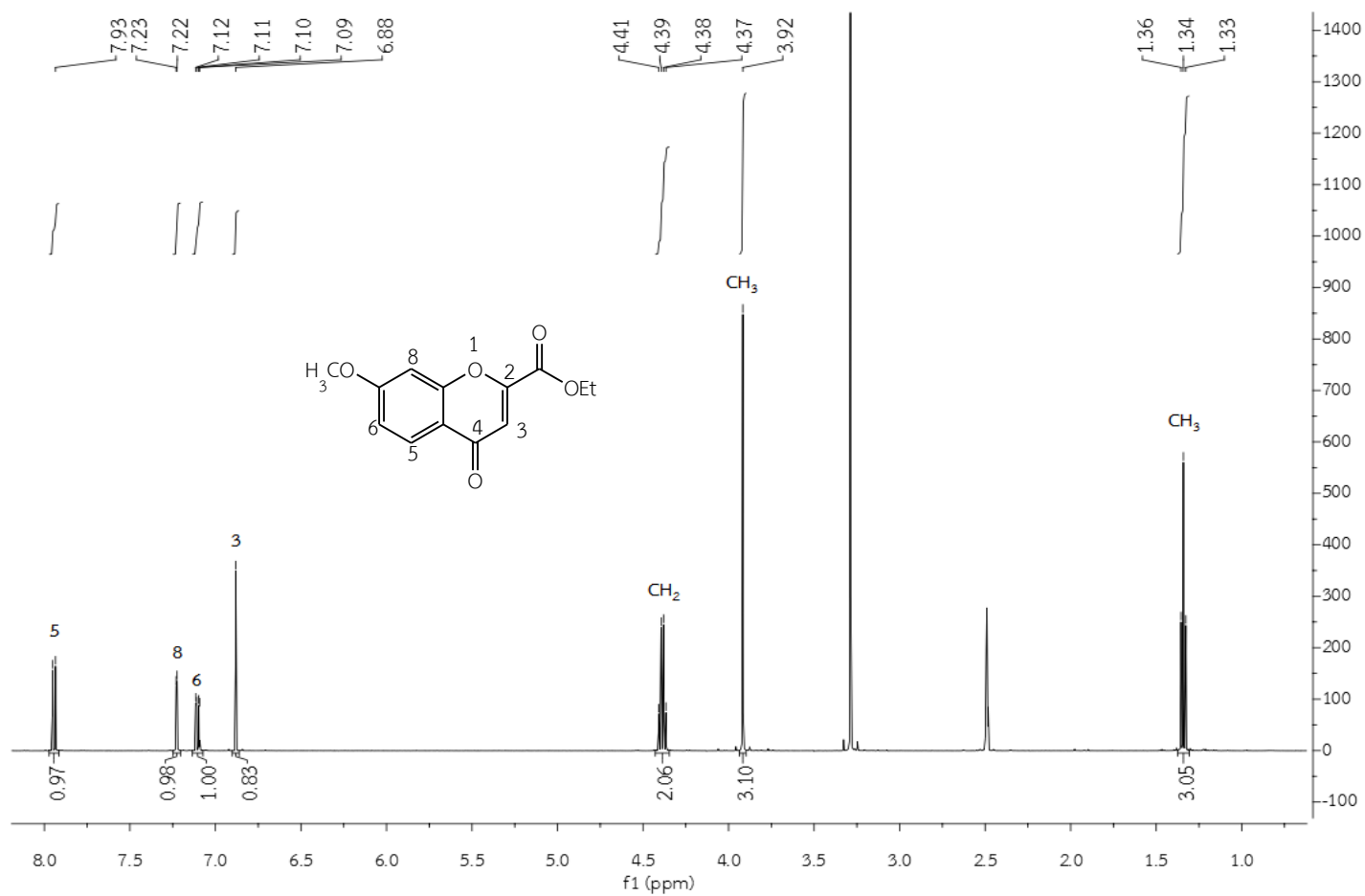


Figure 41. The ¹H-NMR spectrum of Ethyl-7-methoxy-4-oxo-4H-chromene-2-carboxylate (5) in DMSO-d₆

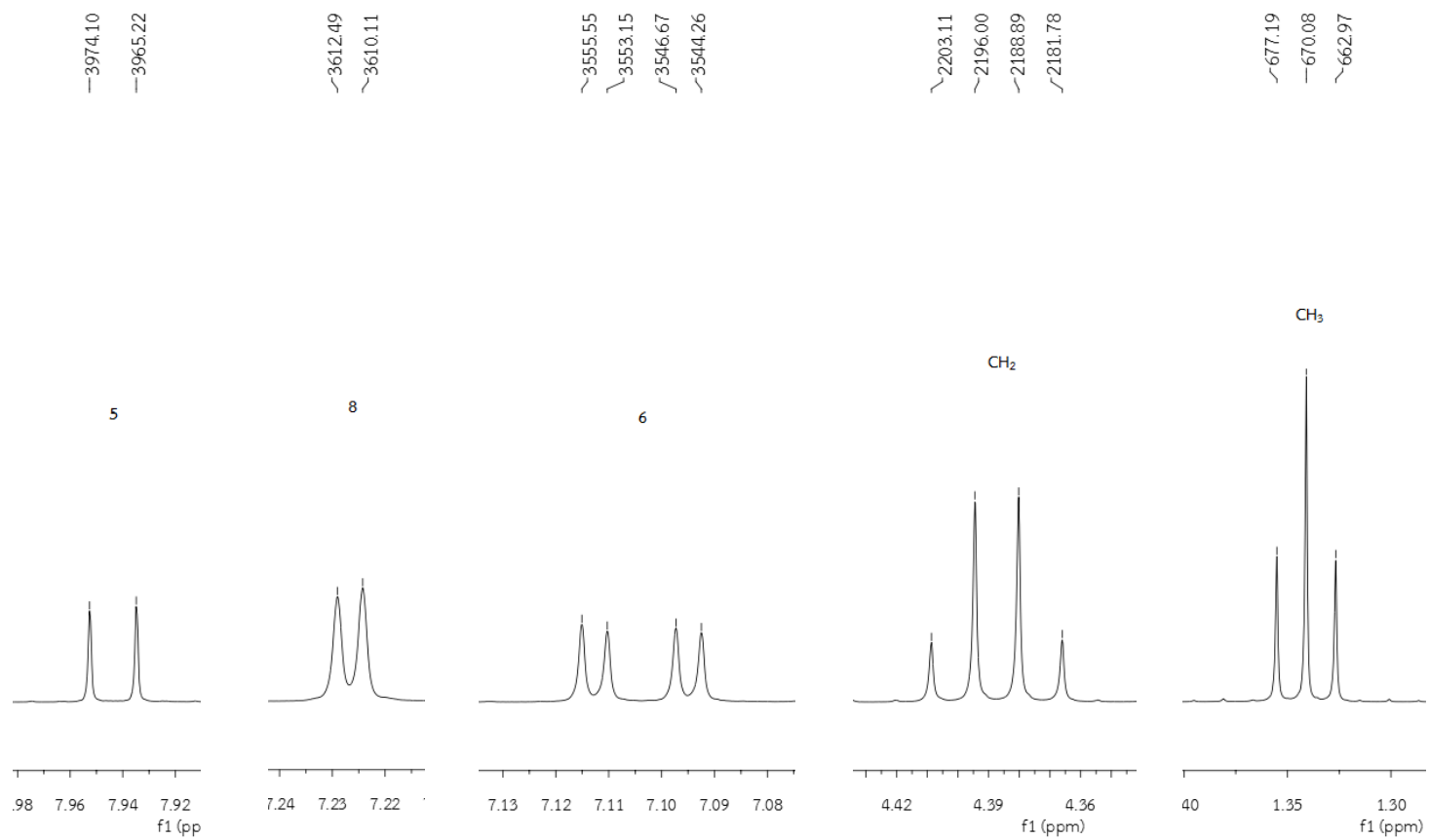


Figure 42. The ¹H-NMR spectrum of Ethyl-7-methoxy-4-oxo-4*H*-chromene-2-carboxylate (**5**) in DMSO-*d*₆ (Enlarged scale)

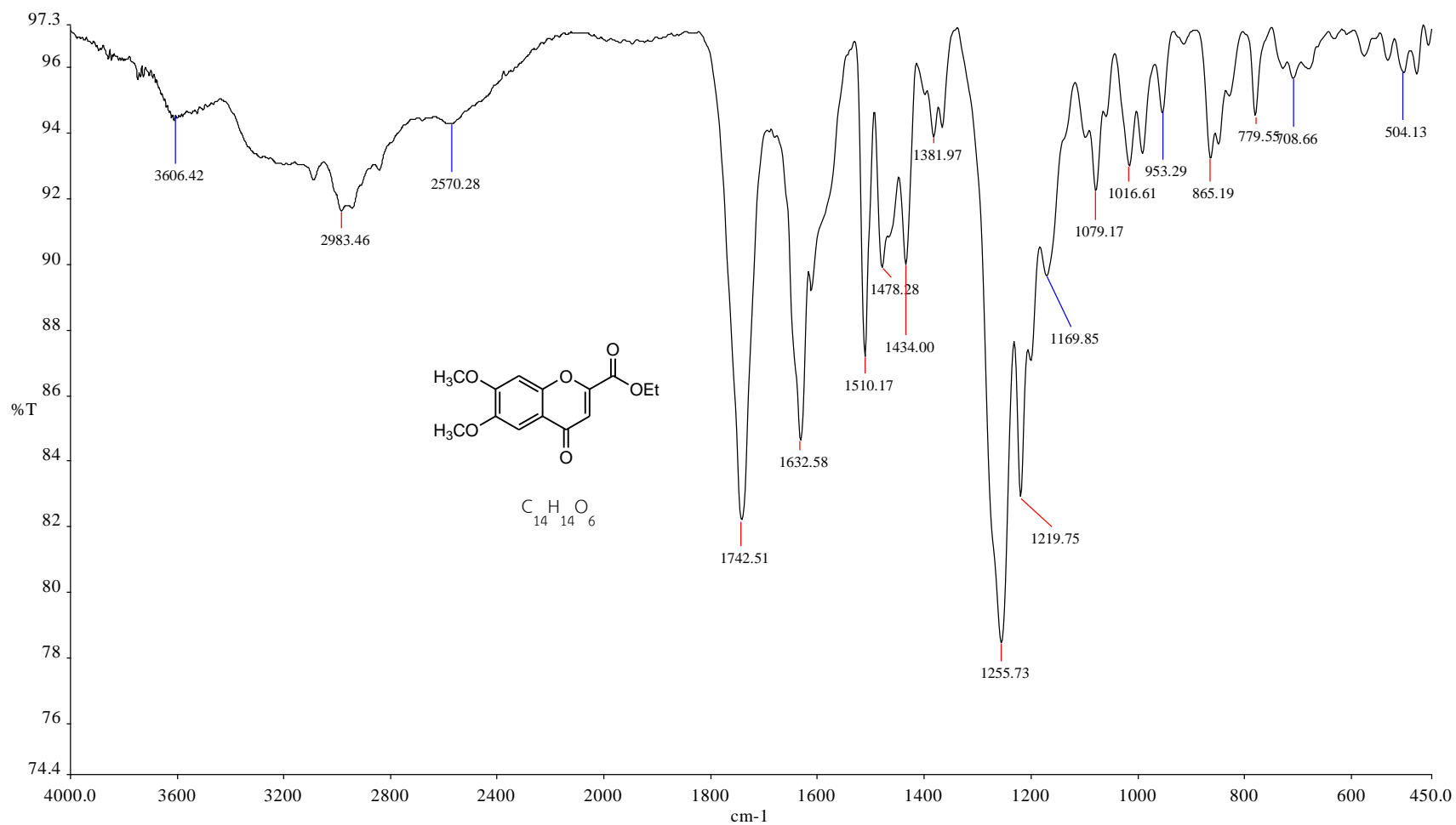


Figure 43. The IR spectrum of Ethyl-6, 7-dimethoxy-4-oxo-4H-chromene-2-carboxylate (6)

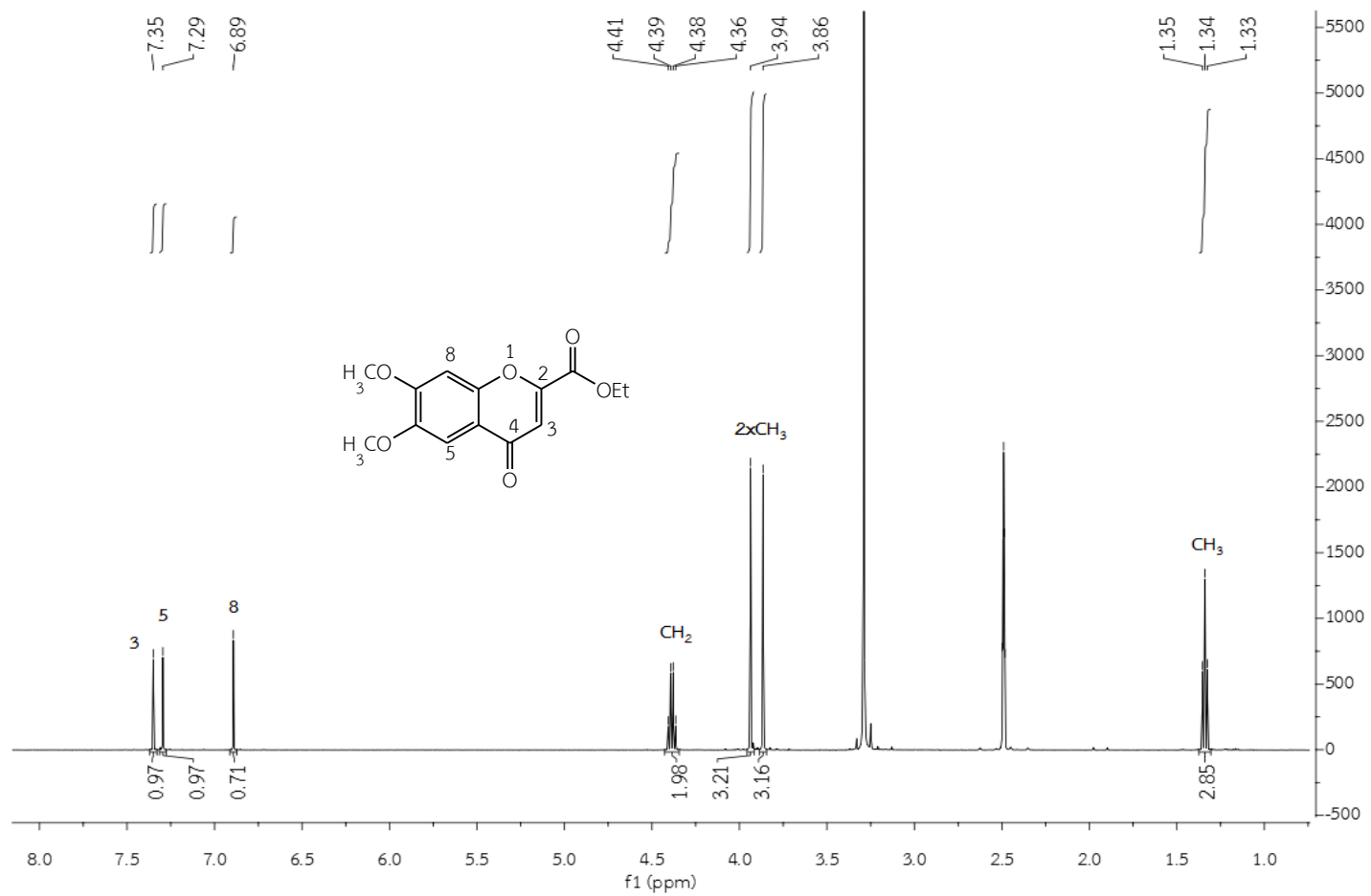


Figure 44. The $^1\text{H-NMR}$ spectrum of Ethyl-6,7-dimethoxy-4-oxo-4H-chromene-2-carboxylate (**6**) in $\text{DMSO-}d_6$

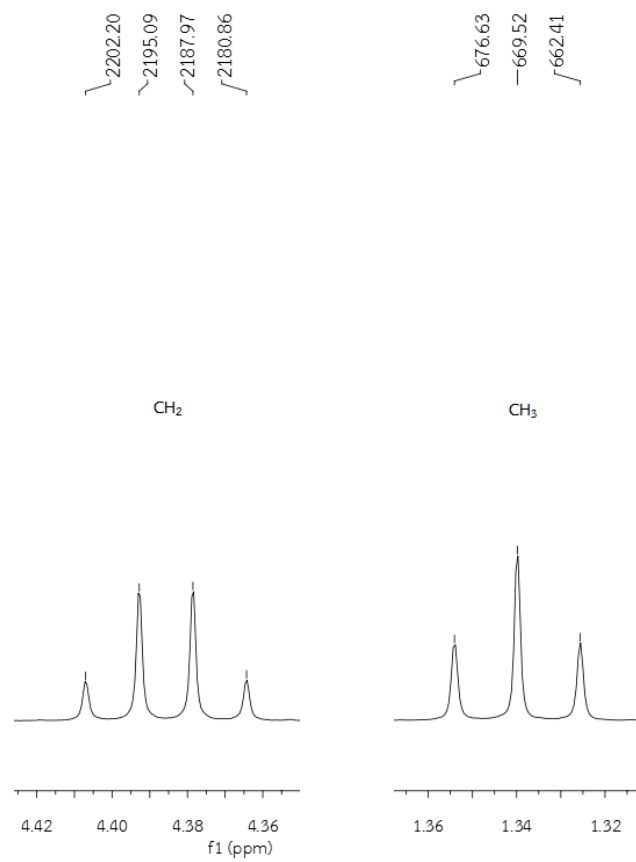


Figure 45. The ^1H -NMR spectrum of Ethyl-6,7-dimethoxy-4-oxo-4*H*-chromene-2-carboxylate (**6**) in $\text{DMSO-}d_6$ (Enlarged scale)

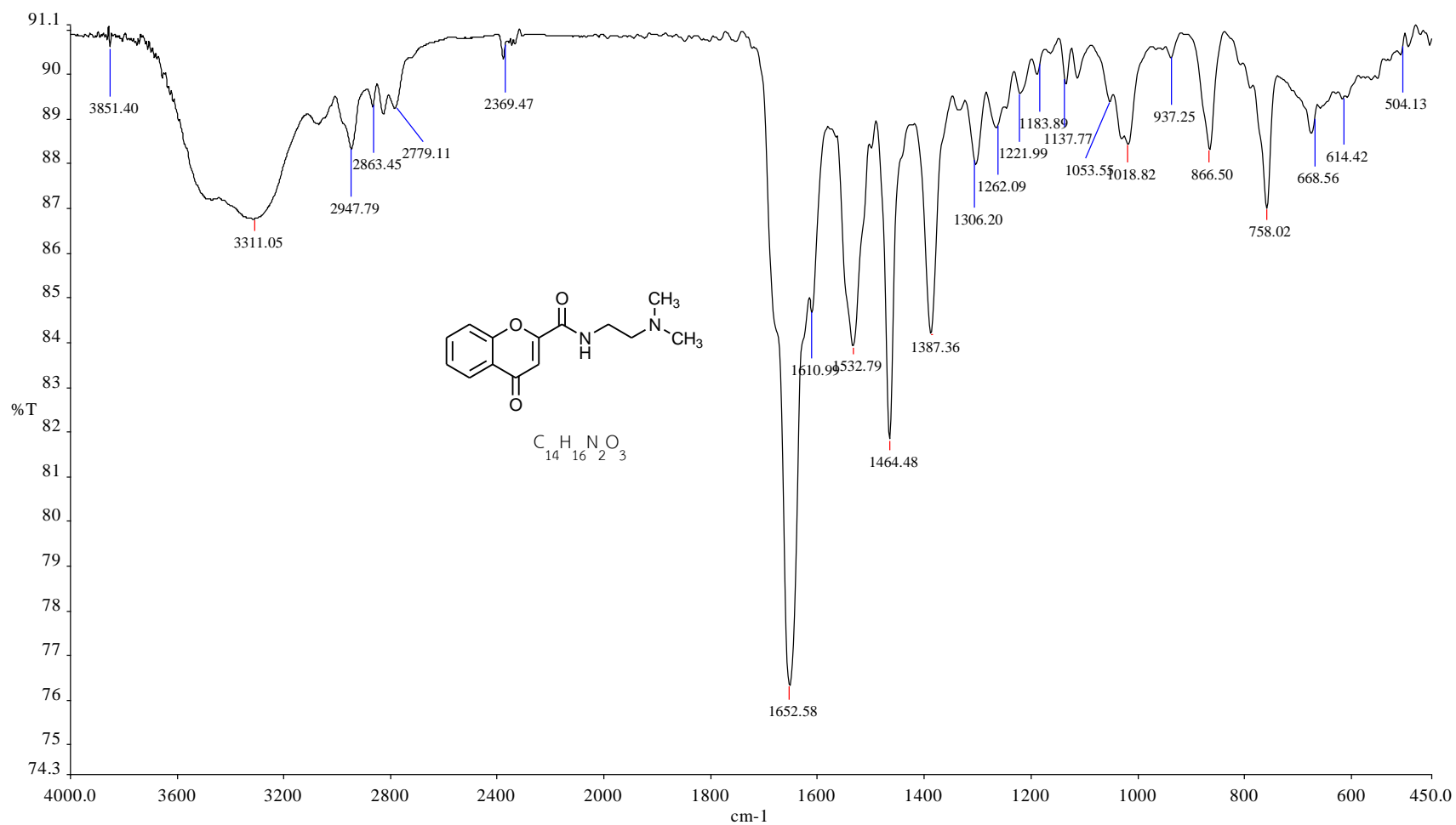


Figure 46. The IR spectrum of *N*-(2-(dimethylamino)ethyl)-4-oxo-4*H*-chromene-2-carboxamide (**7**)

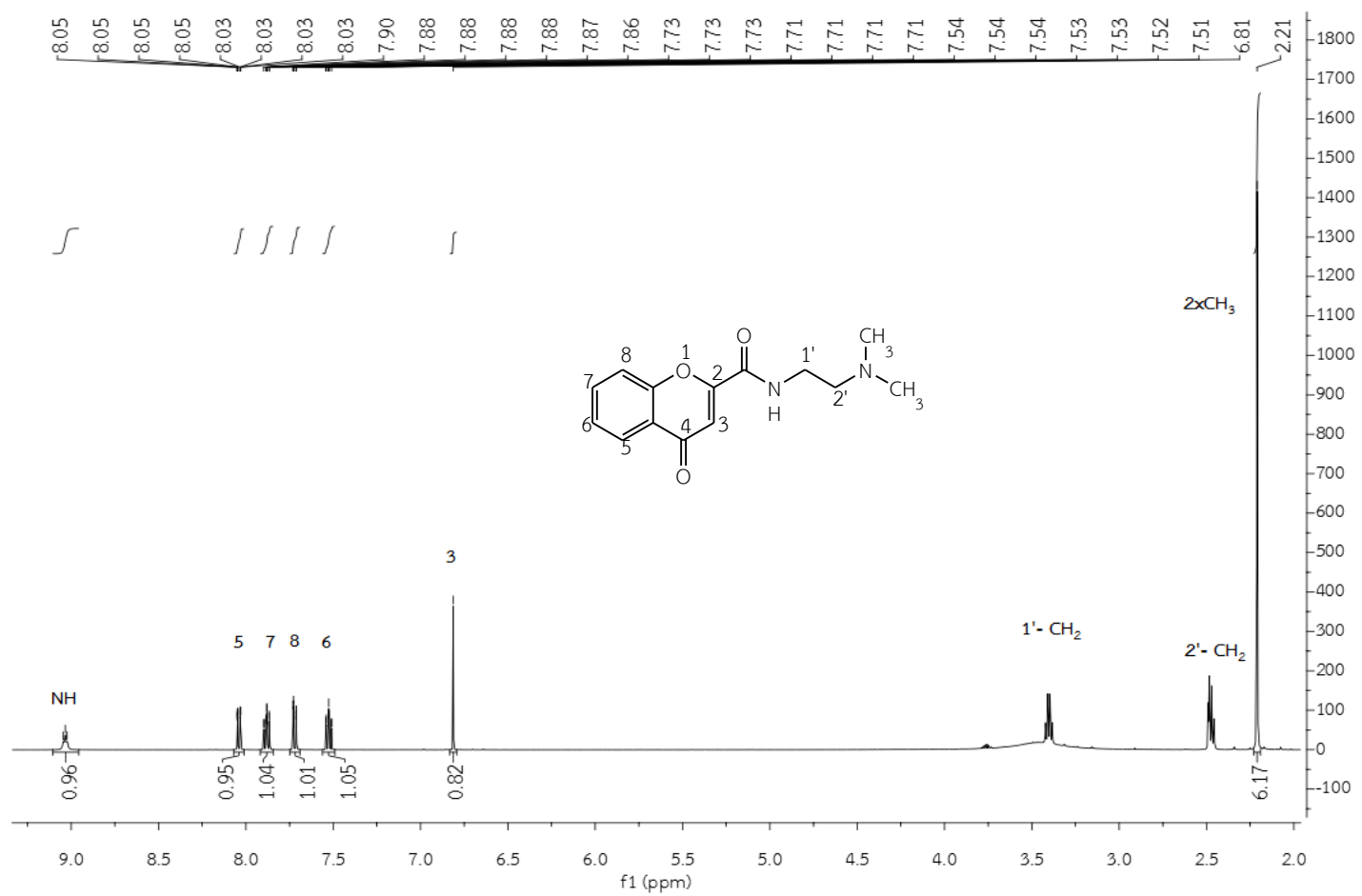


Figure 47. The ¹H-NMR spectrum of *N*-(2-(dimethylamino)ethyl)-4-oxo-4*H*-chromene-2-carboxamide (7) in DMSO-*d*₆

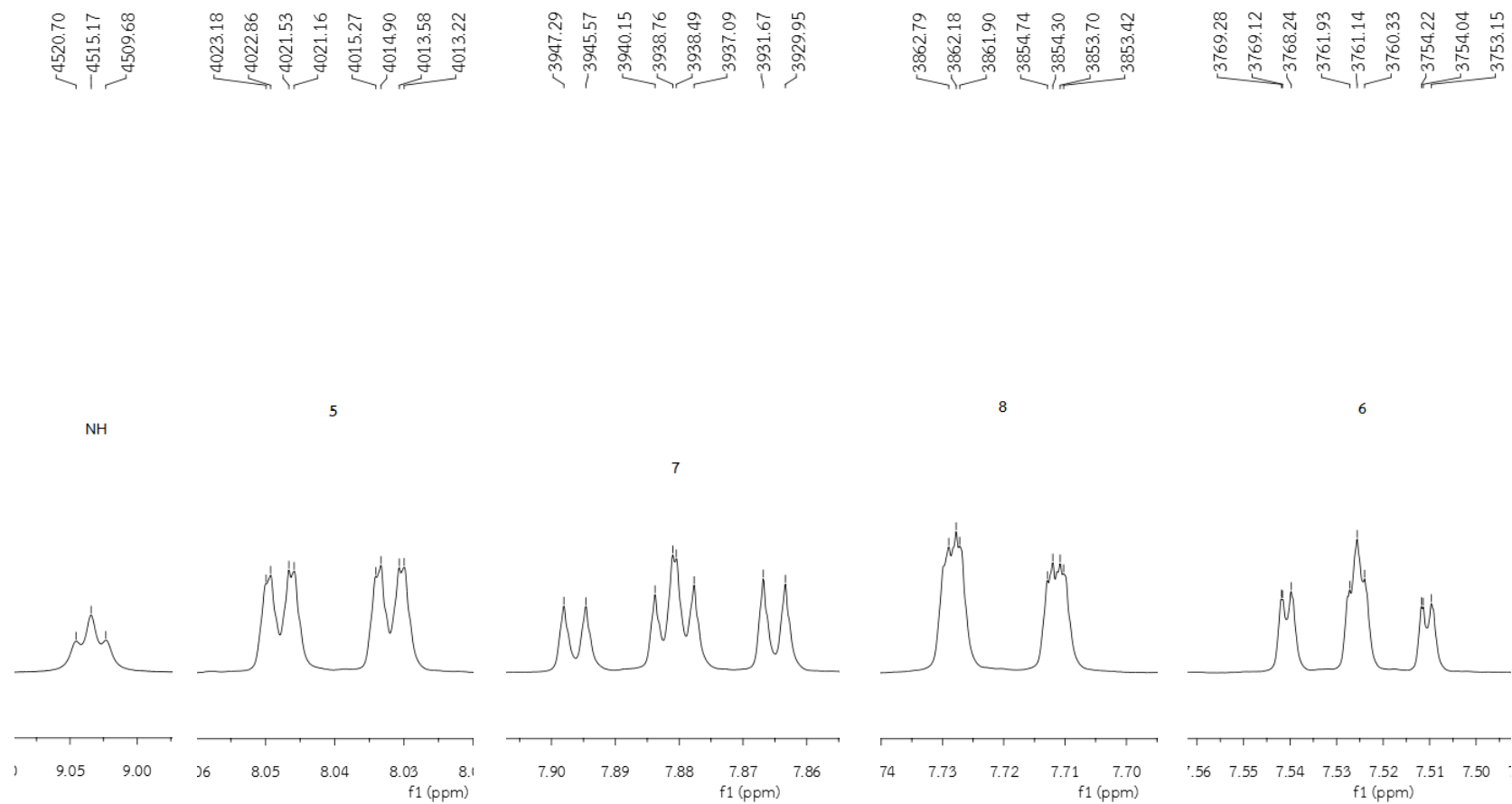


Figure 48. The ¹H-NMR spectrum of *N*-(2-(dimethylamino)ethyl)-4-oxo-4*H*-chromene-2-carboxamide (**7**) in DMSO-*d*₆ (Enlarged scale)

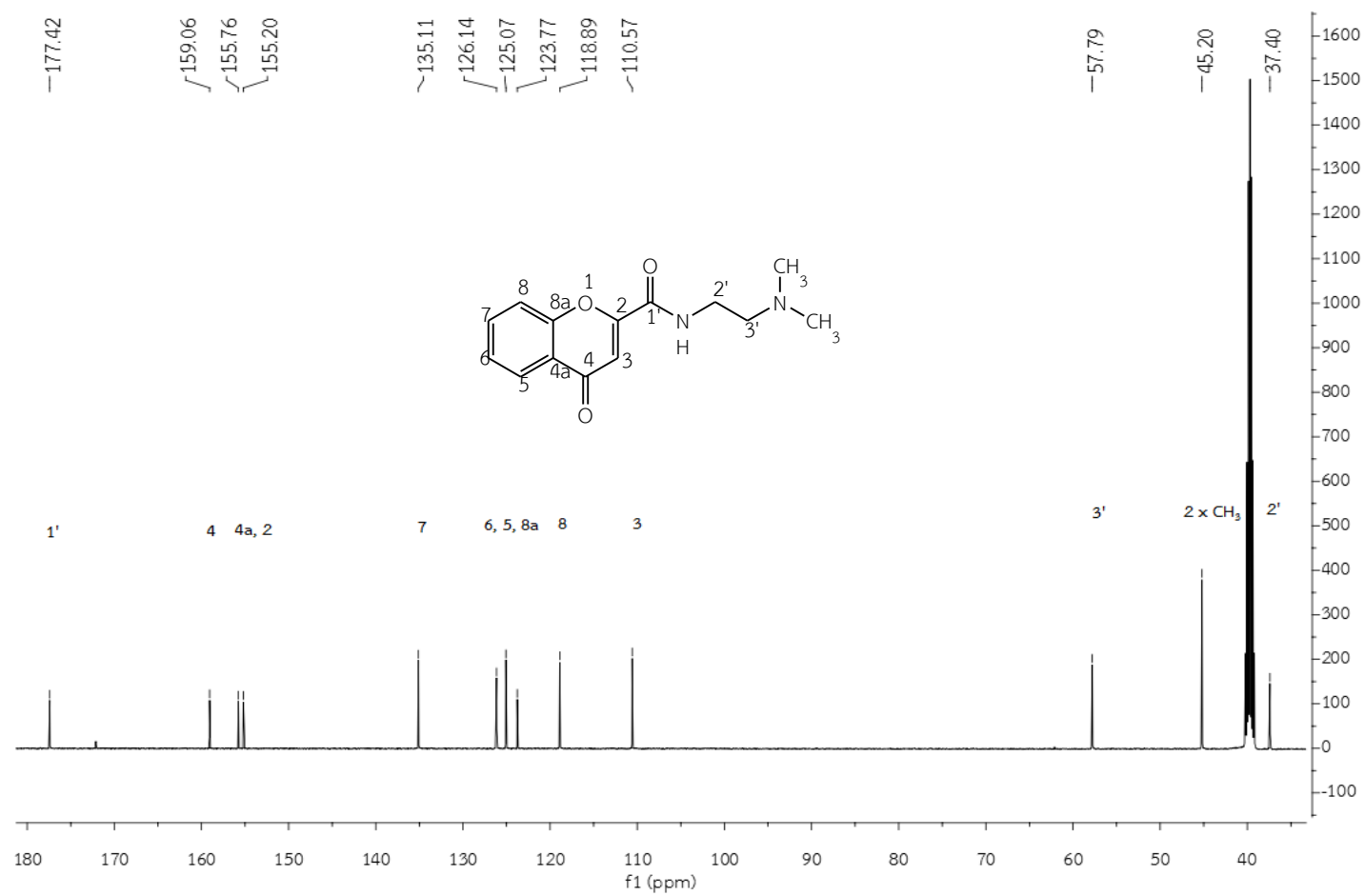


Figure 49. The ¹³C-NMR spectrum of *N*-(2-(dimethylamino)ethyl)-4-oxo-4*H*-chromene-2-carboxamide (7) in DMSO-*d*₆

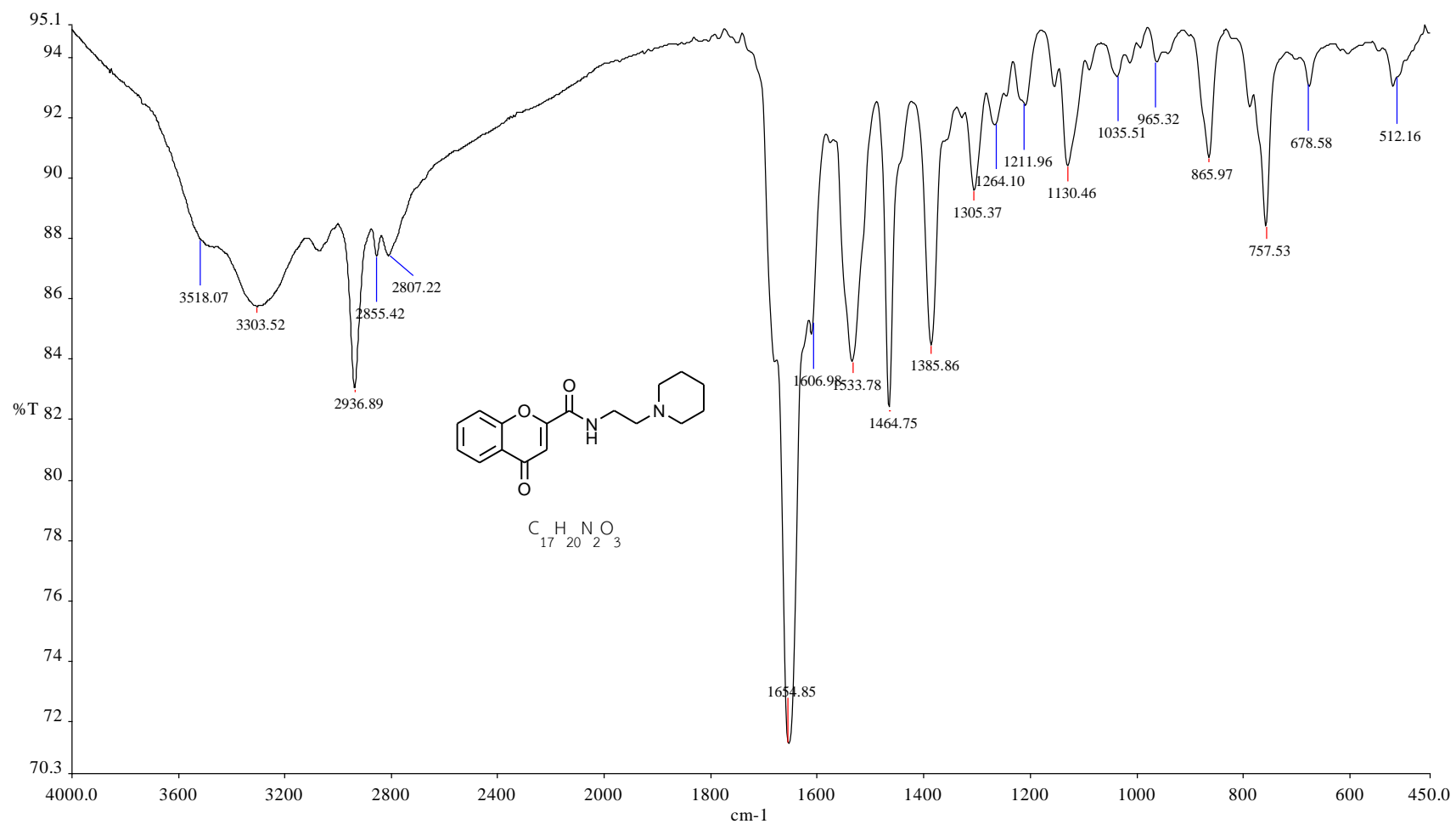


Figure 50. The IR spectrum of 4-oxo-N-(2-(piperidin-1-yl)ethyl)-4H-chromene-2-carboxamide (**8**)

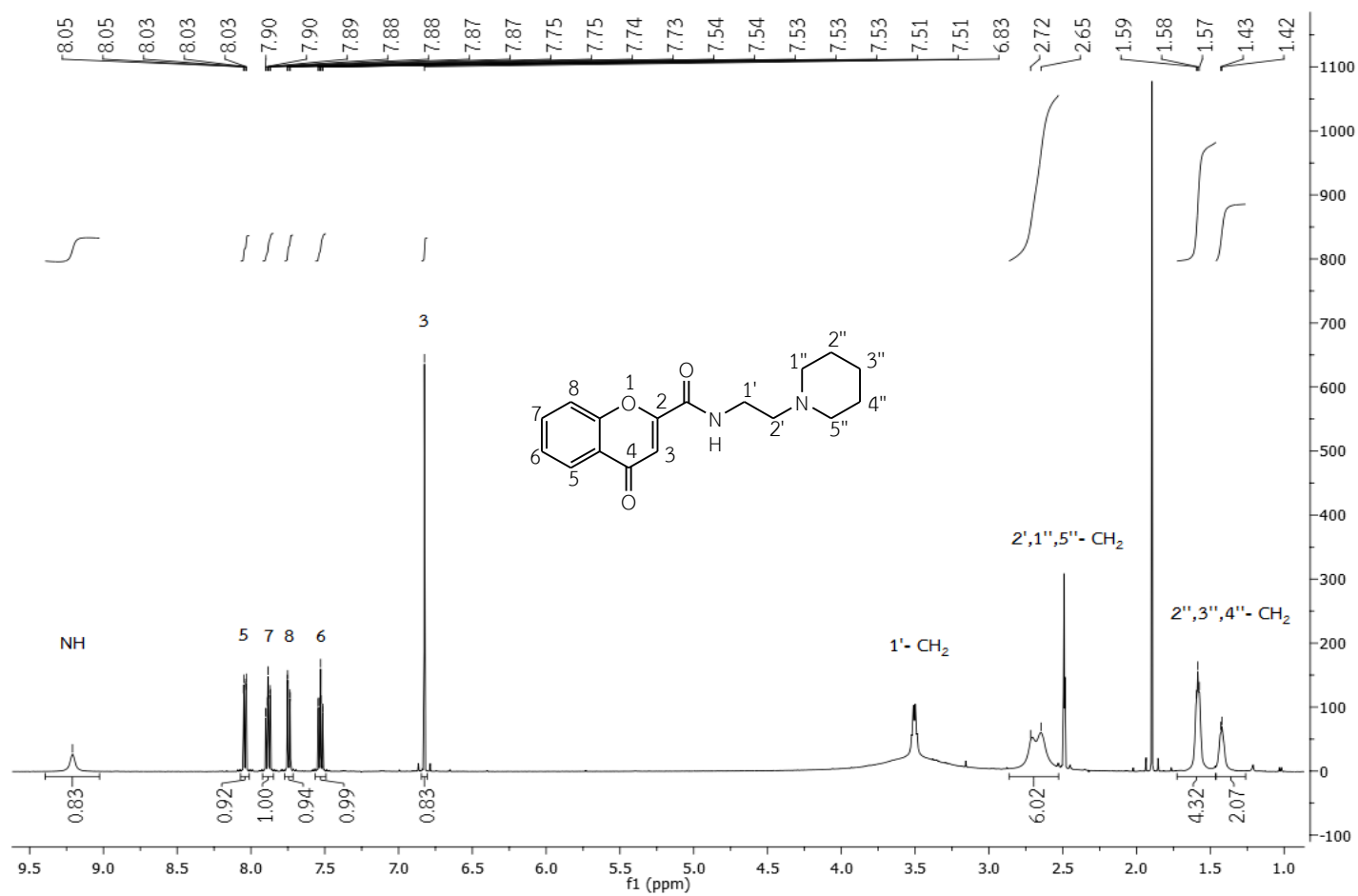


Figure 51. The ¹H-NMR spectrum of 4-oxo-N-(2-(piperidin-1-yl)ethyl)-4H-chromene-2-carboxamide (**8**) in DMSO-*d*₆

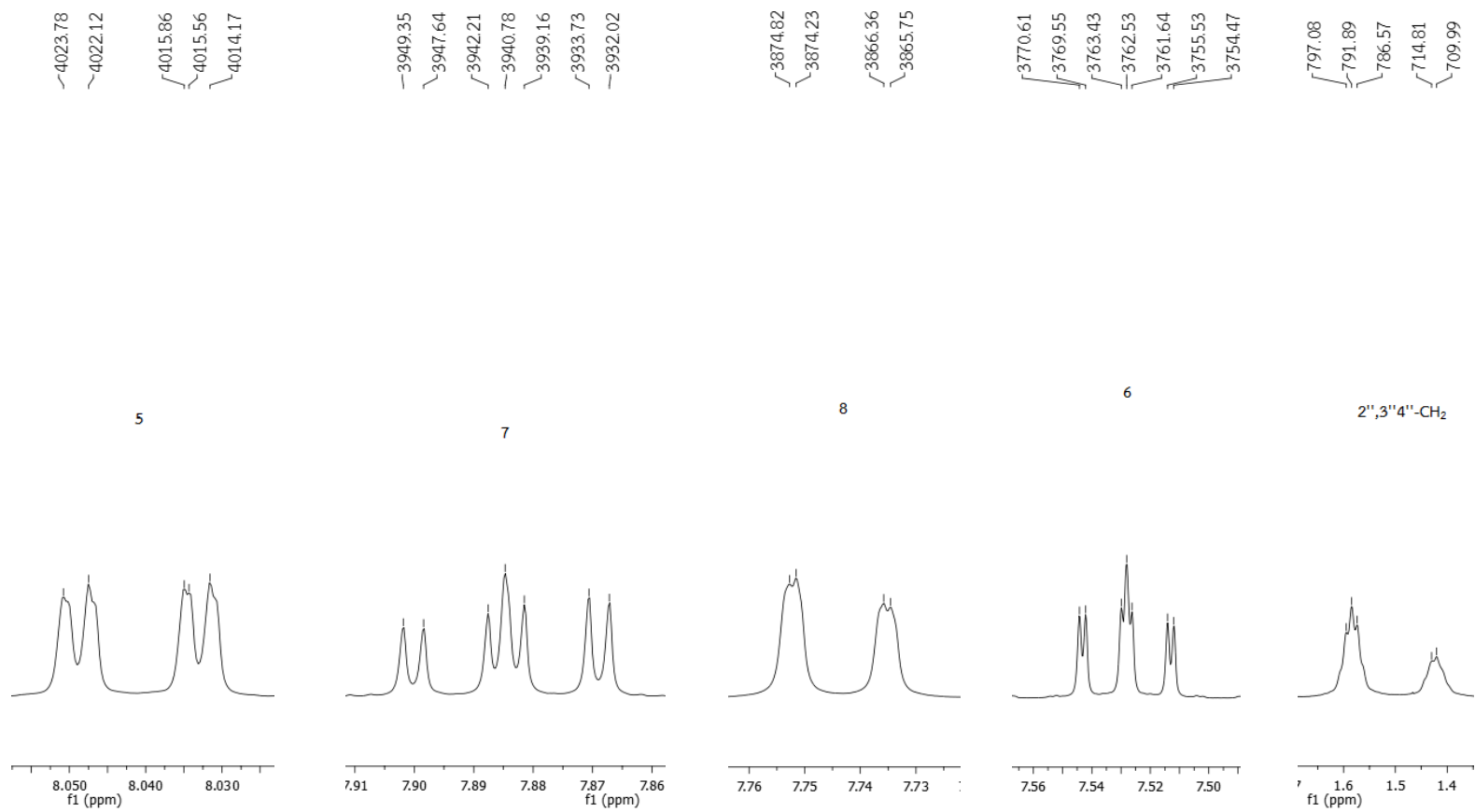


Figure 52. The ¹H-NMR spectrum of 4-oxo-*N*-(2-(piperidin-1-yl)ethyl)-4*H*-chromene-2-carboxamide (**8**) in DMSO-*d*₆ (Enlarged scale)

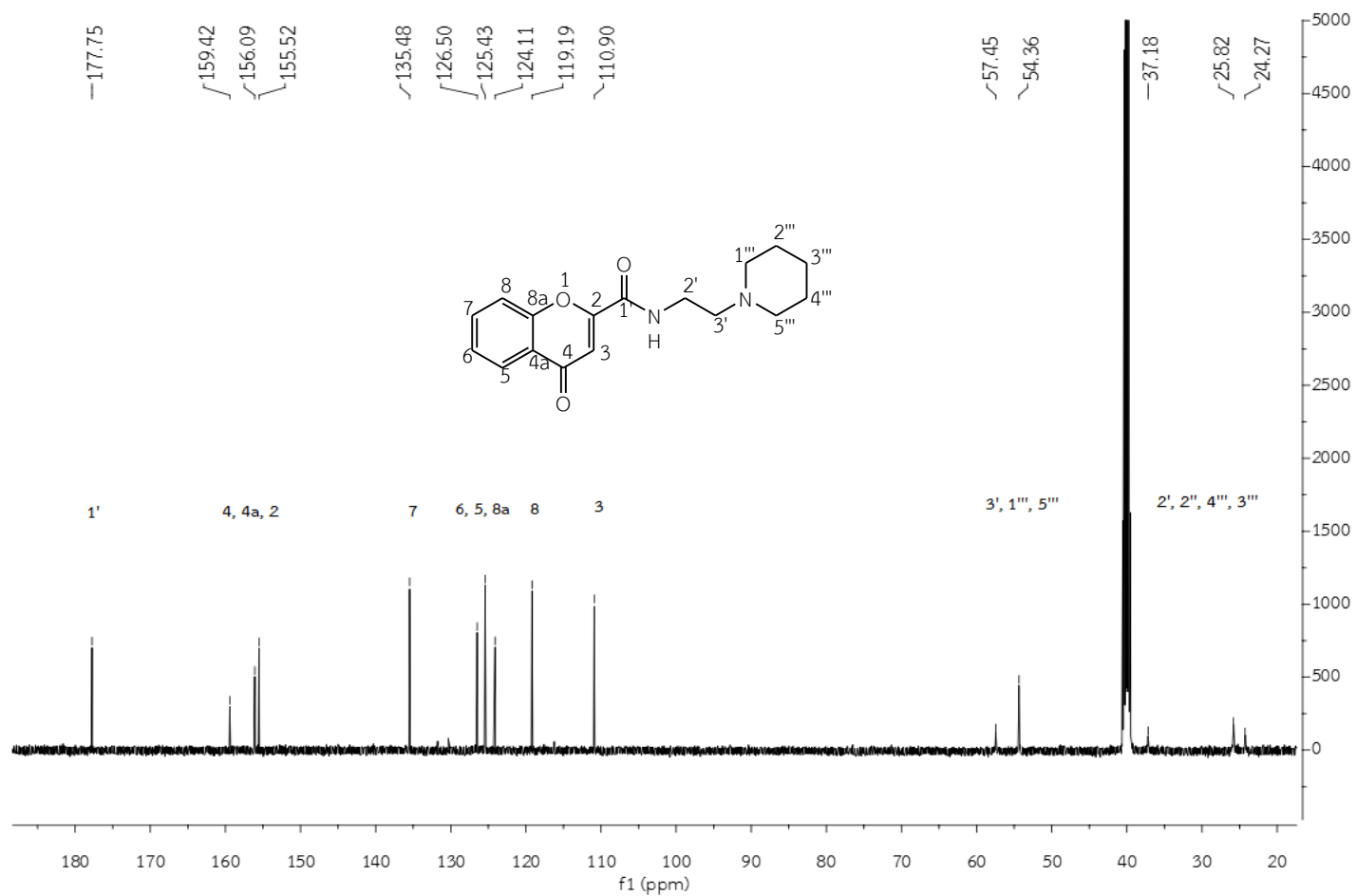


Figure 53. The ^{13}C -NMR spectrum of 4-oxo-*N*-(2-(piperidin-1-yl)ethyl)-4*H*-chromene-2-carboxamide (**8**) in $\text{DMSO-}d_6$

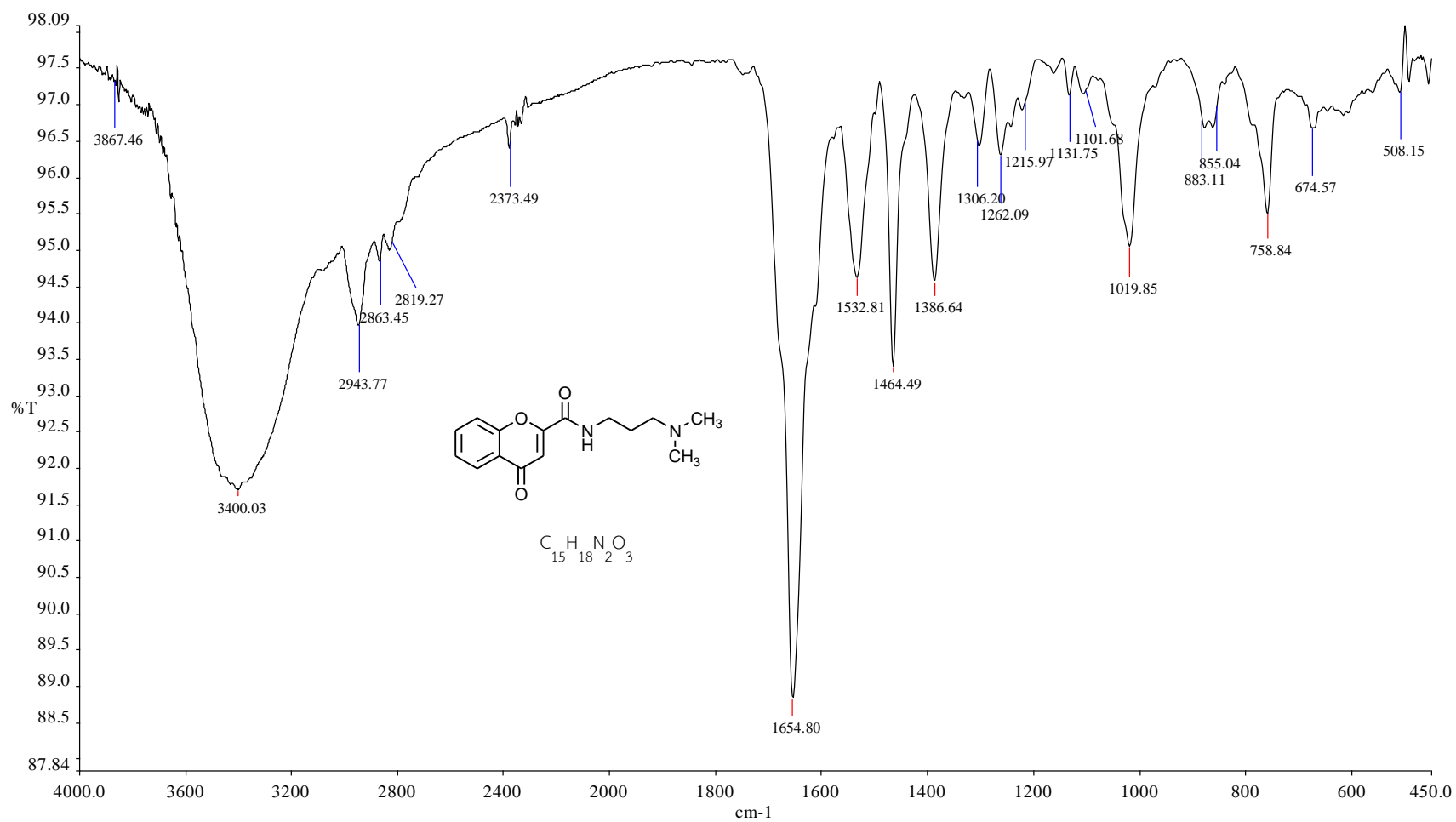


Figure 54. The IR spectrum of *N*-(3-(dimethylamino)propyl)-4-oxo-4*H*-chromene-2-carboxamide (9)

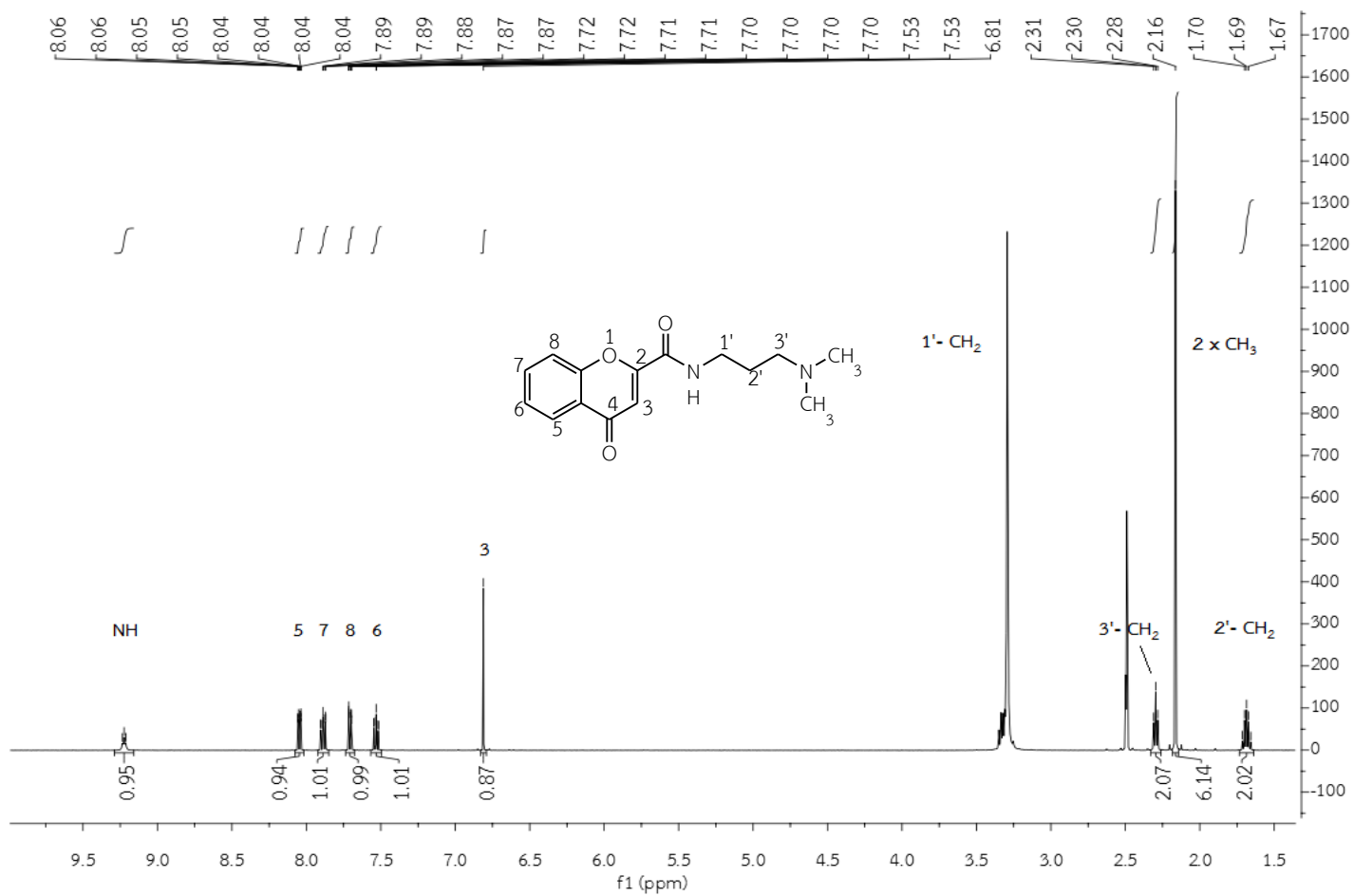


Figure 55. The $^1\text{H-NMR}$ spectrum of *N*-(3-(dimethylamino)propyl)-4-oxo-4*H*-chromene-2-carboxamide (**9**) in $\text{DMSO-}d_6$

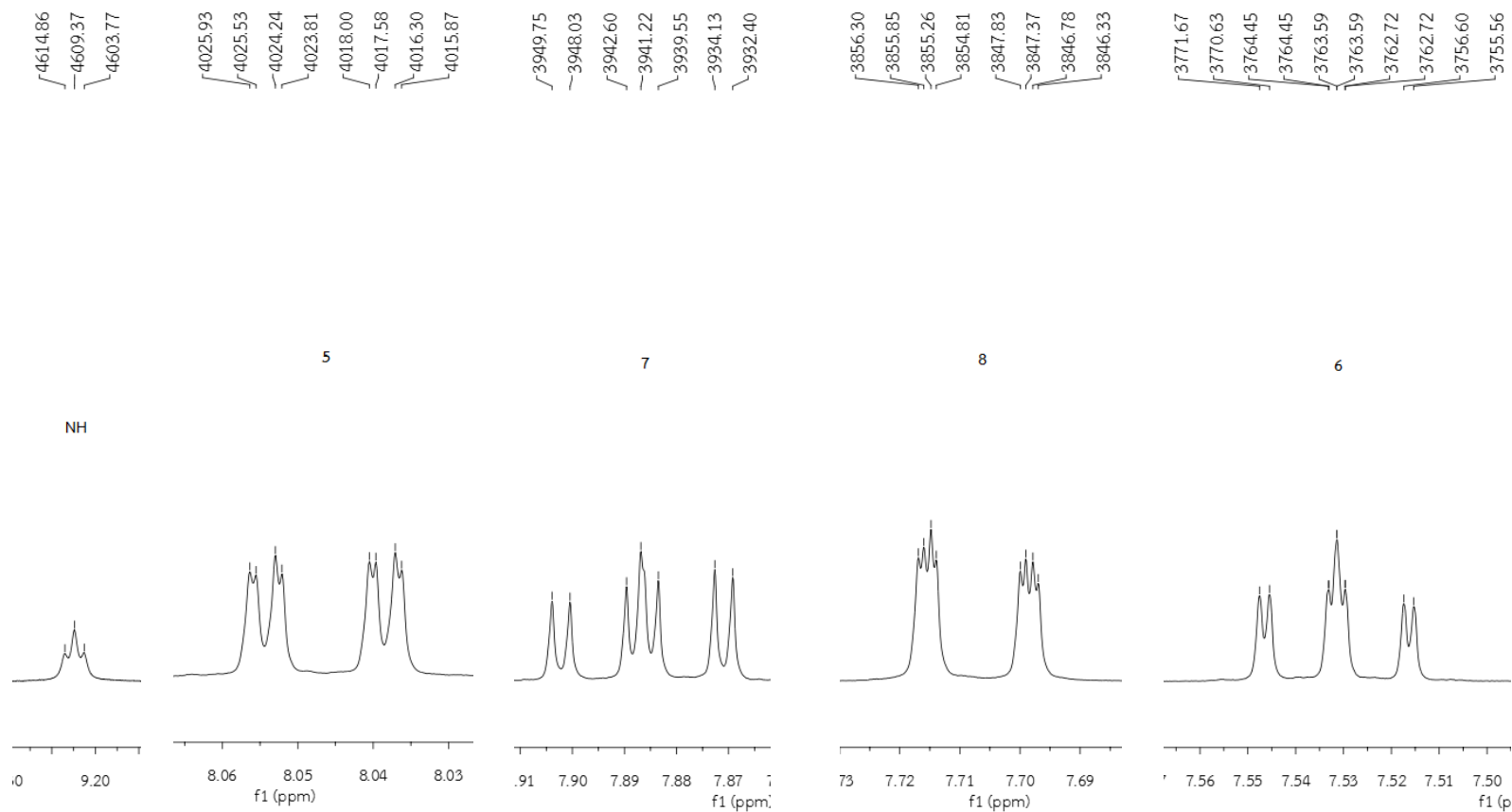


Figure 56. The ^1H -NMR spectrum of *N*-(3-(dimethylamino)propyl)-4-oxo-4*H*-chromene-2-carboxamide (**9**) in $\text{DMSO-}d_6$ (Enlarged scale)

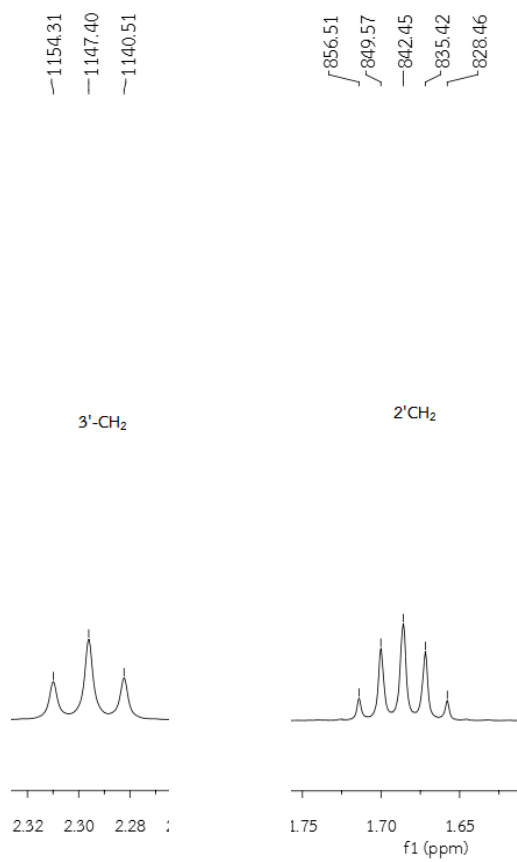


Figure 57. The ¹H-NMR spectrum of *N*-(3-(dimethylamino)propyl)-4-oxo-4*H*-chromene-2-carboxamide (**9**) in DMSO-*d*₆ (Enlarged scale)

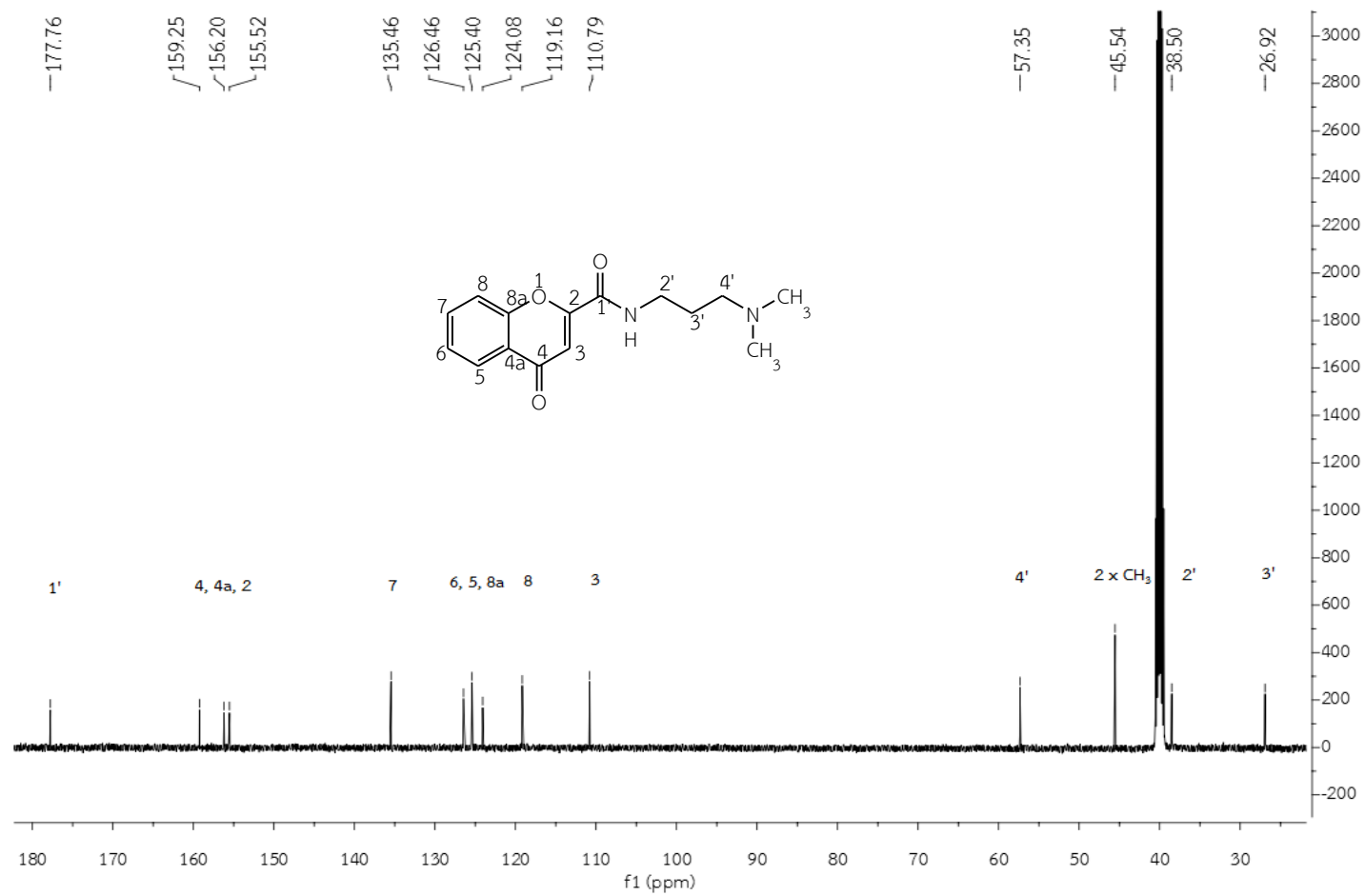


Figure 58. The ^{13}C -NMR spectrum of *N*-(3-(dimethylamino)propyl)-4-oxo-4*H*-chromene-2-carboxamide (**9**) in $\text{DMSO-}d_6$

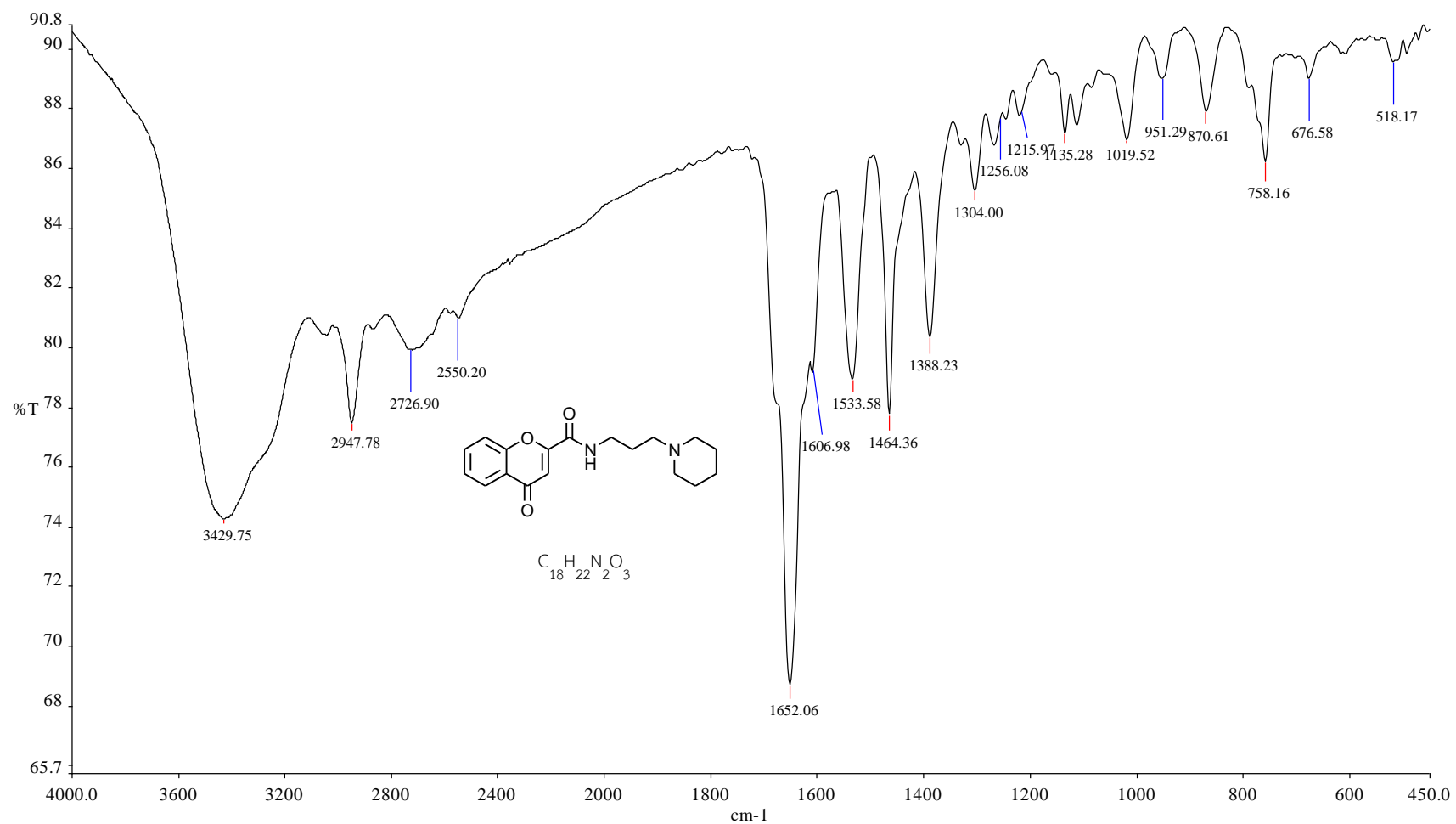


Figure 59. The IR spectrum of 4-oxo-*N*-(3-(piperidin-1-yl)propyl)-4*H*-chromene-2-carboxamide (10)

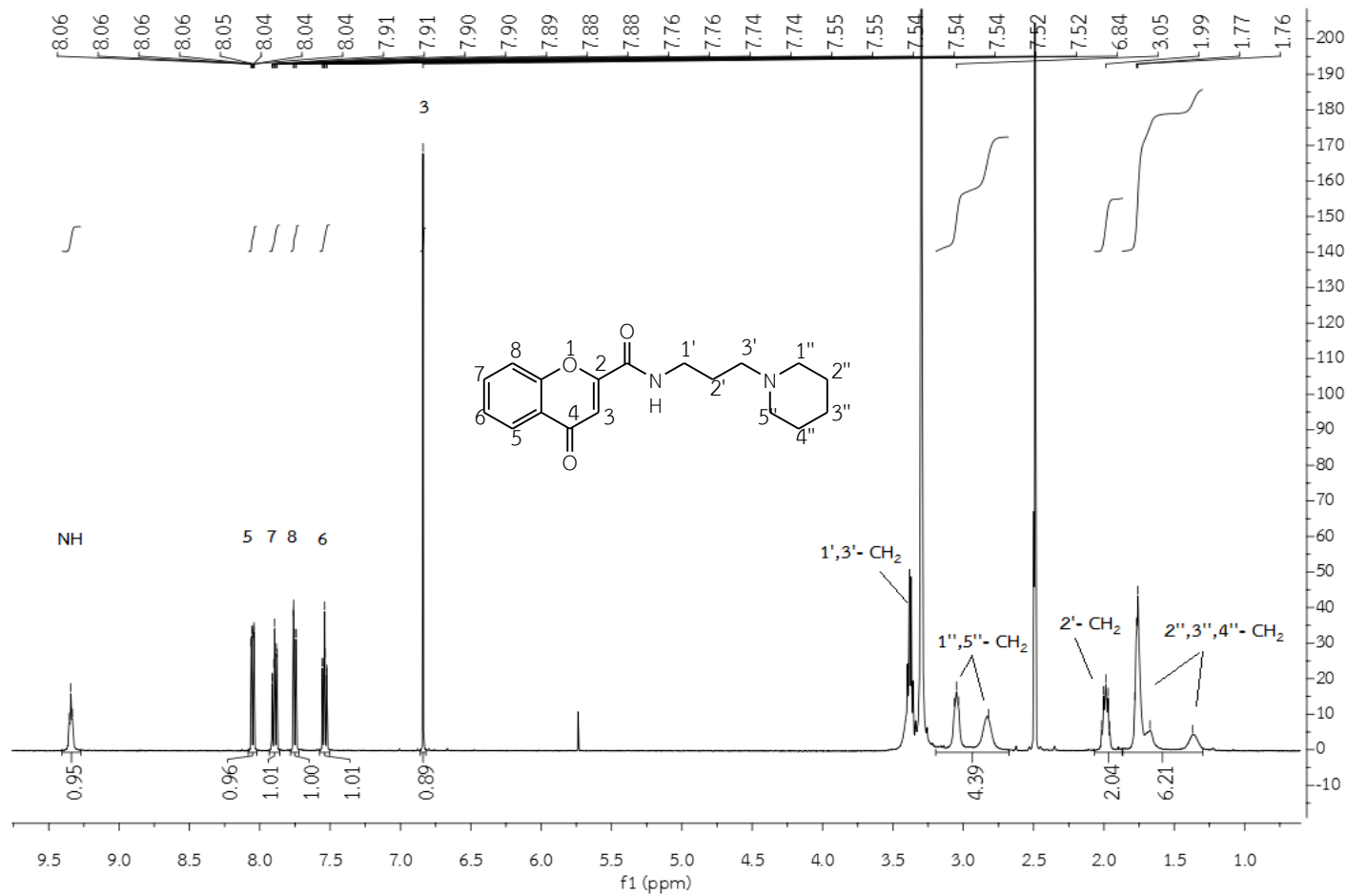


Figure 60. The $^1\text{H-NMR}$ spectrum of 4-oxo-*N*-(3-(piperidin-1-yl)propyl)-4*H*-chromene-2-carboxamide (**10**) in $\text{DMSO-}d_6$

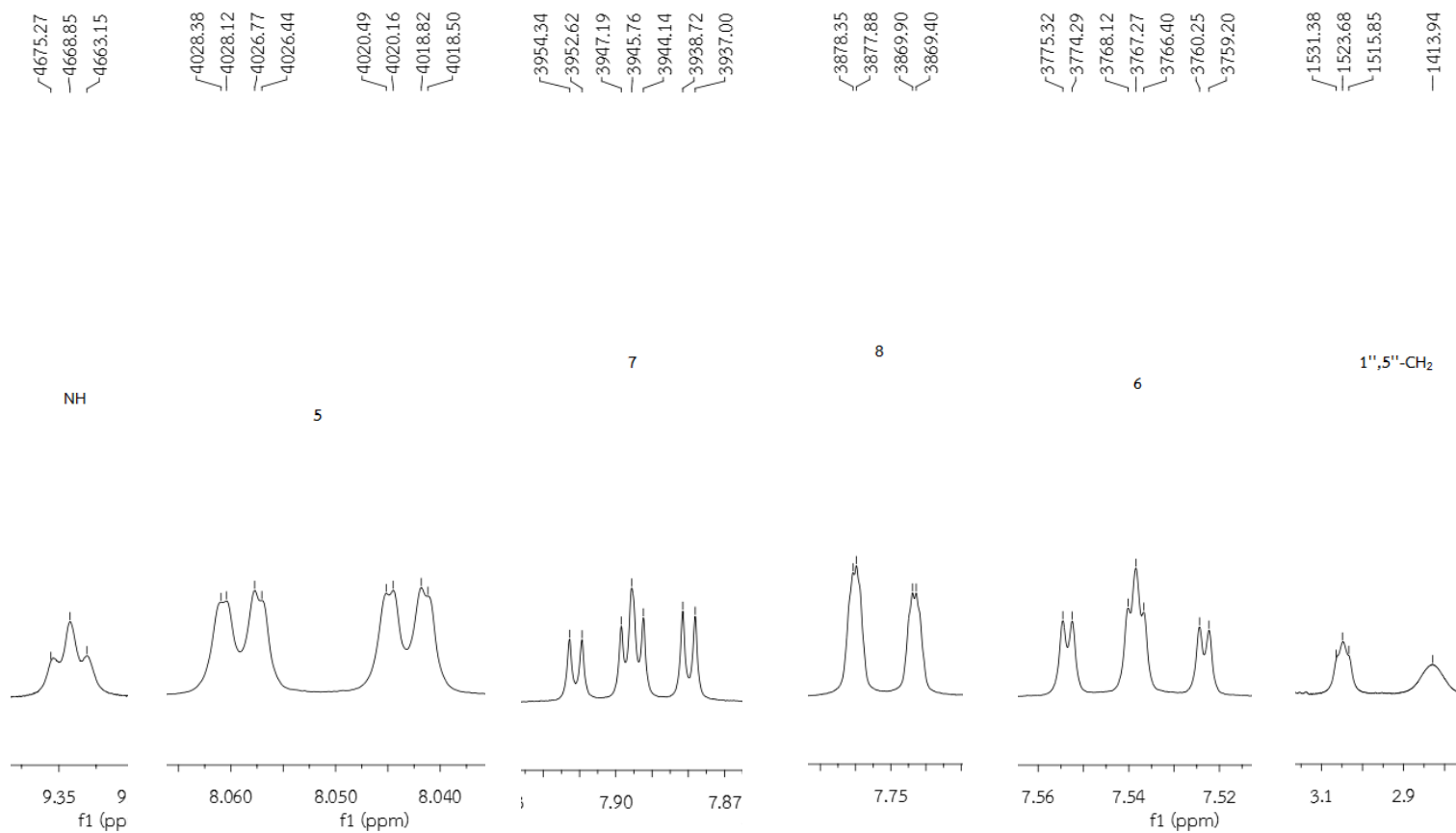


Figure 61. The ¹H-NMR spectrum of 4-oxo-*N*-(3-(piperidin-1-yl)propyl)-4*H*-chromene-2-carboxamide (**10**) in DMSO-*d*₆ (Enlarged scale)

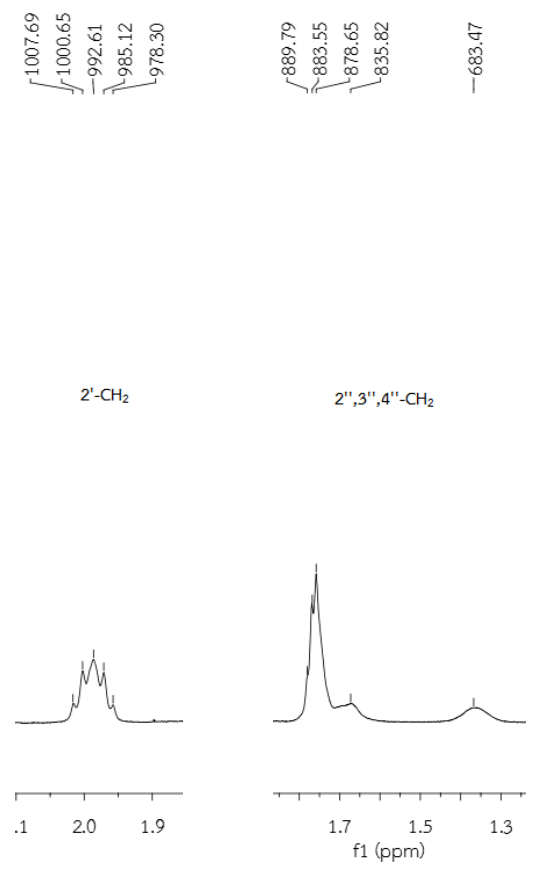


Figure 62. The ¹H-NMR spectrum of 4-oxo-*N*-(3-(piperidin-1-yl)propyl)-4*H*-chromene-2-carboxamide (**10**) in DMSO-*d*₆ (Enlarged scale)

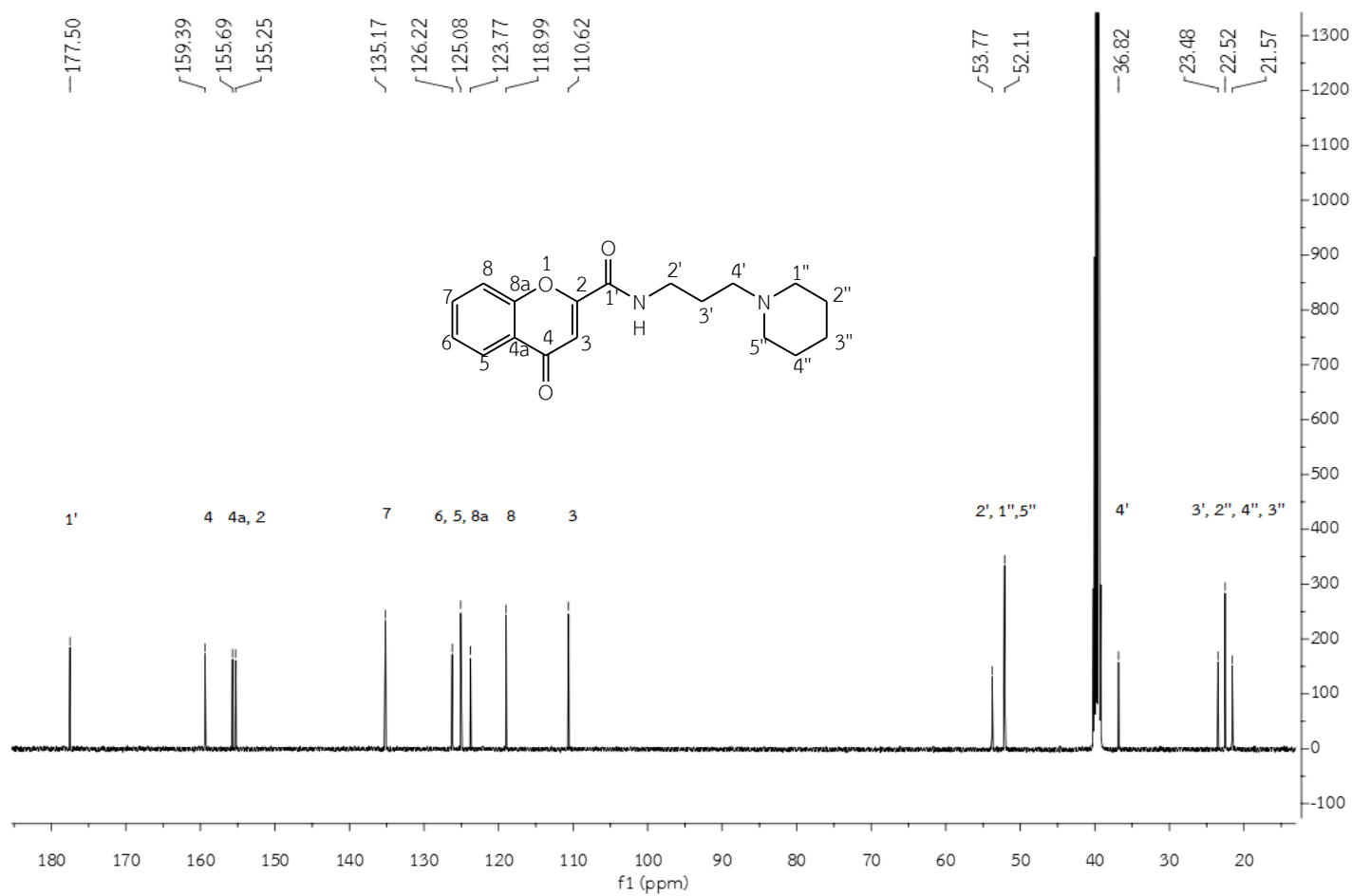


Figure 63. The ^{13}C -NMR spectrum of 4-oxo-*N*-(3-(piperidin-1-yl)propyl)-4*H*-chromene-2-carboxamide (**10**) in $\text{DMSO-}d_6$

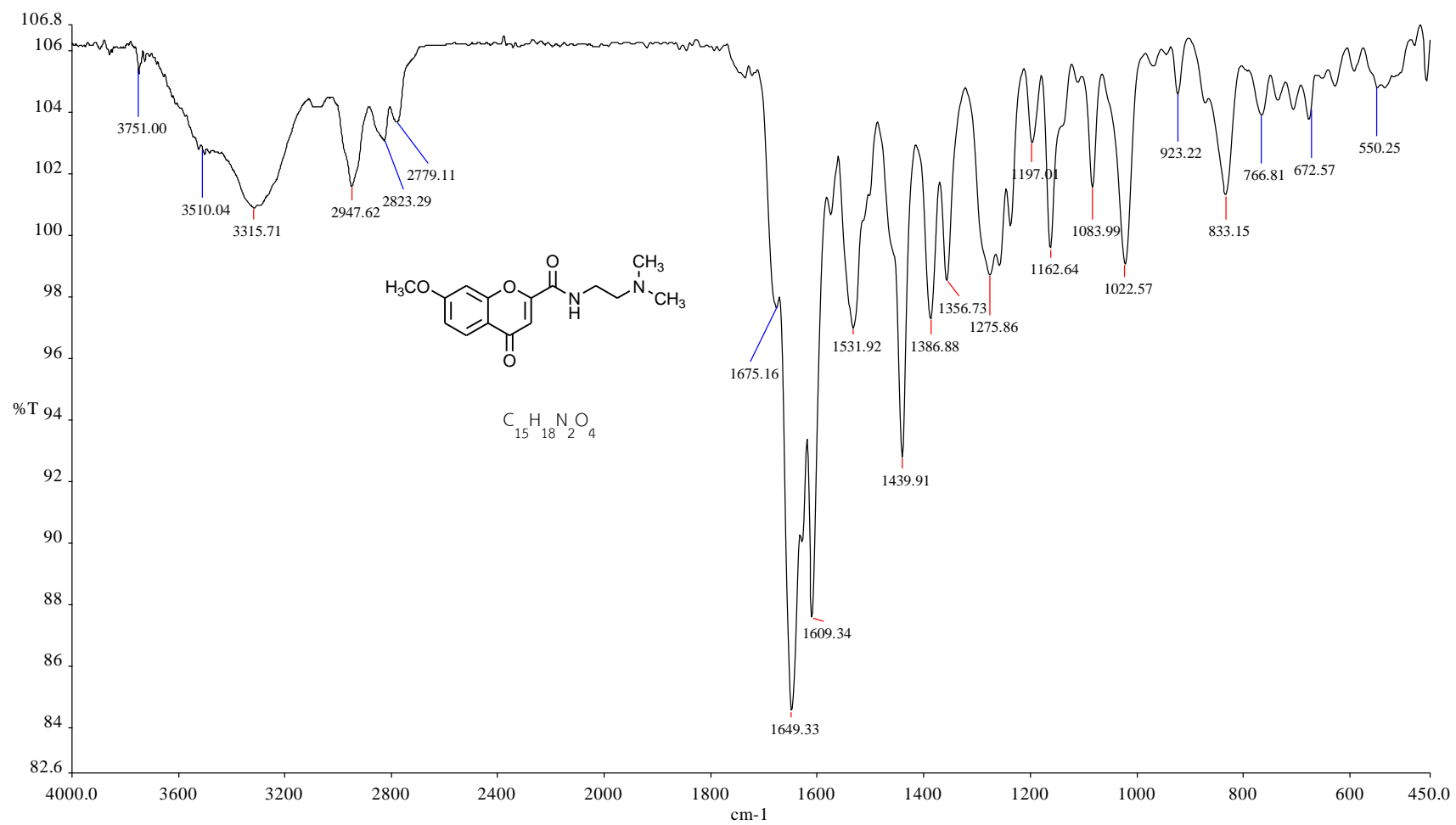


Figure 64. The IR spectrum of *N*-(2-(dimethylamino)ethyl)-7-methoxy-4-oxo-4*H*-chromene-2-carboxamide (**11**)

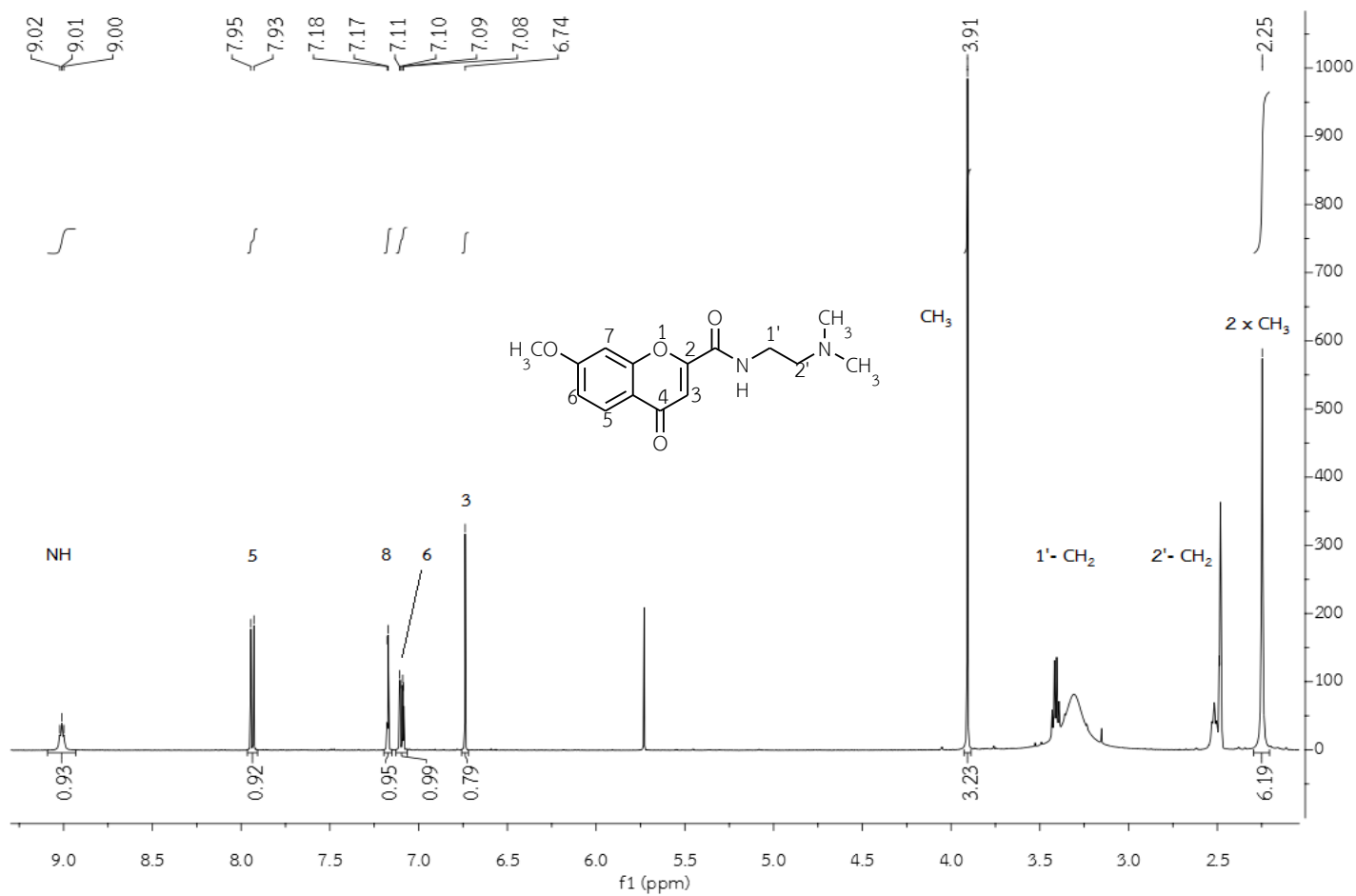


Figure 65. The ¹H-NMR spectrum of *N*-(2-(dimethylamino)ethyl)-7-methoxy-4-oxo-4*H*-chromene-2-carboxamide (**11**) in DMSO-*d*₆

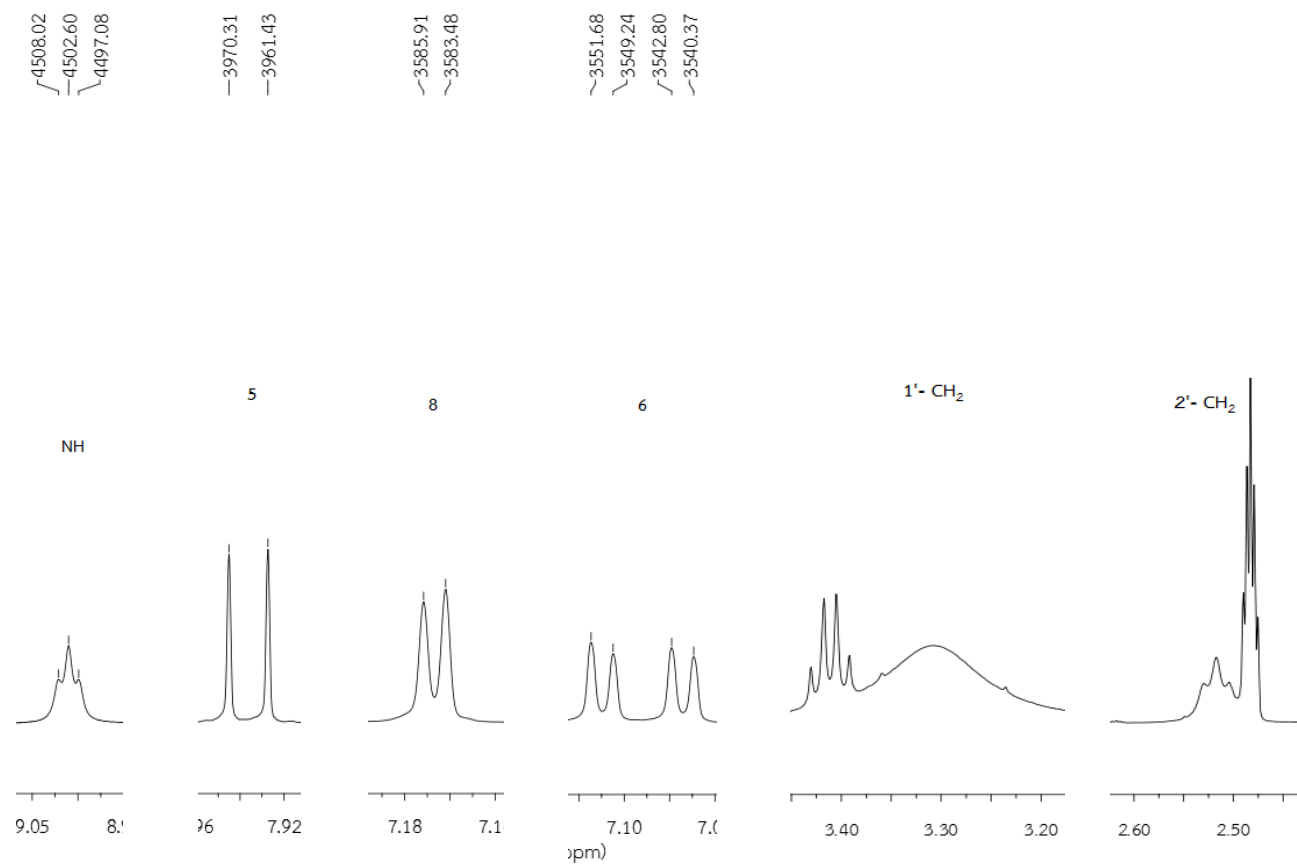


Figure 66. The ¹H-NMR spectrum of *N*-(2-(dimethylamino)ethyl)-7-methoxy-4-oxo-4*H*-chromene-2-carboxamide (**11**) in DMSO-*d*₆ (Enlarged scale)

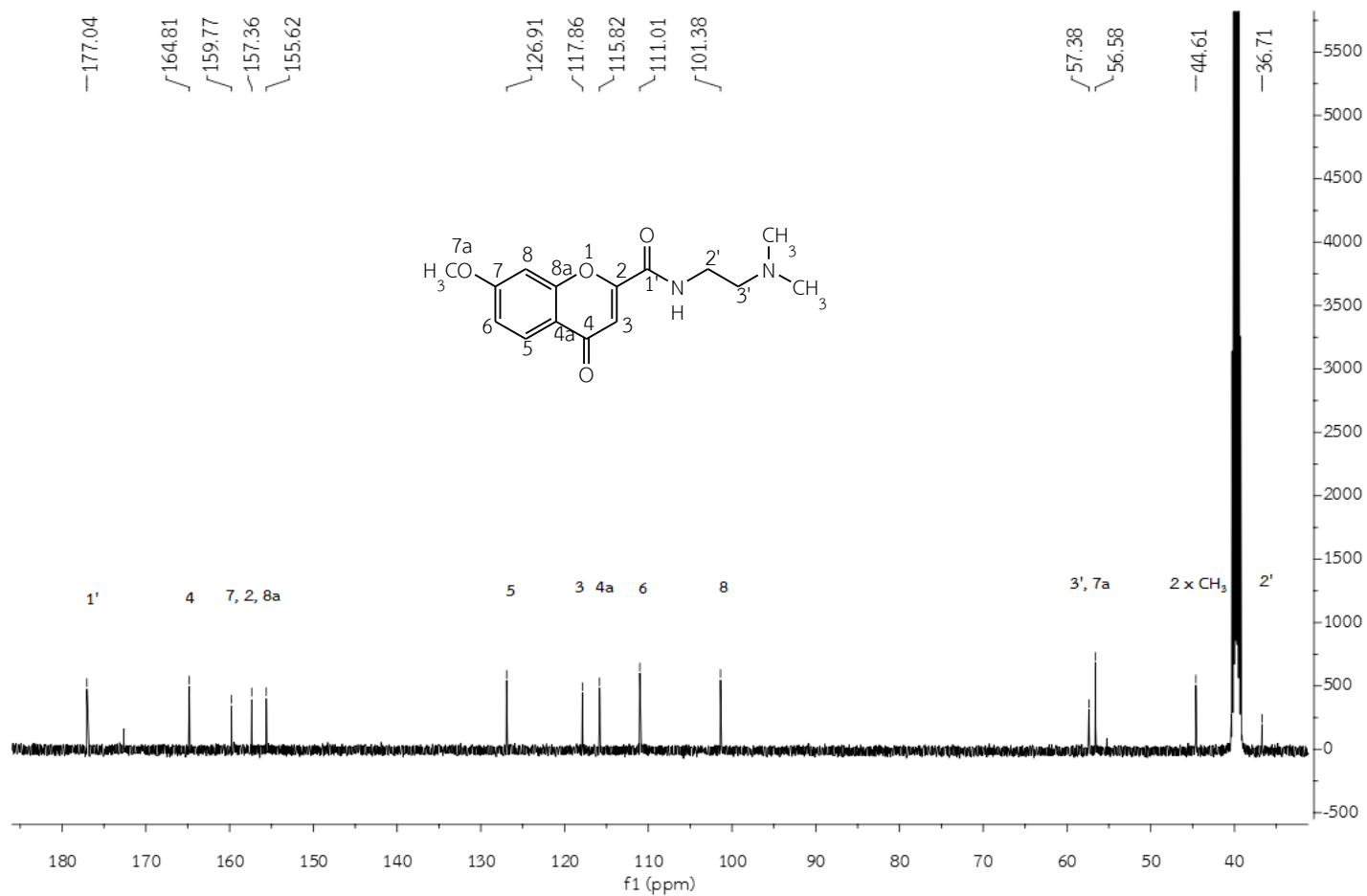


Figure 67. The ^{13}C -NMR spectrum of *N*-(2-(dimethylamino)ethyl)-7-methoxy-4-oxo-4*H*-chromene-2-carboxamide (**11**) in $\text{DMSO-}d_6$

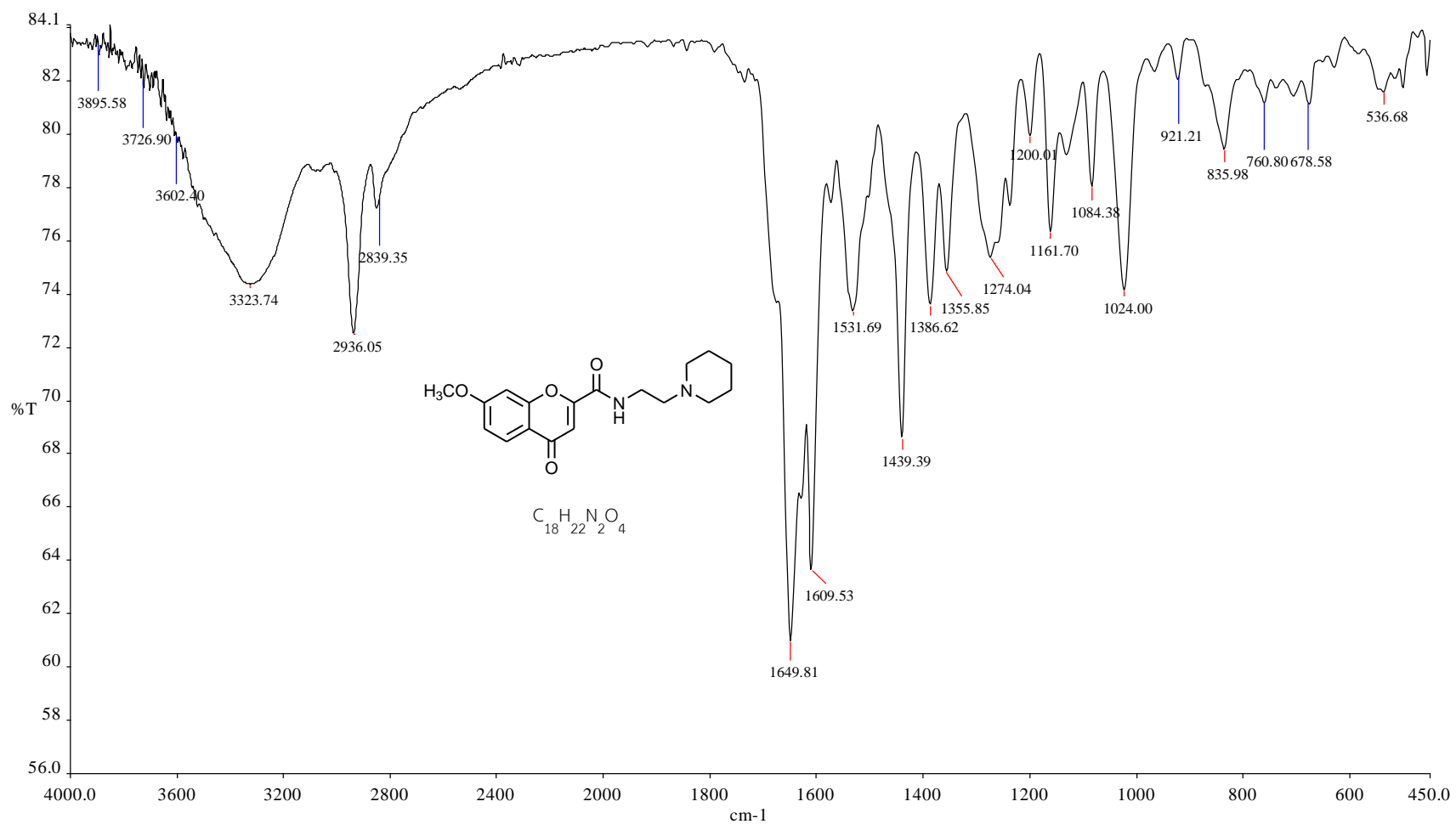


Figure 68. The IR spectrum of 7-methoxy-4-oxo-*N*-(2-(piperidin-1-yl)ethyl)-4*H*-chromene-2-carboxamide (**12**)

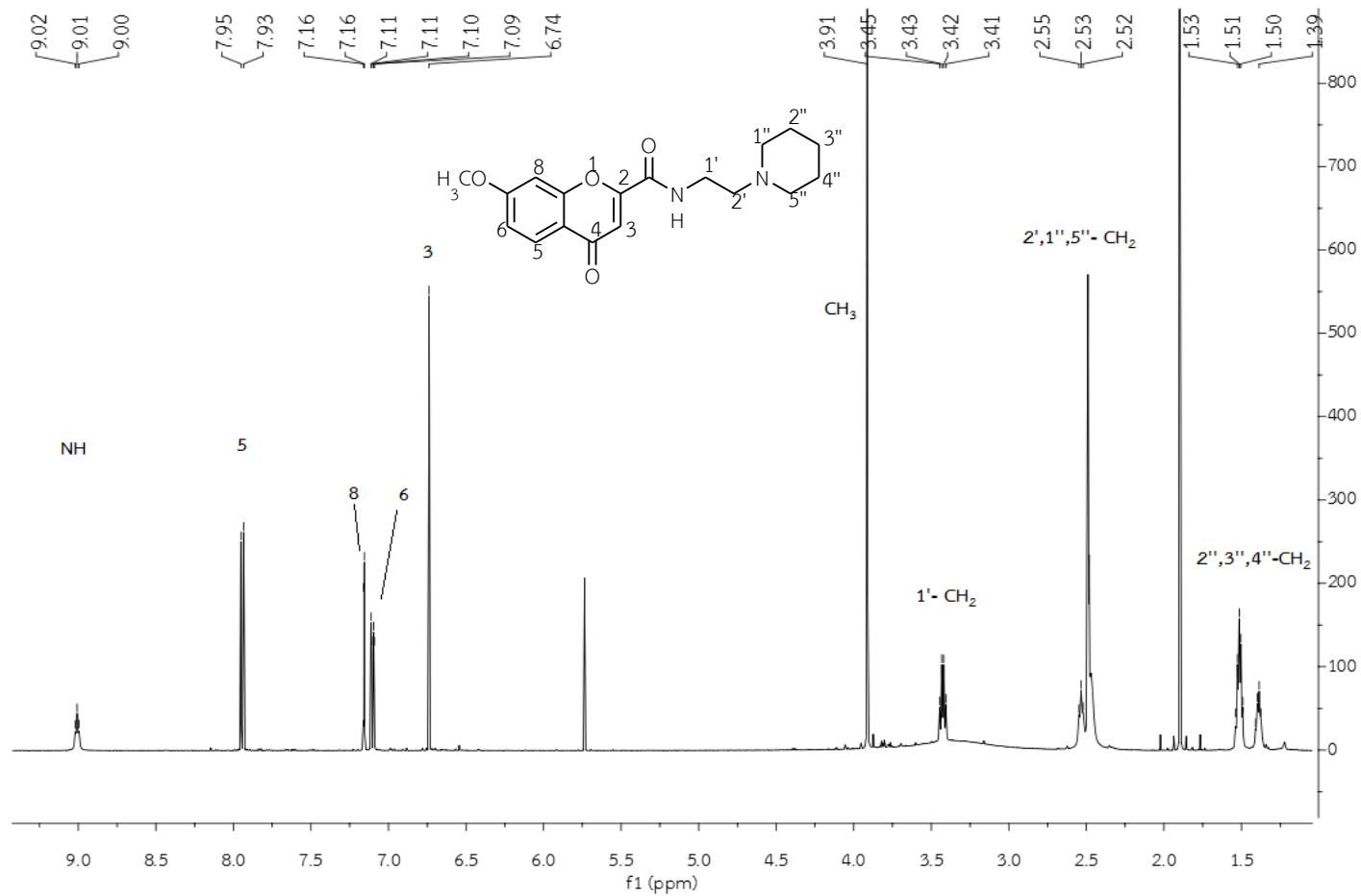


Figure 69. The ¹H-NMR spectrum of 7-methoxy-4-oxo-N-(2-(piperidin-1-yl)ethyl)-4H-chromene-2-carboxamide (**12**) in DMSO-*d*₆

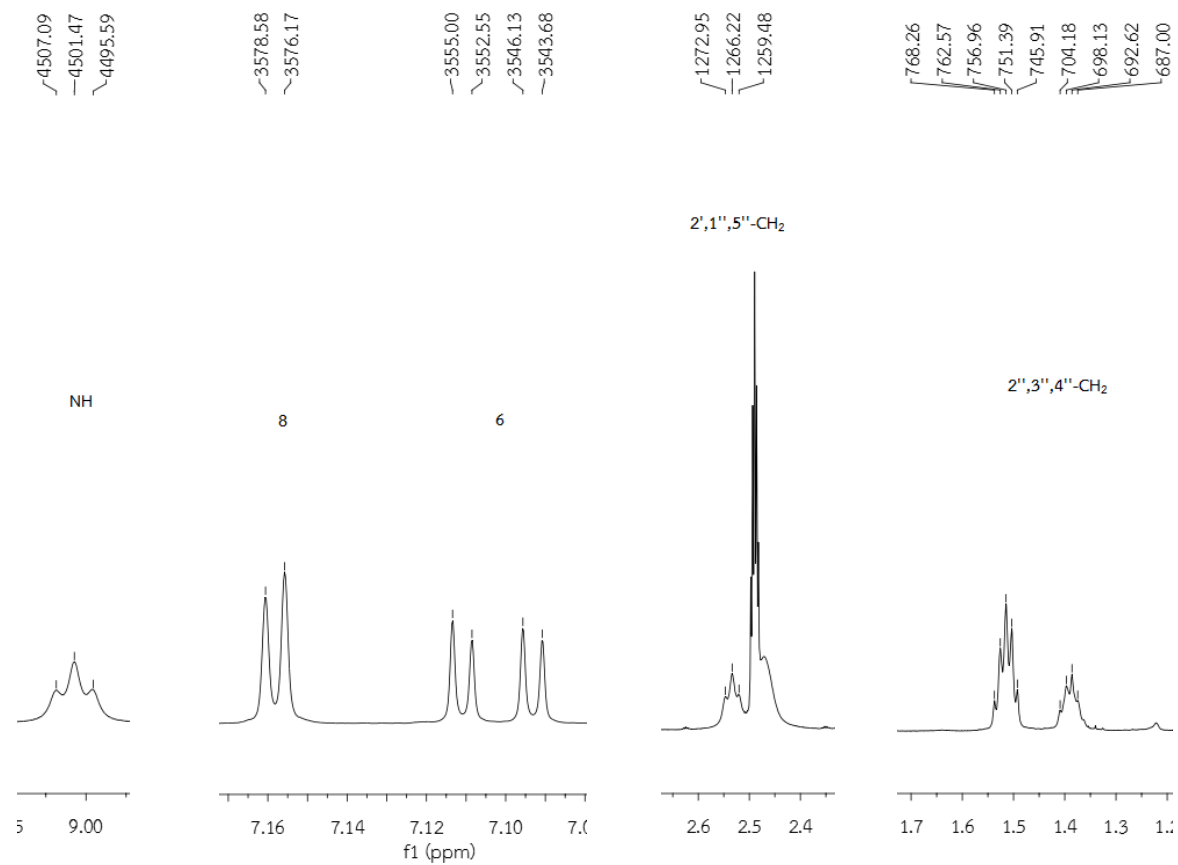


Figure 70. The ¹H-NMR spectrum of 7-methoxy-4-oxo-N-(2-(piperidin-1-yl)ethyl)-4H-chromene-2-carboxamide (**12**) in DMSO-*d*₆ (Enlarged scale)

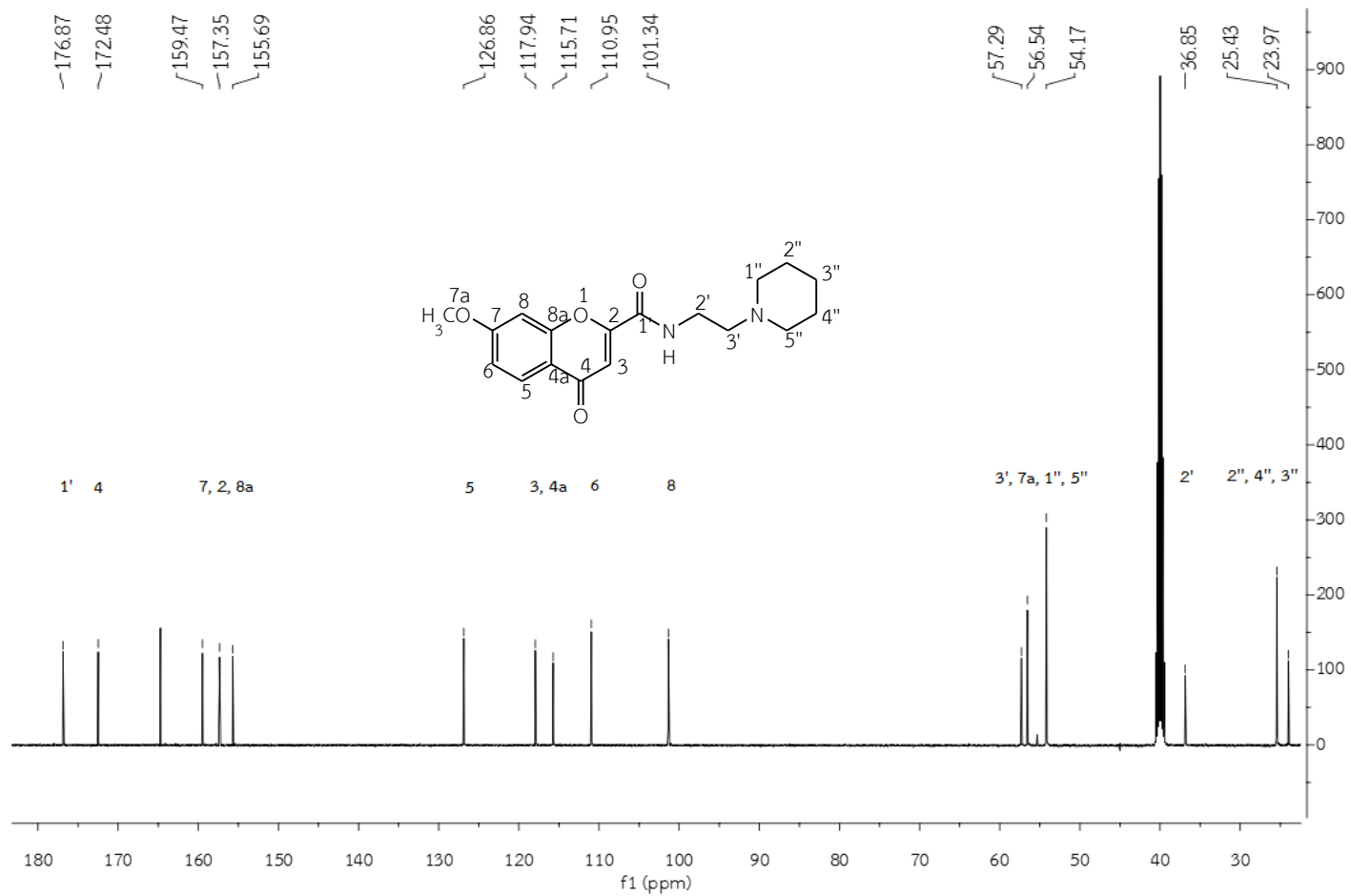


Figure 71. The ^{13}C -NMR spectrum of 7-methoxy-4-oxo-N-(2-(piperidin-1-yl)ethyl)-4H-chromene-2-carboxamide (**12**) in $\text{DMSO-}d_6$

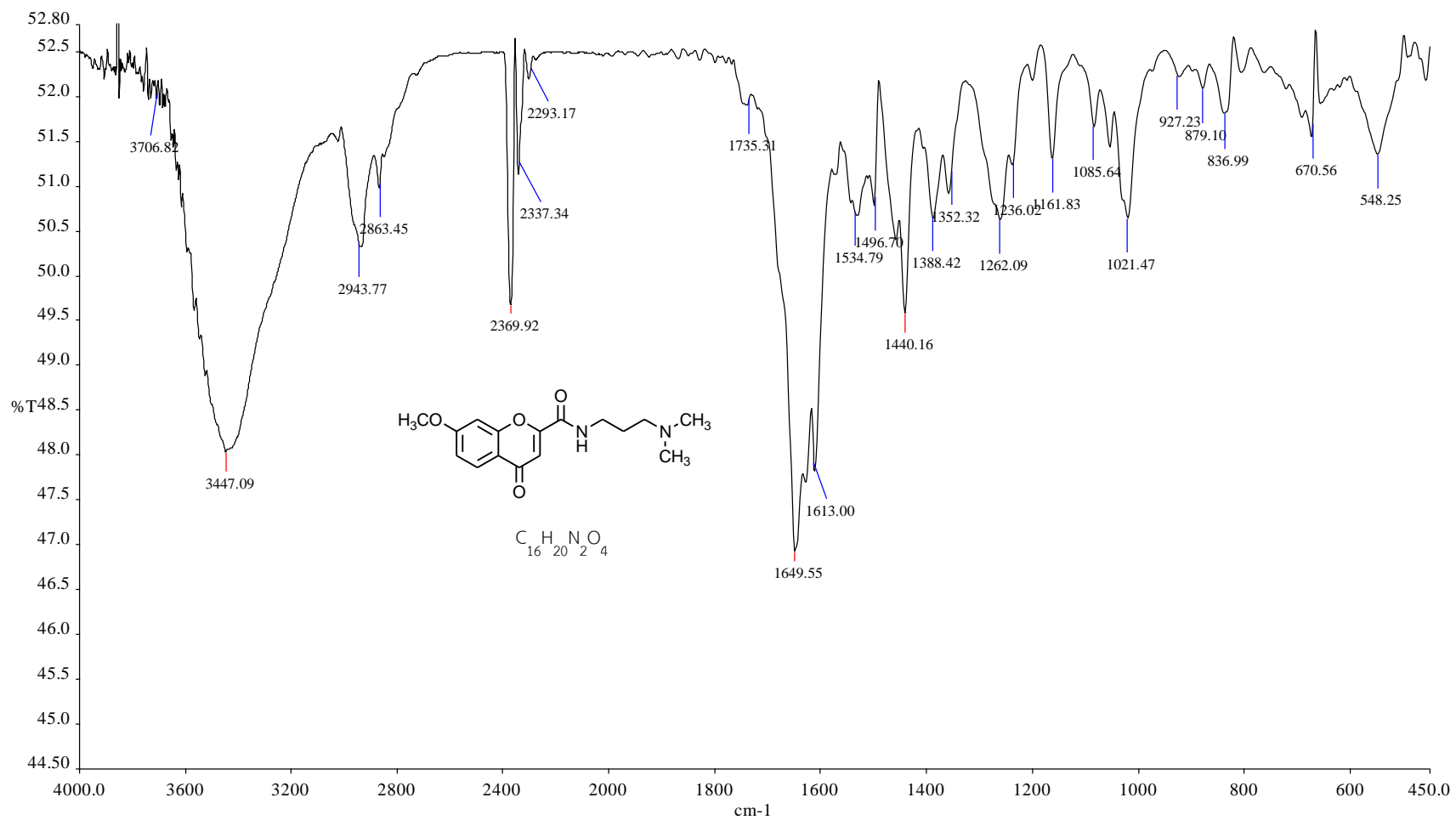


Figure 72. The IR spectrum of *N*-(3-(dimethylamino)propyl)-7-methoxy-4-oxo-4*H*-chromene-2-carboxamide (13)

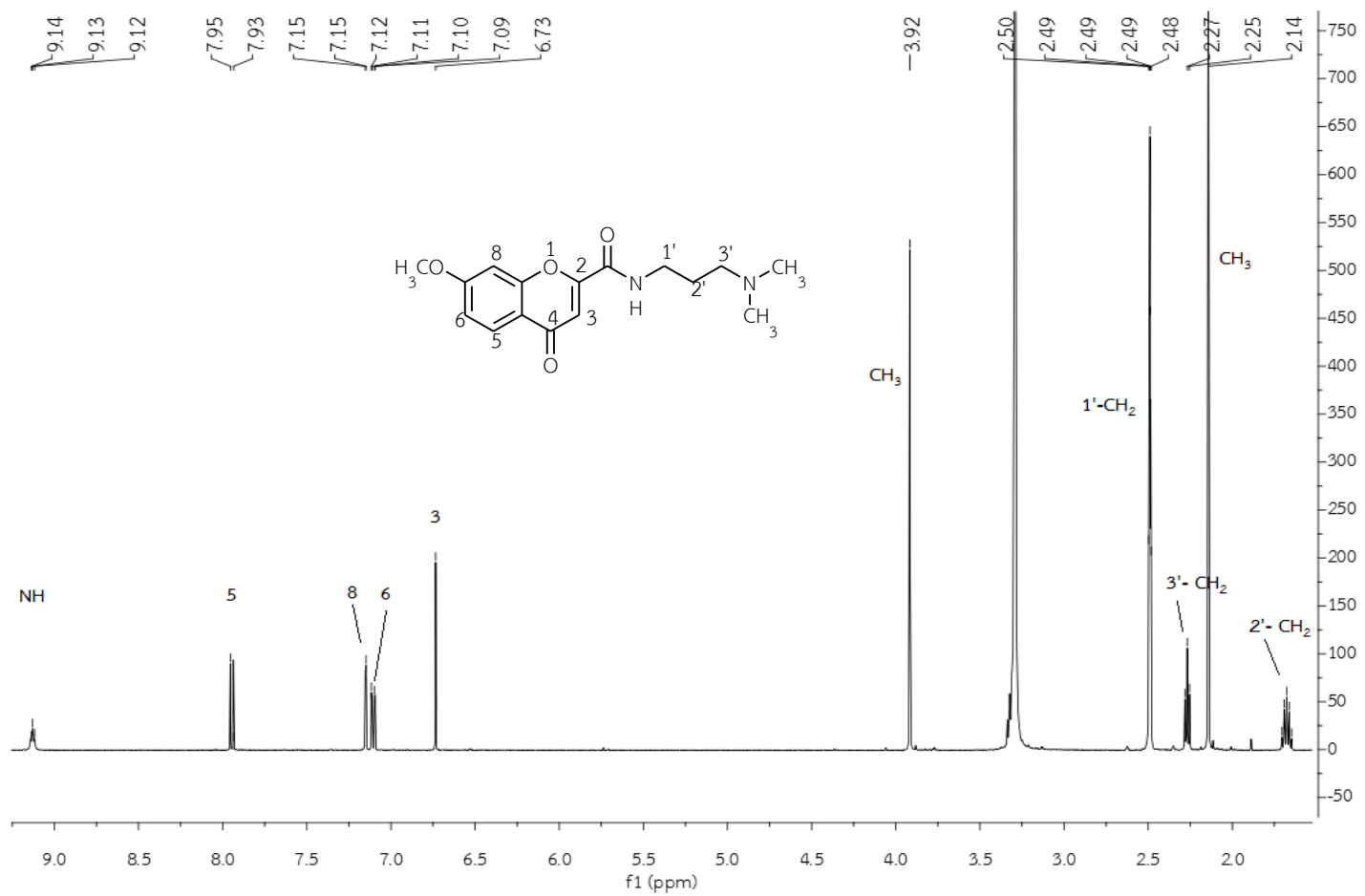


Figure 73. The ¹H-NMR spectrum of *N*-(3-(dimethylamino)propyl)-7-methoxy-4-oxo-4*H*-chromene-2-carboxamide (**13**) in DMSO-*d*₆

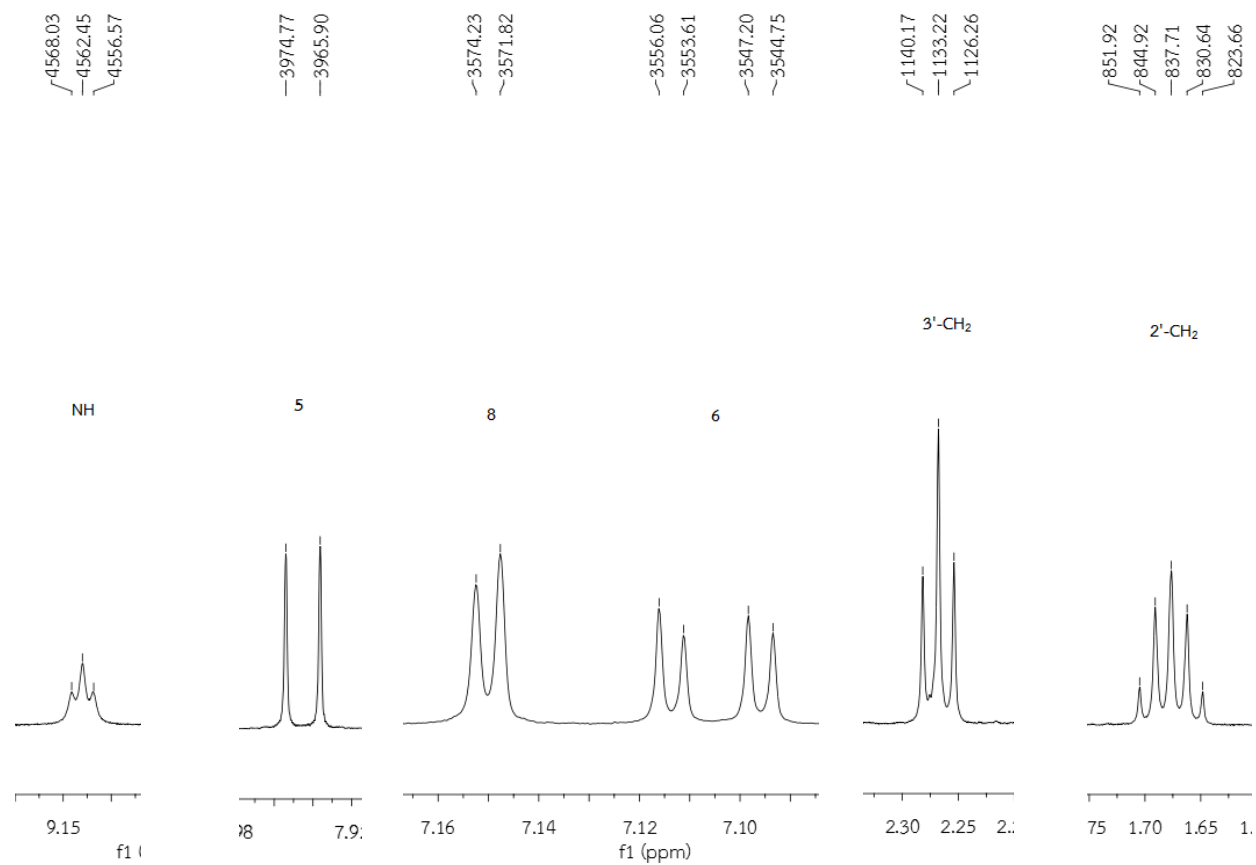


Figure 74. The ¹H-NMR spectrum of *N*-(3-(dimethylamino)propyl)-7-methoxy-4-oxo-4*H*-chromene-2-carboxamide (**13**) in DMSO-*d*₆ (Enlarged scale)

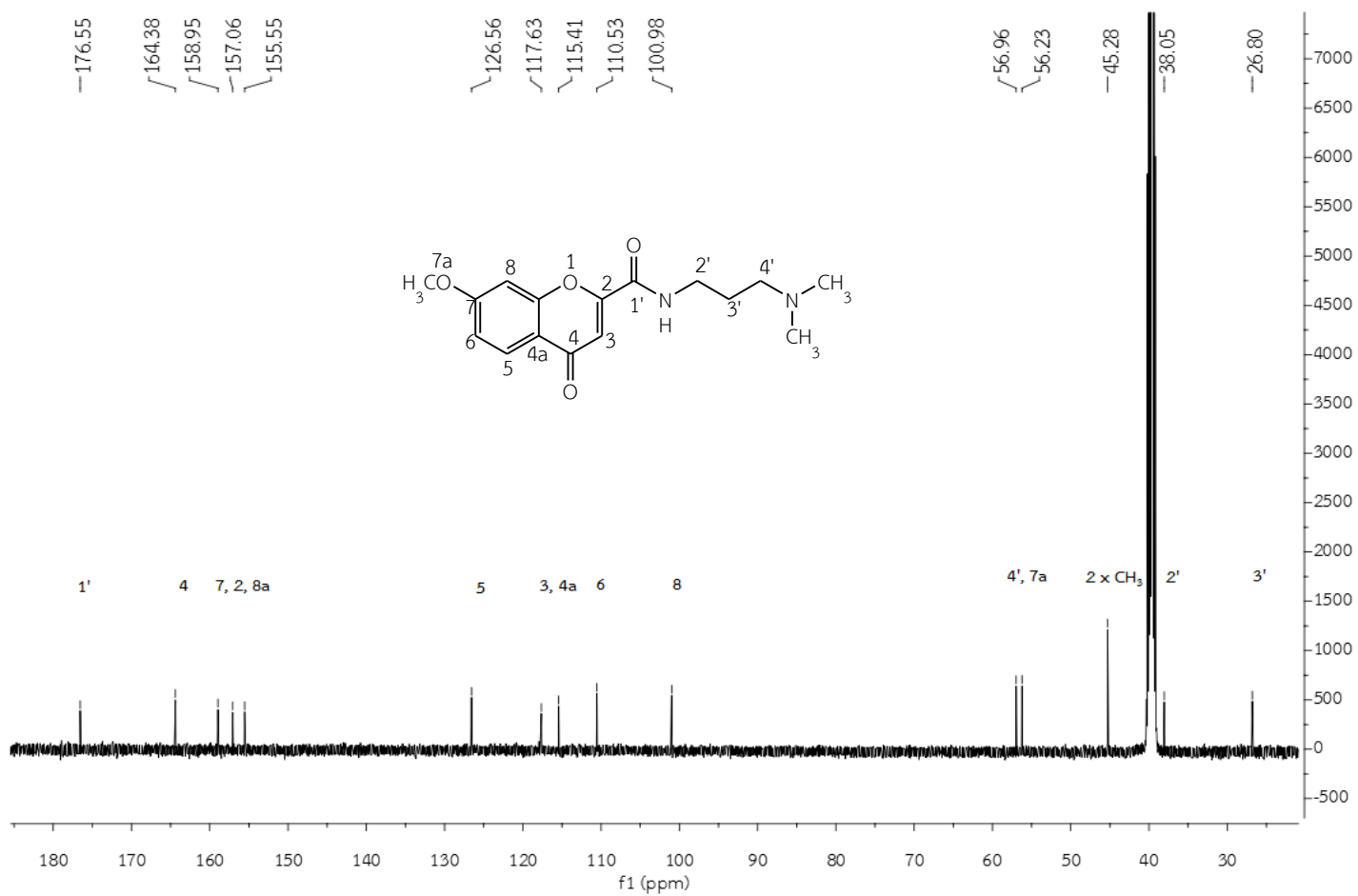


Figure 75. The ^{13}C -NMR spectrum of *N*-(3-(dimethylamino)propyl)-7-methoxy-4-oxo-4*H*-chromene-2-carboxamide (**13**) in $\text{DMSO-}d_6$

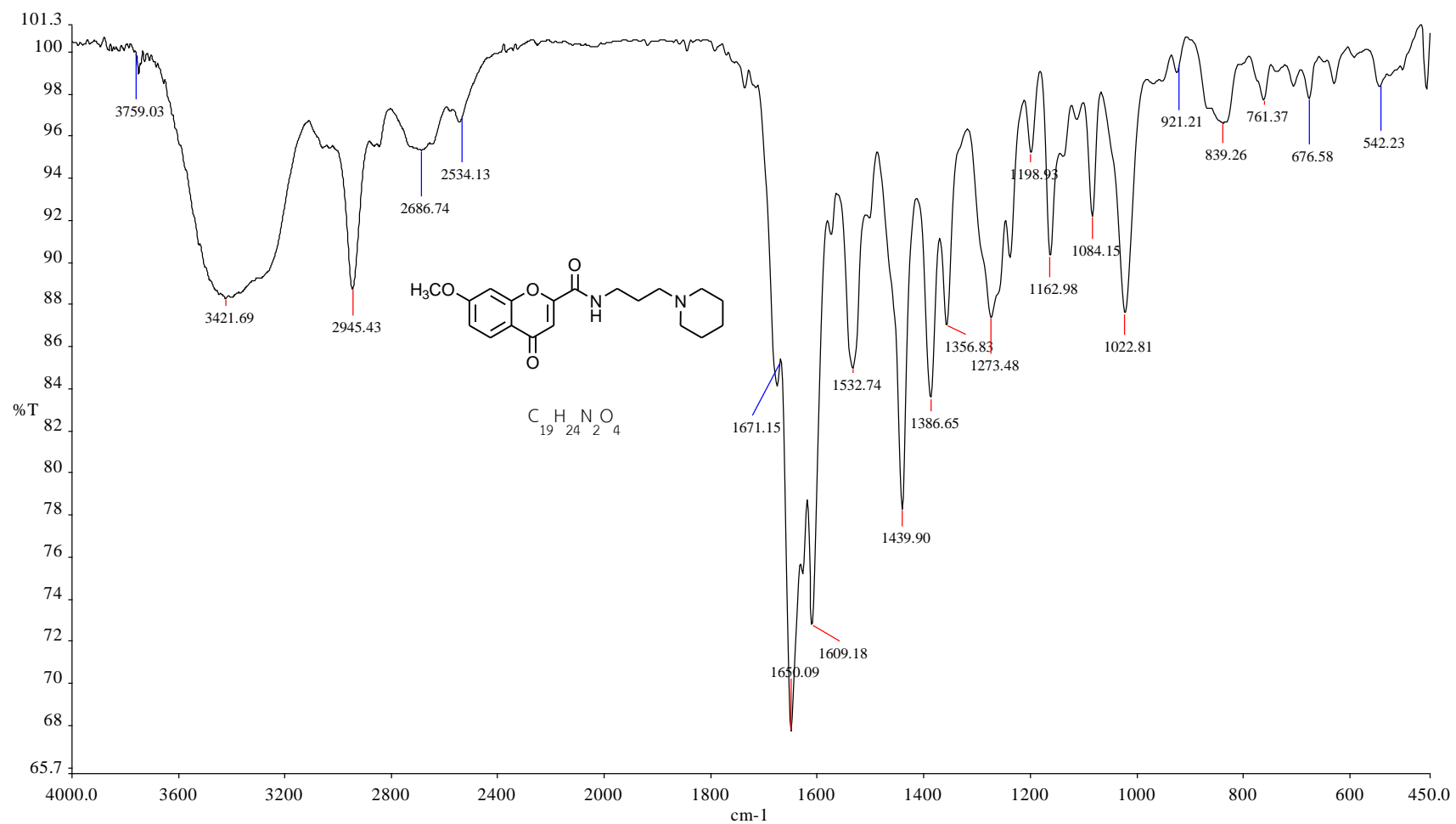


Figure 76. The IR spectrum of 7-methoxy-4-oxo-N-(3-(piperidin-1-yl)propyl)-4H-chromene-2-carboxamide (**14**)

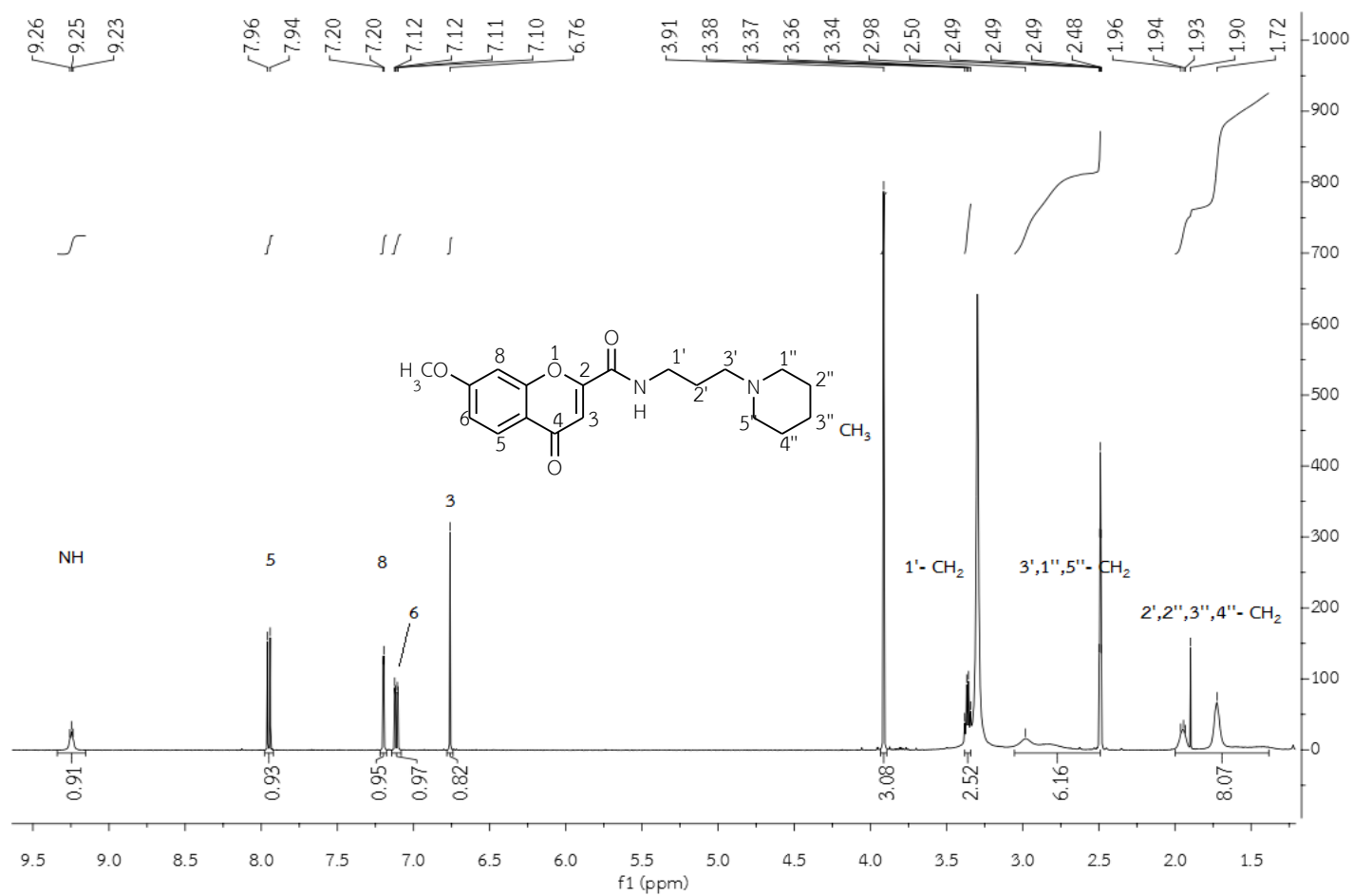


Figure 77. The ¹H-NMR spectrum of 7-methoxy-4-oxo-*N*-(3-(piperidin-1-yl)propyl)-4*H*-chromene-2-carboxamide (**14**) in DMSO-*d*₆

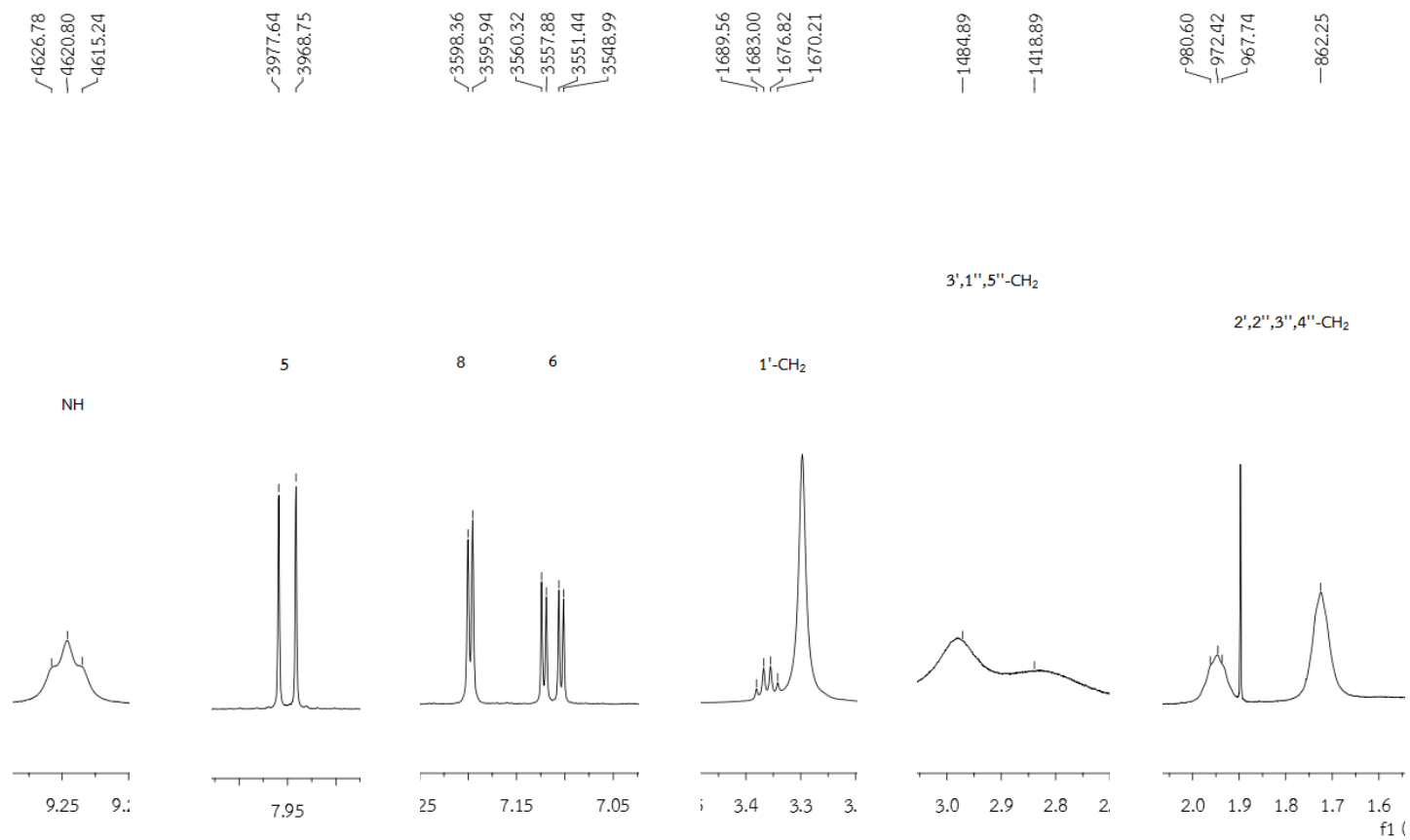


Figure 78. The ¹H-NMR spectrum of 7-methoxy-4-oxo-*N*-(3-(piperidin-1-yl)propyl)-4*H*-chromene-2-carboxamide (**14**) in DMSO-*d*₆ (Enlarged scale)

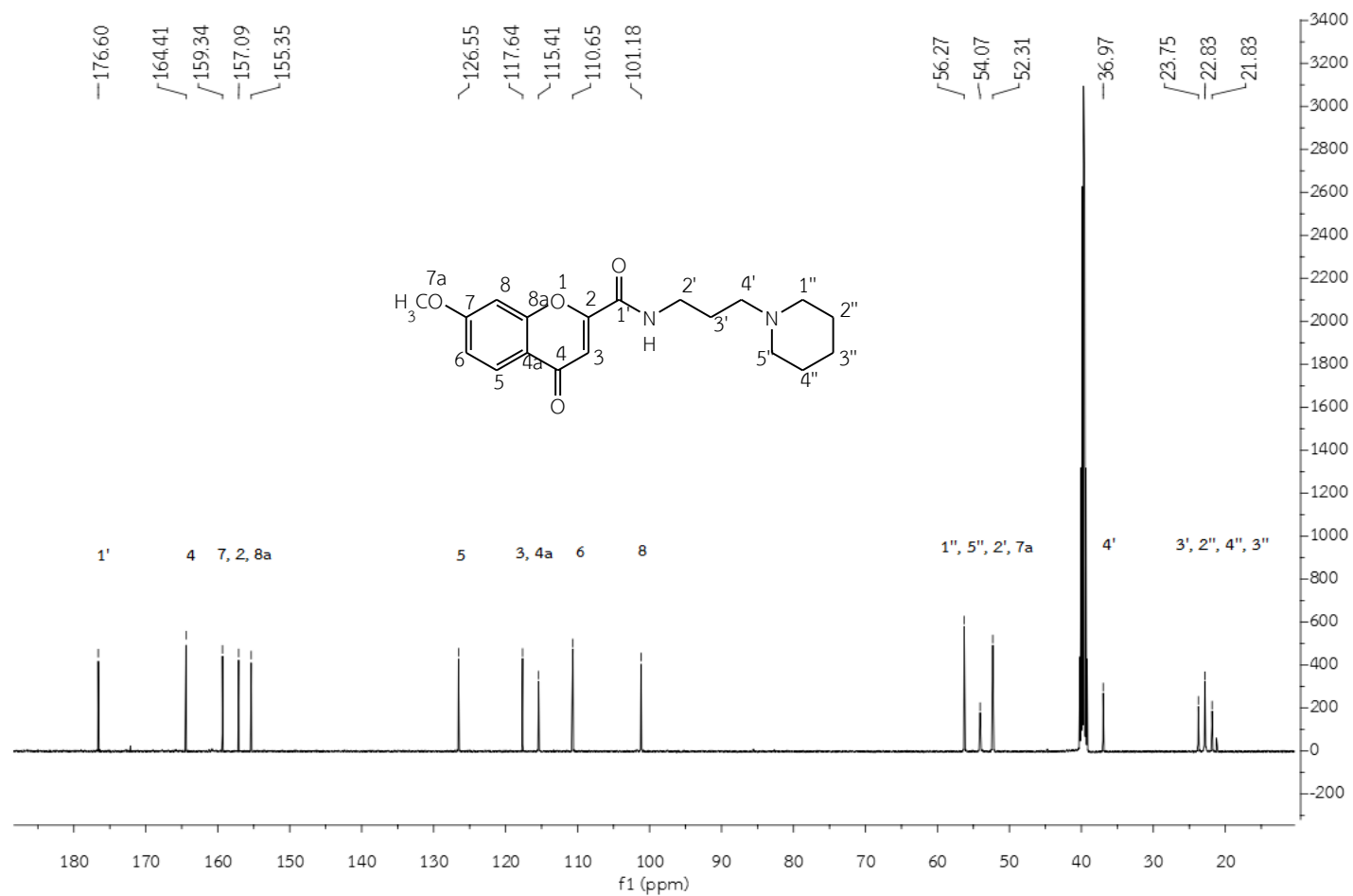


Figure 79. The ^{13}C -NMR spectrum of 7-methoxy-4-oxo-*N*-(3-(piperidin-1-yl)propyl)-4*H*-chromene-2-carboxamide (**14**) in $\text{DMSO-}d_6$

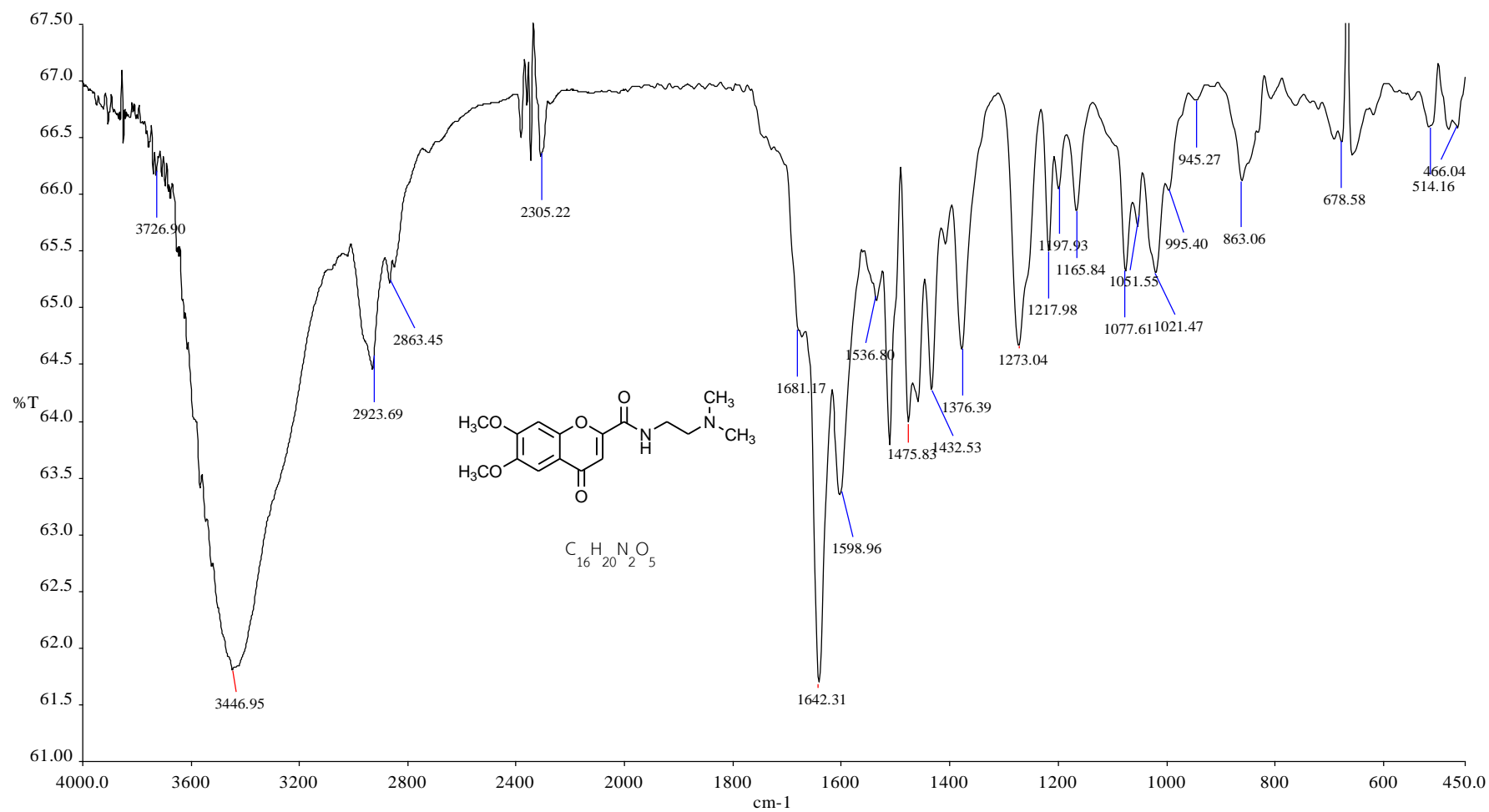


Figure 80. The IR spectrum of *N*-(2-(dimethylamino)ethyl)-6, 7-dimethoxy-4-oxo-4*H*-chromene-2-carboxamide (**15**)

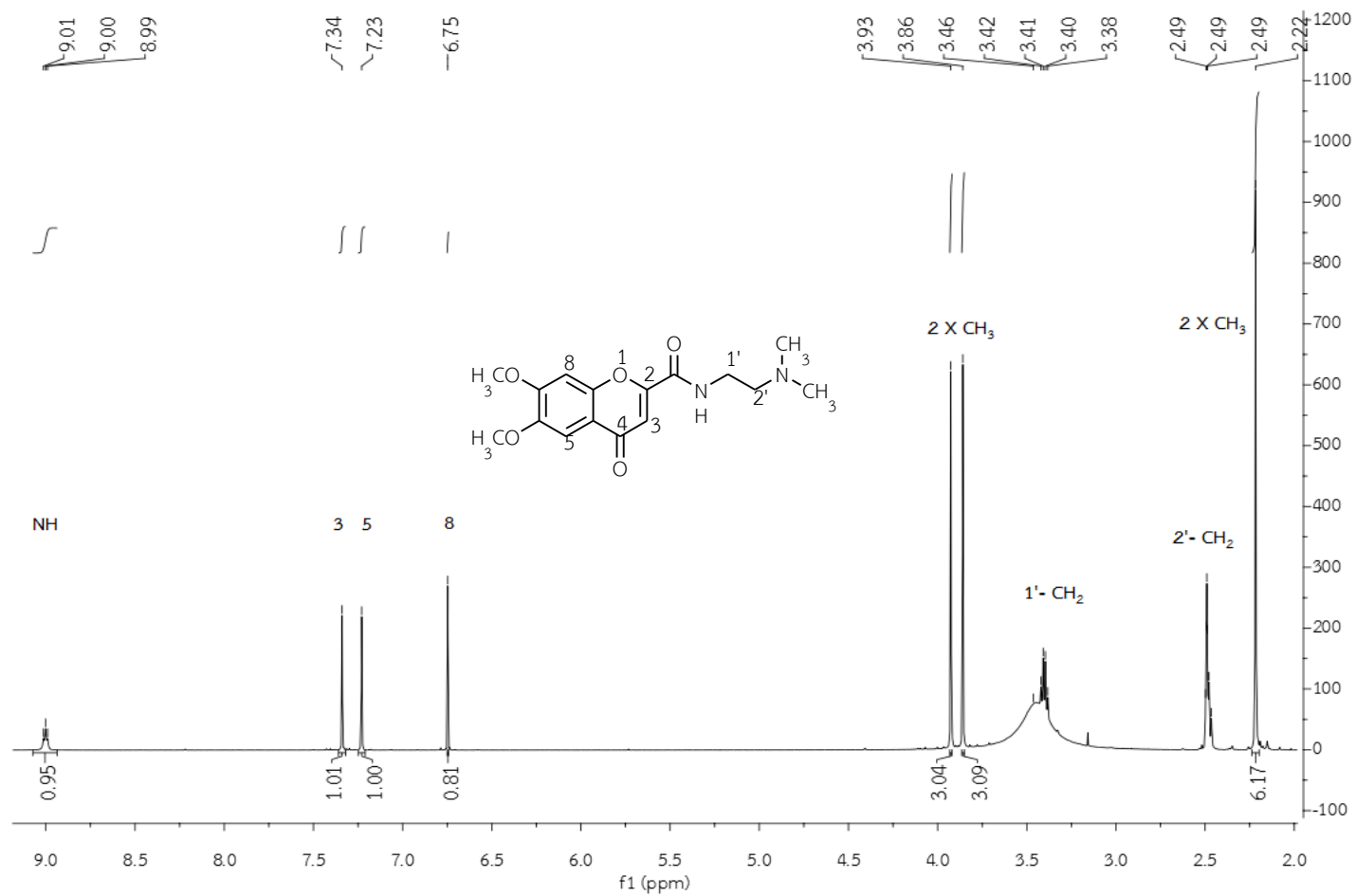


Figure 81. The ¹H-NMR spectrum of *N*-(2-(dimethylamino)ethyl)-6,7-dimethoxy-4-oxo-4*H*-chromene-2-carboxamide (15) in DMSO-*d*₆

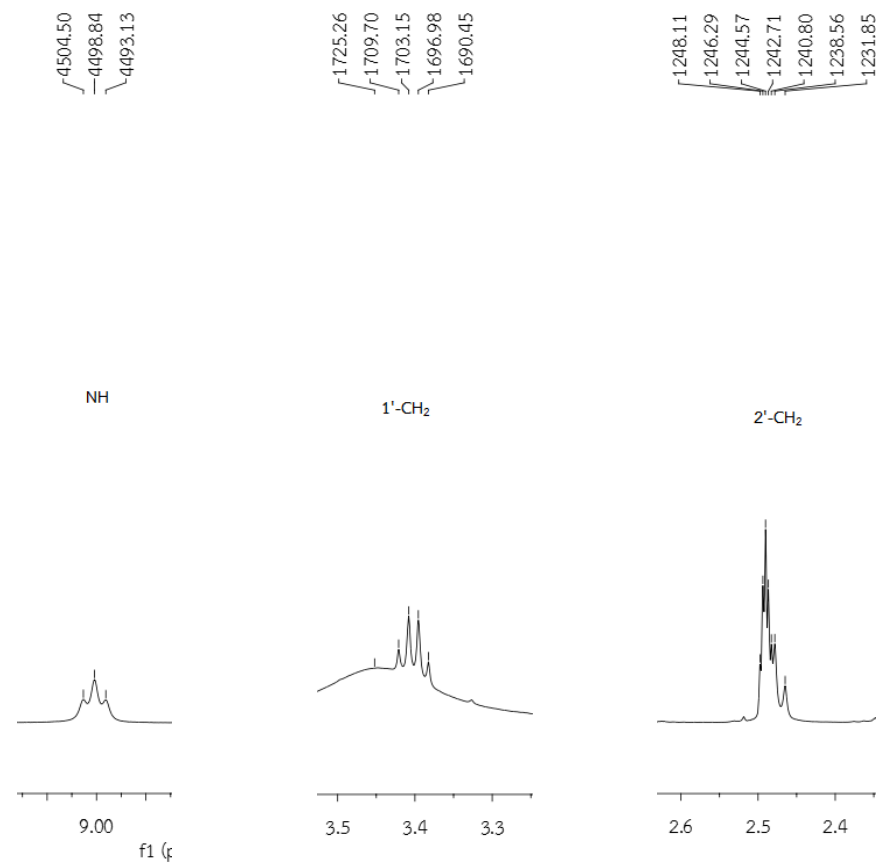


Figure 82. The ¹H-NMR spectrum of *N*-(2-(dimethylamino)ethyl)-6,7-dimethoxy-4-oxo-4*H*-chromene-2-carboxamide (**15**) in DMSO-*d*₆ (Enlarged scale)

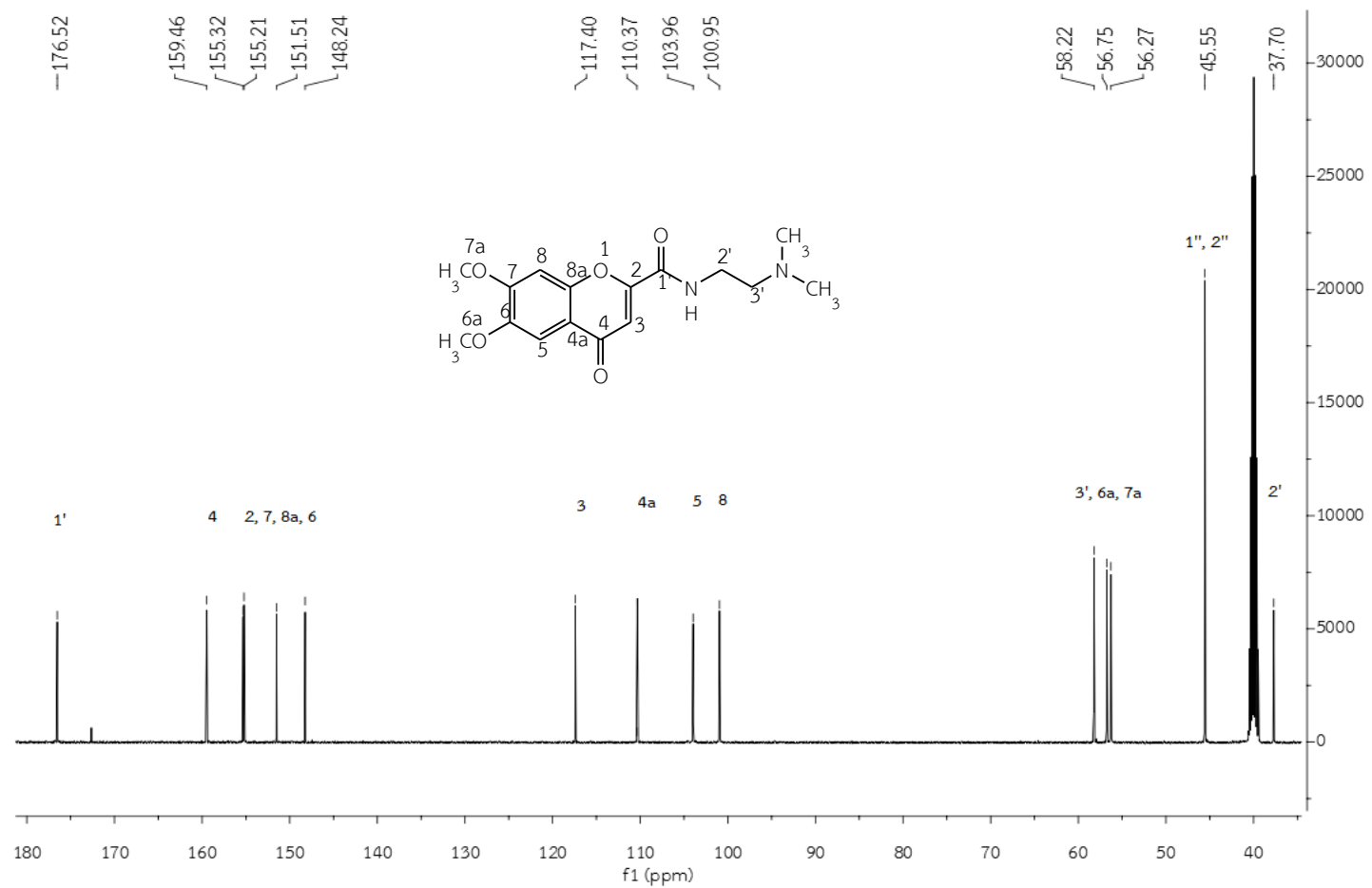


Figure 83. The ^{13}C -NMR spectrum of *N*-(2-(dimethylamino)ethyl)-6,7-dimethoxy-4-oxo-4*H*-chromene-2-carboxamide (15) in $\text{DMSO-}d_6$

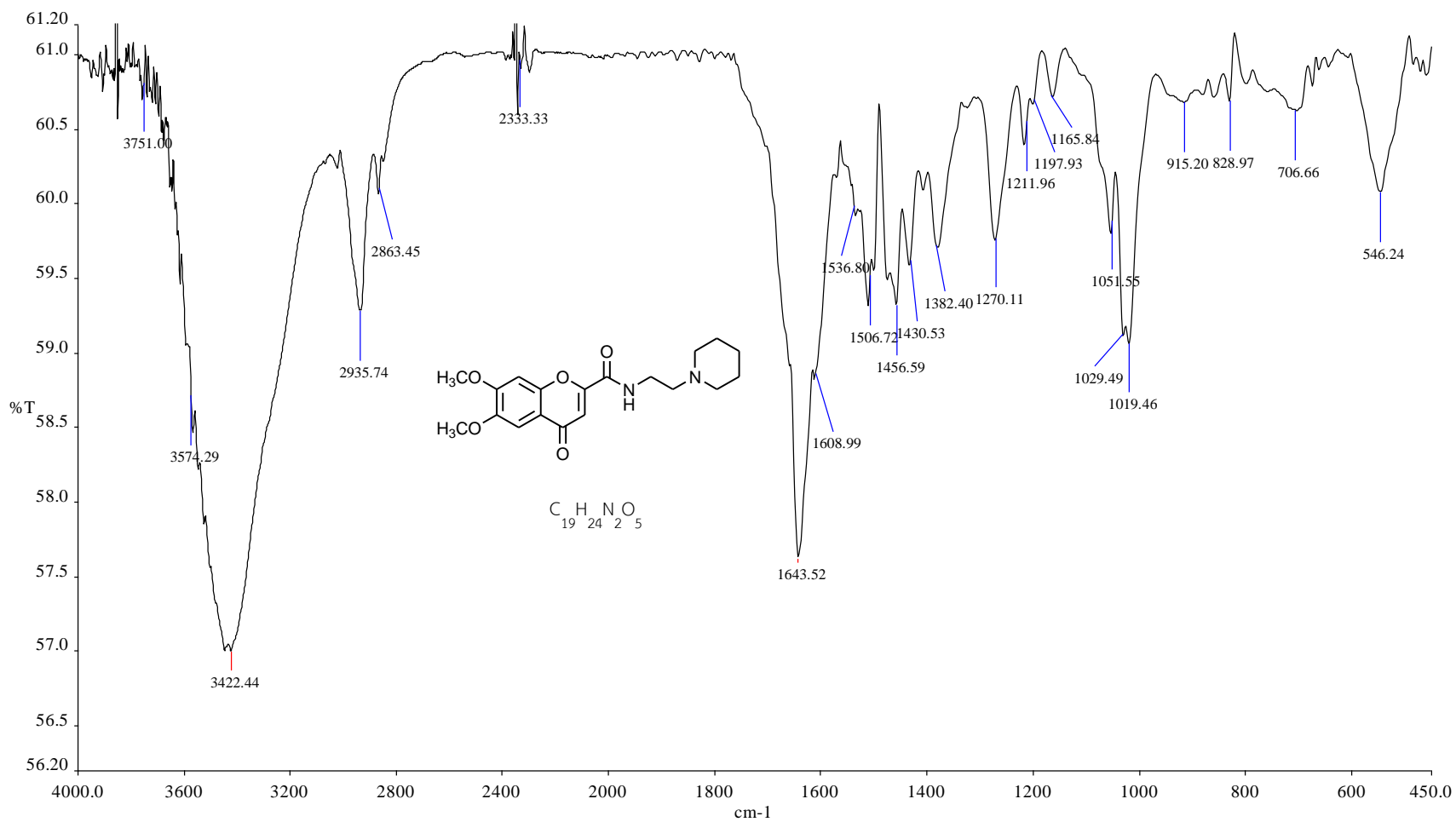


Figure 84. The IR spectrum of 6, 7-dimethoxy-4-oxo-N-(2-(piperidin-1-yl)ethyl)-4H-chromene-2-carboxamide (16)

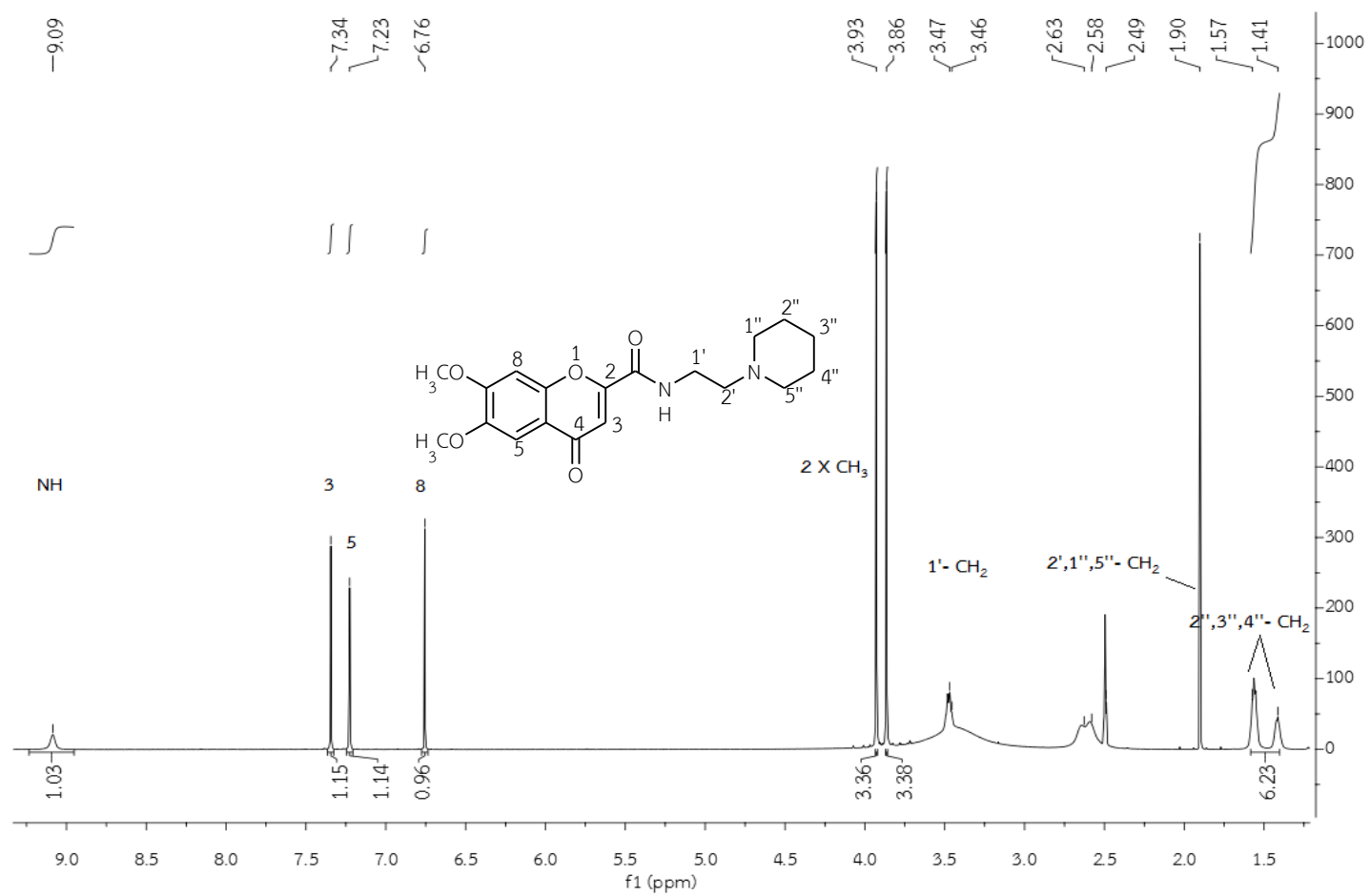


Figure 85. The ¹H-NMR spectrum of 6, 7-dimethoxy-4-oxo-N-(2-(piperidin-1-yl)ethyl)-4H-chromene-2-carboxamide (**16**) in DMSO-*d*₆

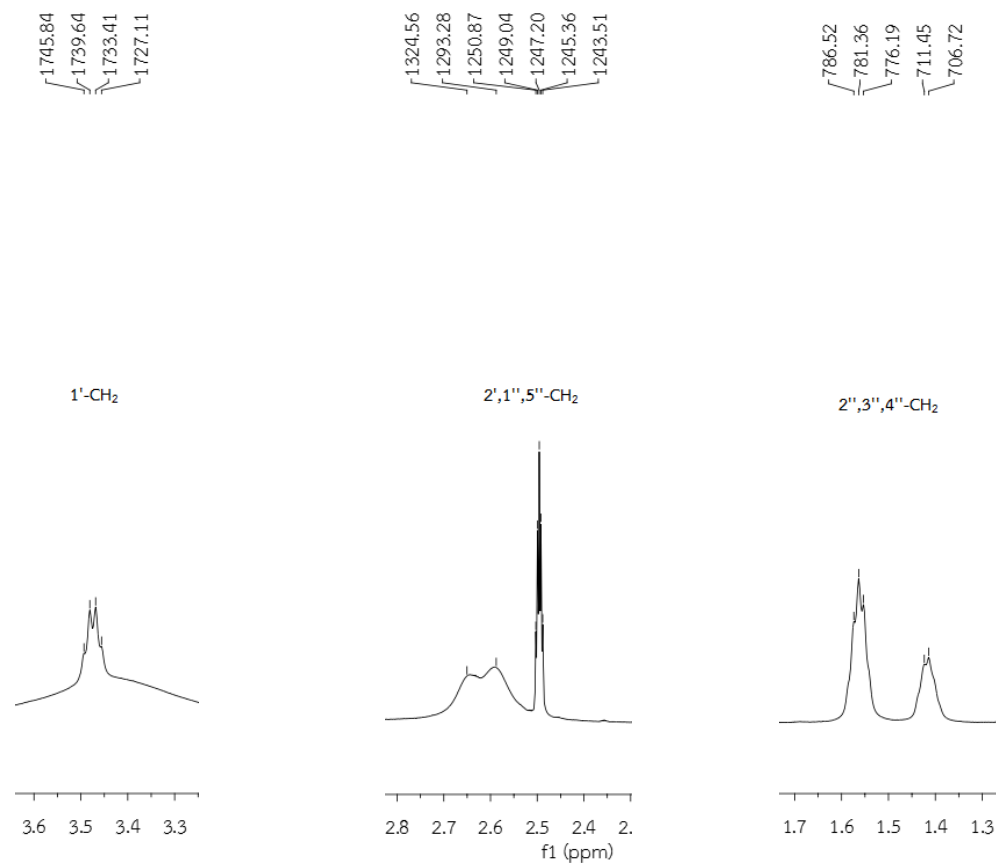


Figure 86. The $^1\text{H-NMR}$ spectrum of 6, 7-dimethoxy-4-oxo-*N*-(2-(piperidin-1-yl)ethyl)-4*H*-chromene-2-carboxamide (**16**) in $\text{DMSO-}d_6$ (Enlarged scale)

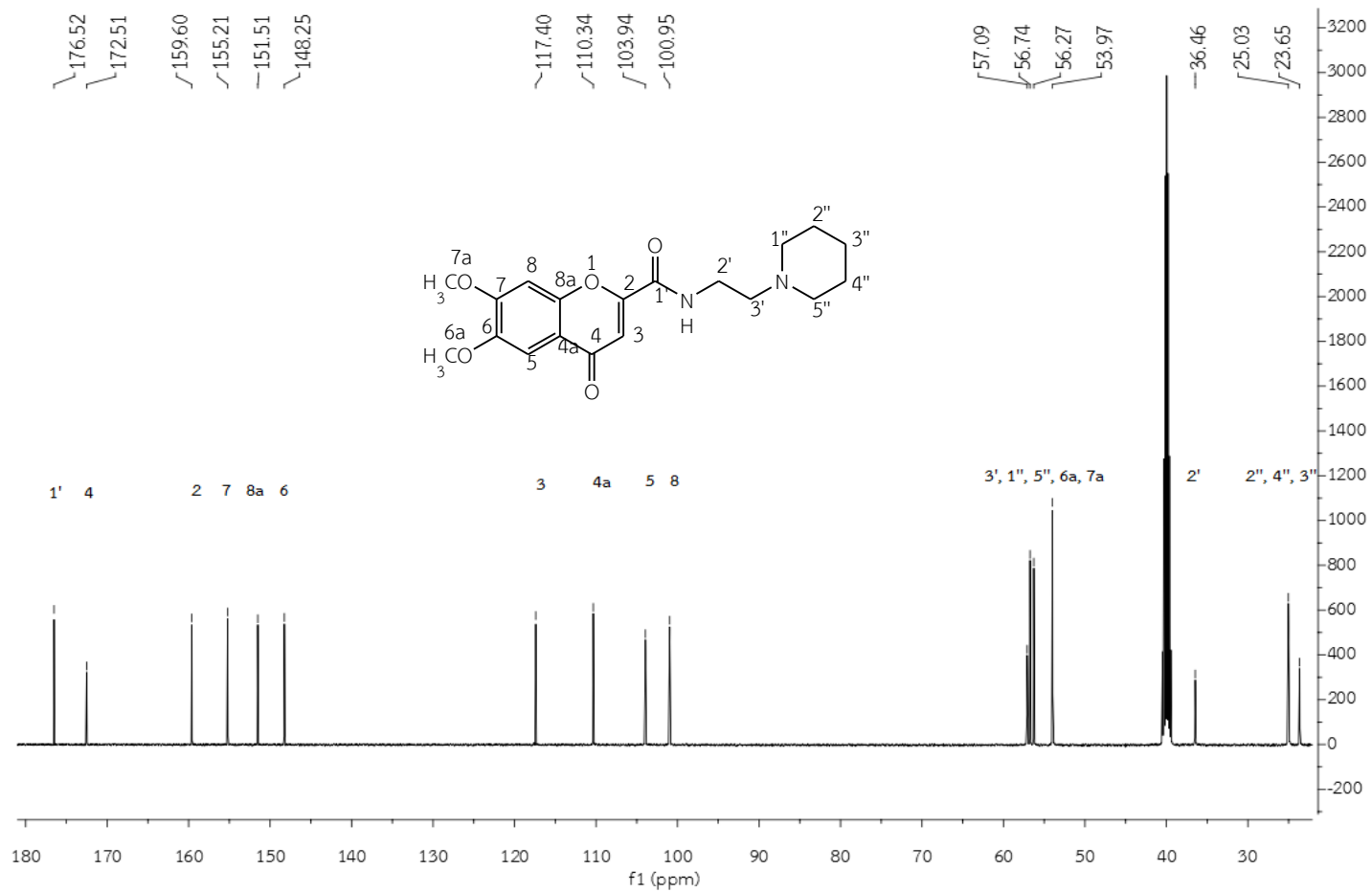


Figure 87. The ¹³C-NMR spectrum of 6, 7-dimethoxy-4-oxo-N-(2-(piperidin-1-yl)ethyl)-4H-chromene-2-carboxamide (**16**) in DMSO-*d*₆

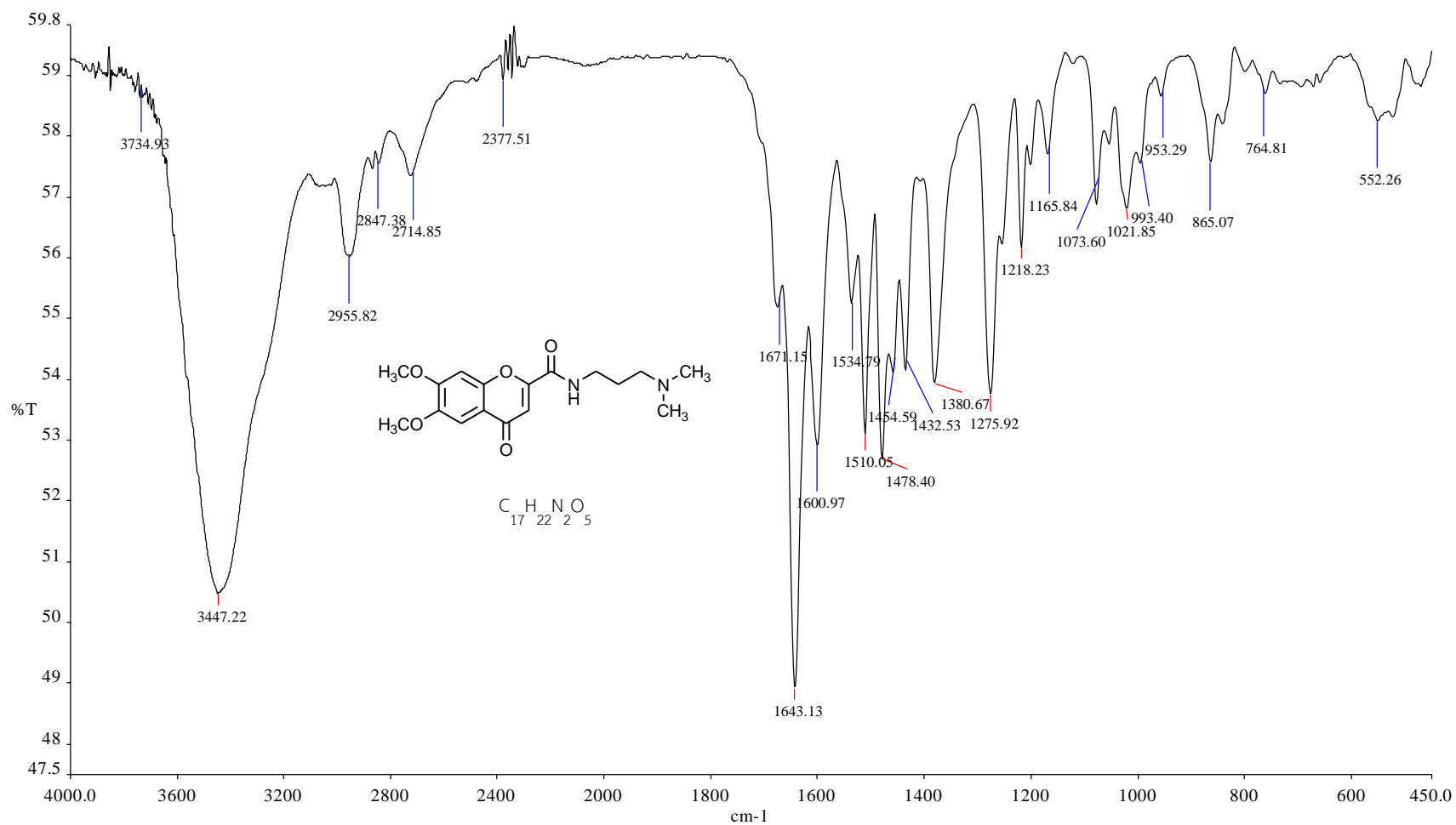


Figure 88. The IR spectrum of *N*-(3-(dimethylamino)propyl)-6,7-dimethoxy-4-oxo-4*H*-chromene-2-carboxamide (17)

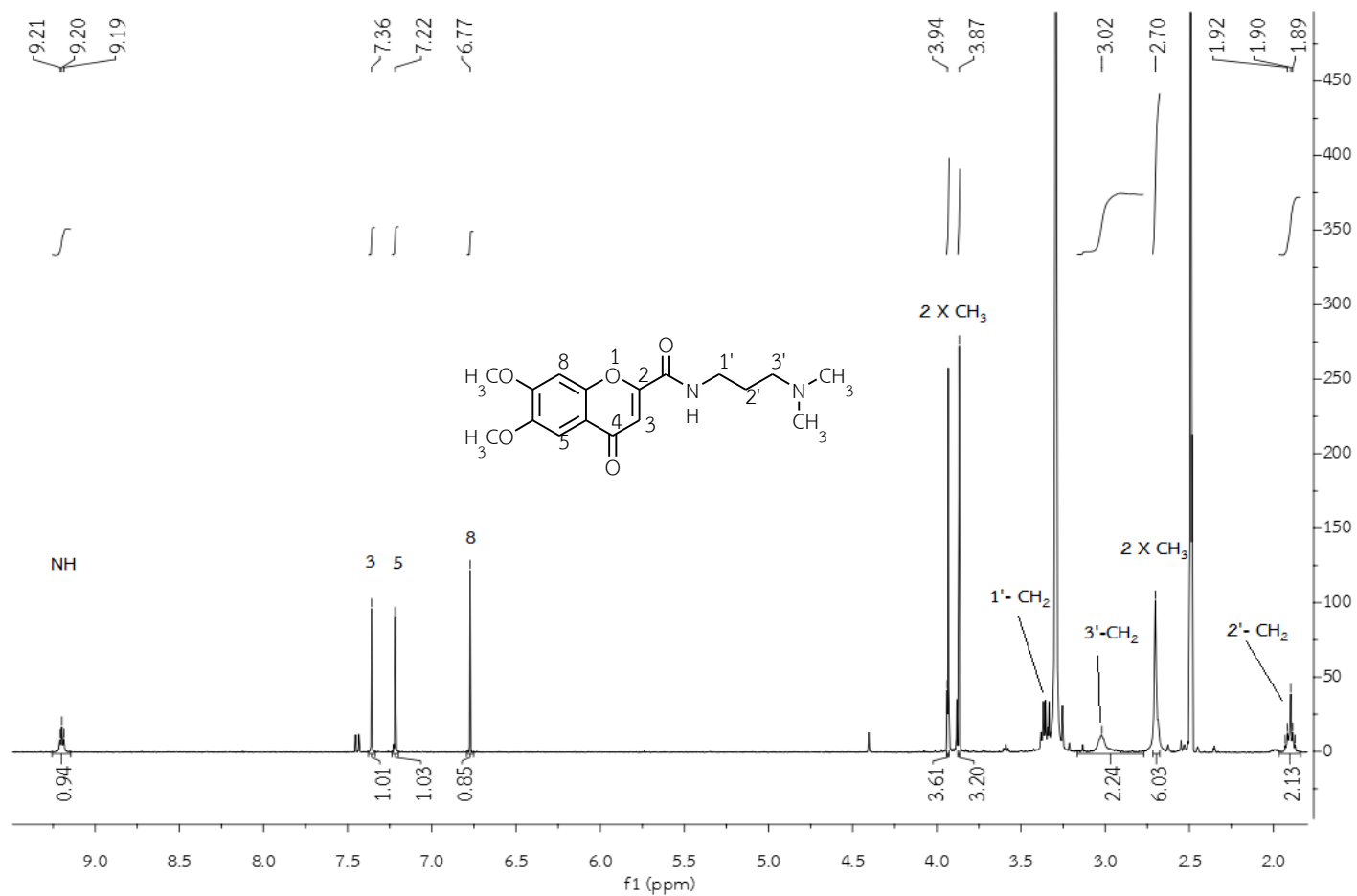


Figure 89. The ¹H-NMR spectrum of *N*-(3-(dimethylamino)propyl)-6,7-dimethoxy-4-oxo-4*H*-chromene-2-carboxamide (**17**) in DMSO-*d*₆

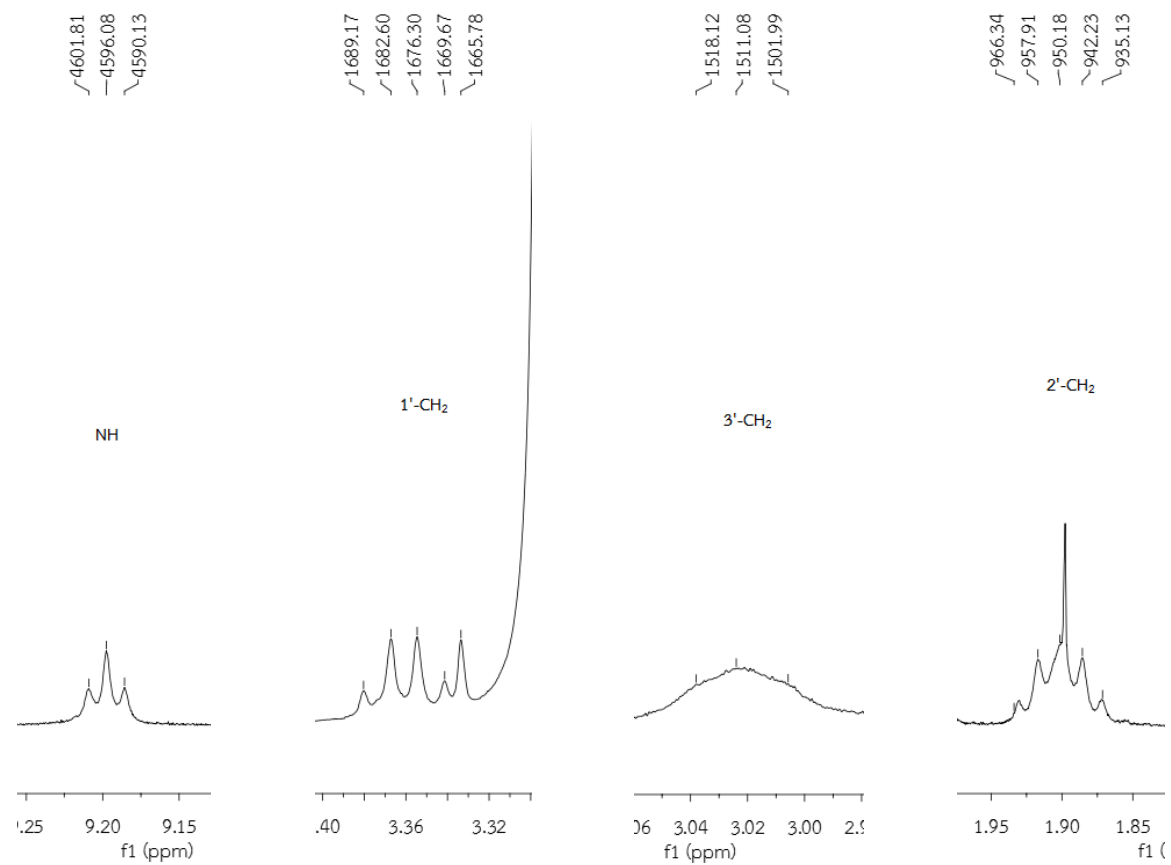


Figure 90. The ¹H-NMR spectrum of *N*-(3-(dimethylamino)propyl)-6,7-dimethoxy-4-oxo-4*H*-chromene-2-carboxamide (**17**) in DMSO-*d*₆ (Enlarged scale)

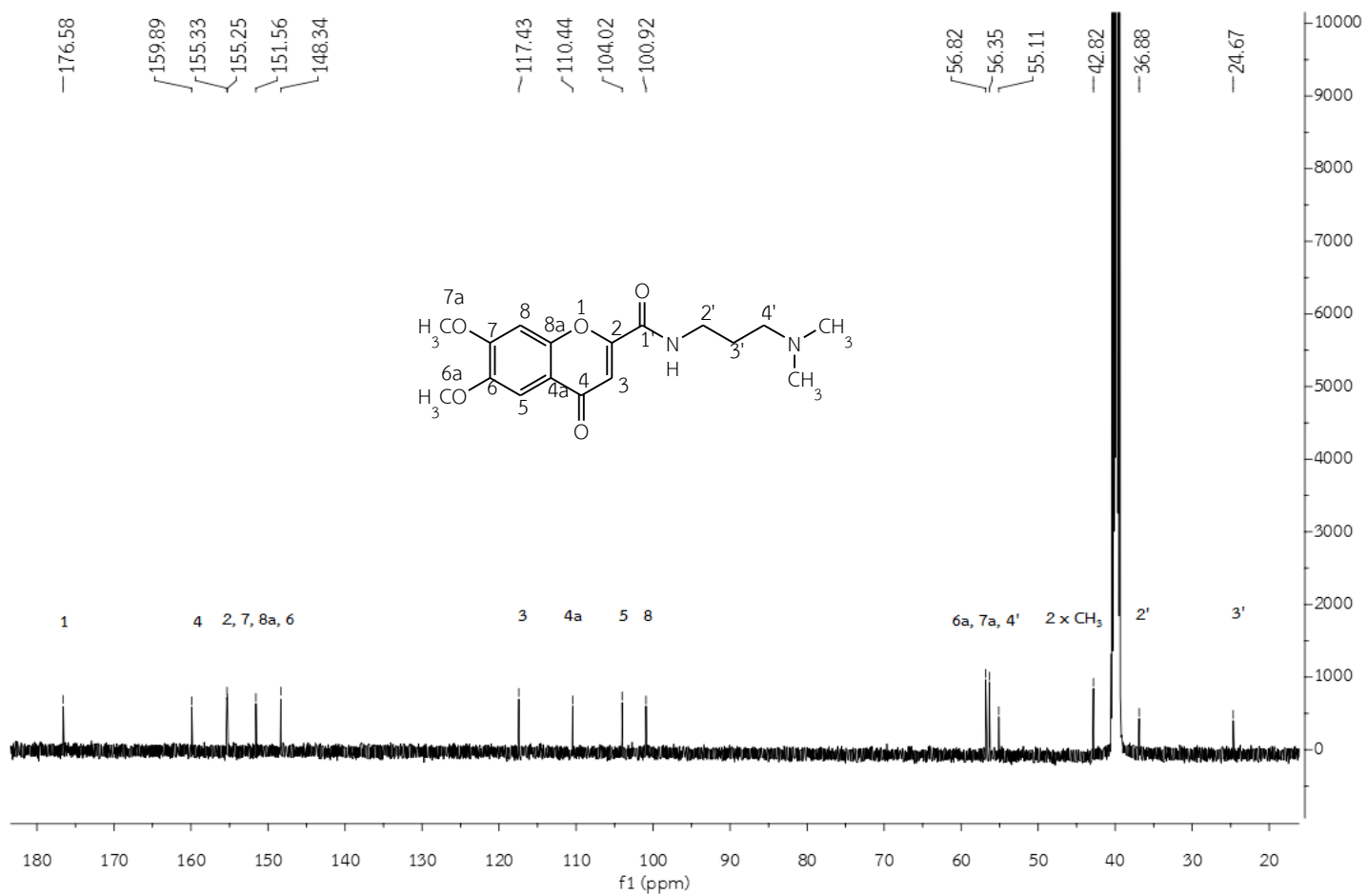


Figure 91. The ¹³C-NMR spectrum of *N*-(3-(dimethylamino)propyl)-6,7-dimethoxy-4-oxo-4*H*-chromene-2-carboxamide (**17**) in DMSO-*d*₆

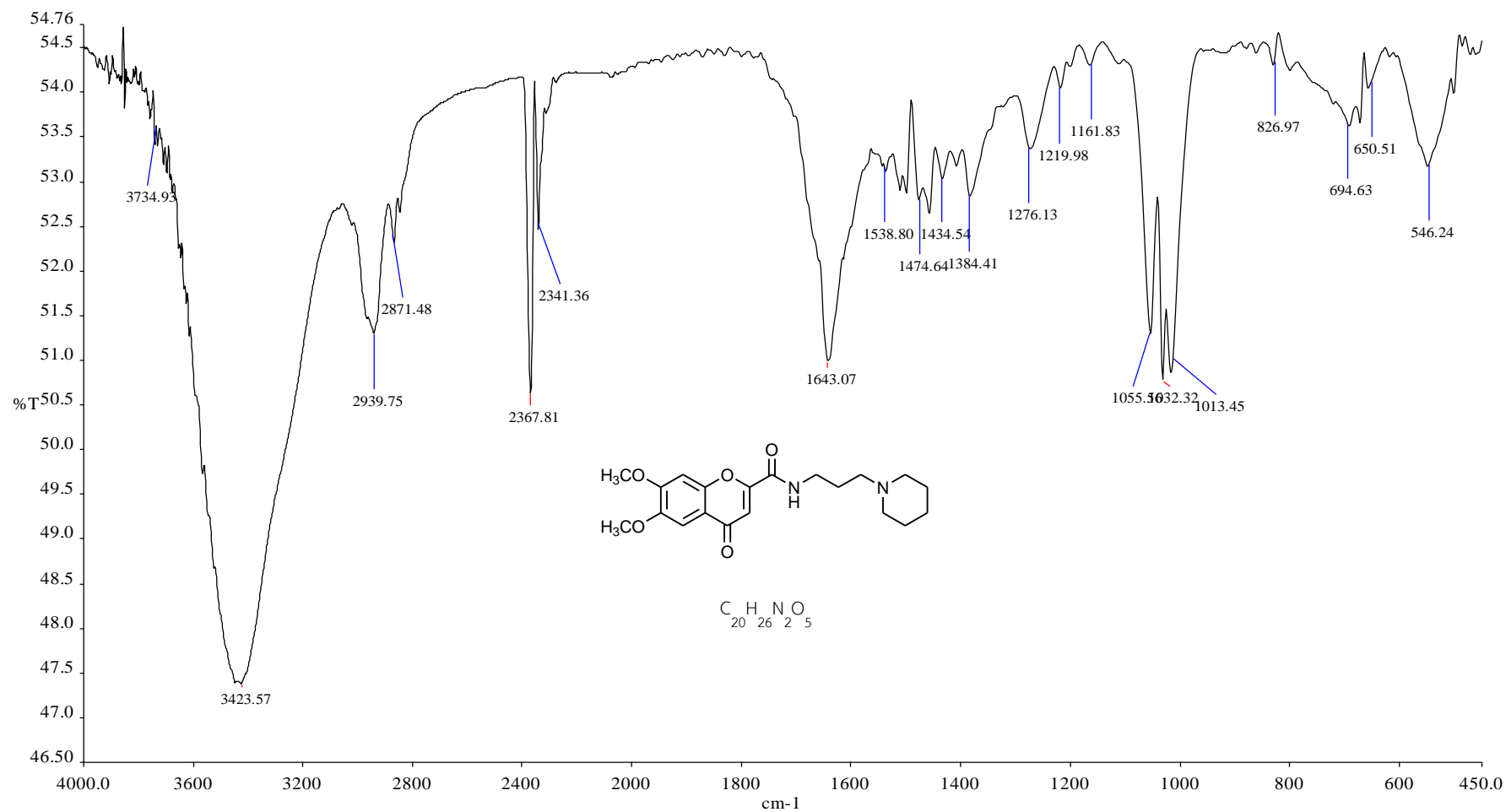


Figure 92. The IR spectrum of 6, 7-dimethoxy-4-oxo-N-(3-(piperidin-1-yl)propyl)-4H-chromene-2-carboxamide (18)

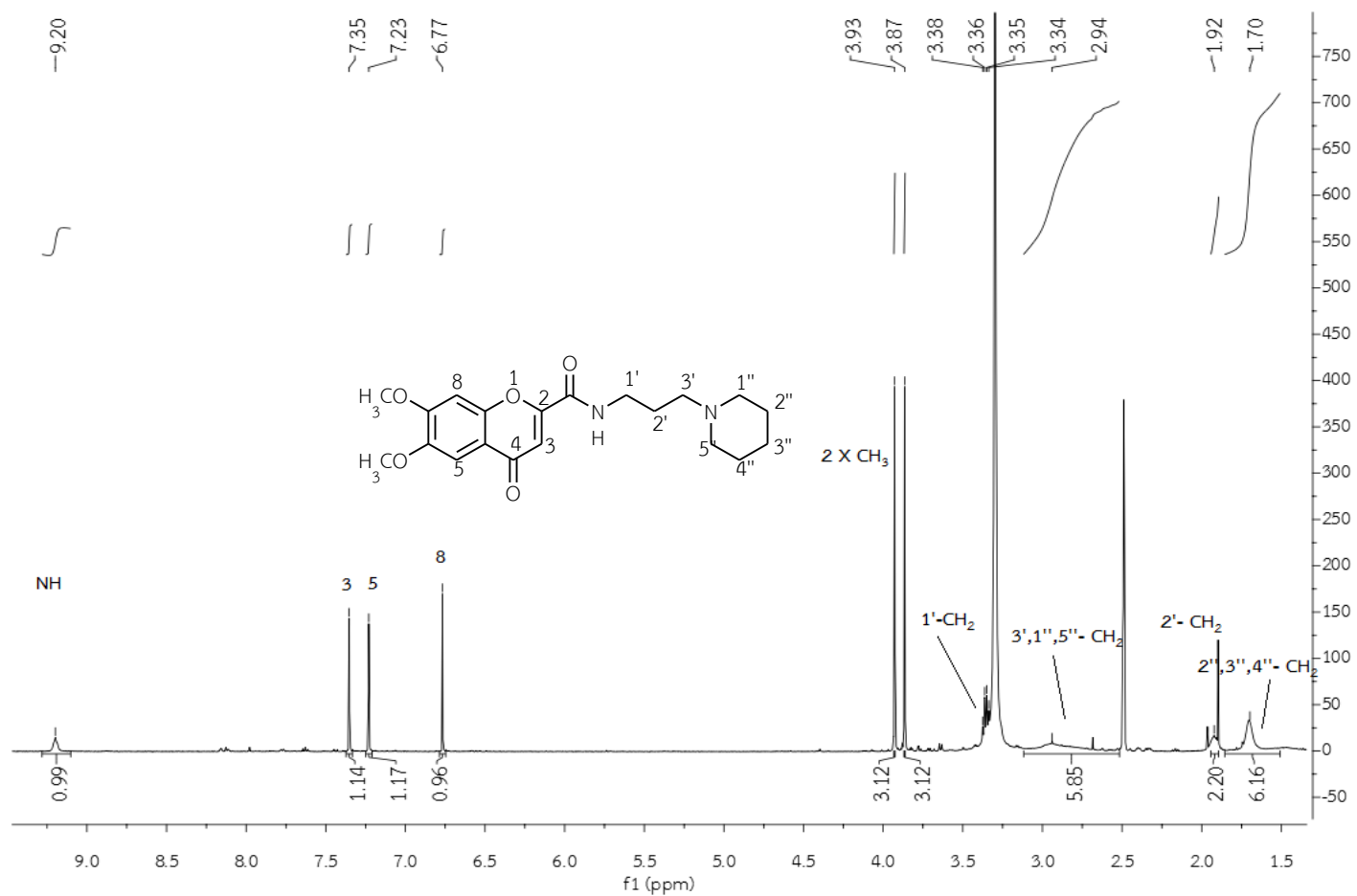


Figure 93. The ¹H-NMR spectrum of 6, 7-dimethoxy-4-oxo-N-(3-(piperidin-1-yl)propyl)-4H-chromene-2-carboxamide (**18**) in DMSO-*d*₆

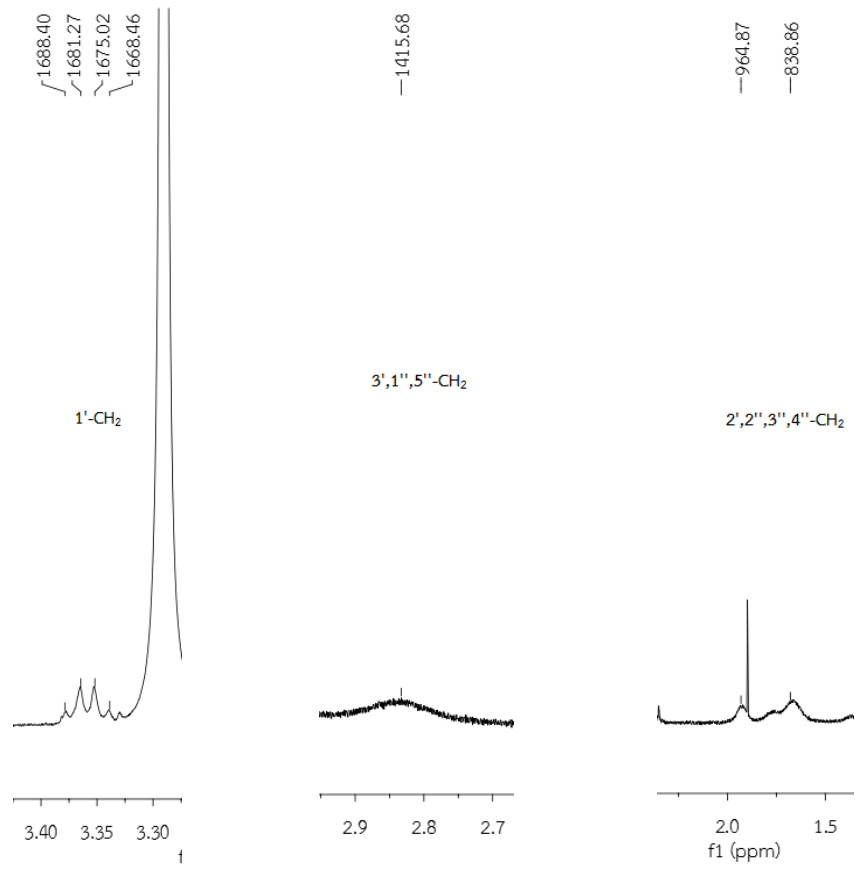


Figure 94. The ¹H-NMR spectrum of 6, 7-dimethoxy-4-oxo-*N*-(3-(piperidin-1-yl)propyl)-4*H*-chromene-2-carboxamide (**18**) in DMSO-*d*₆ (Enlarged scale)

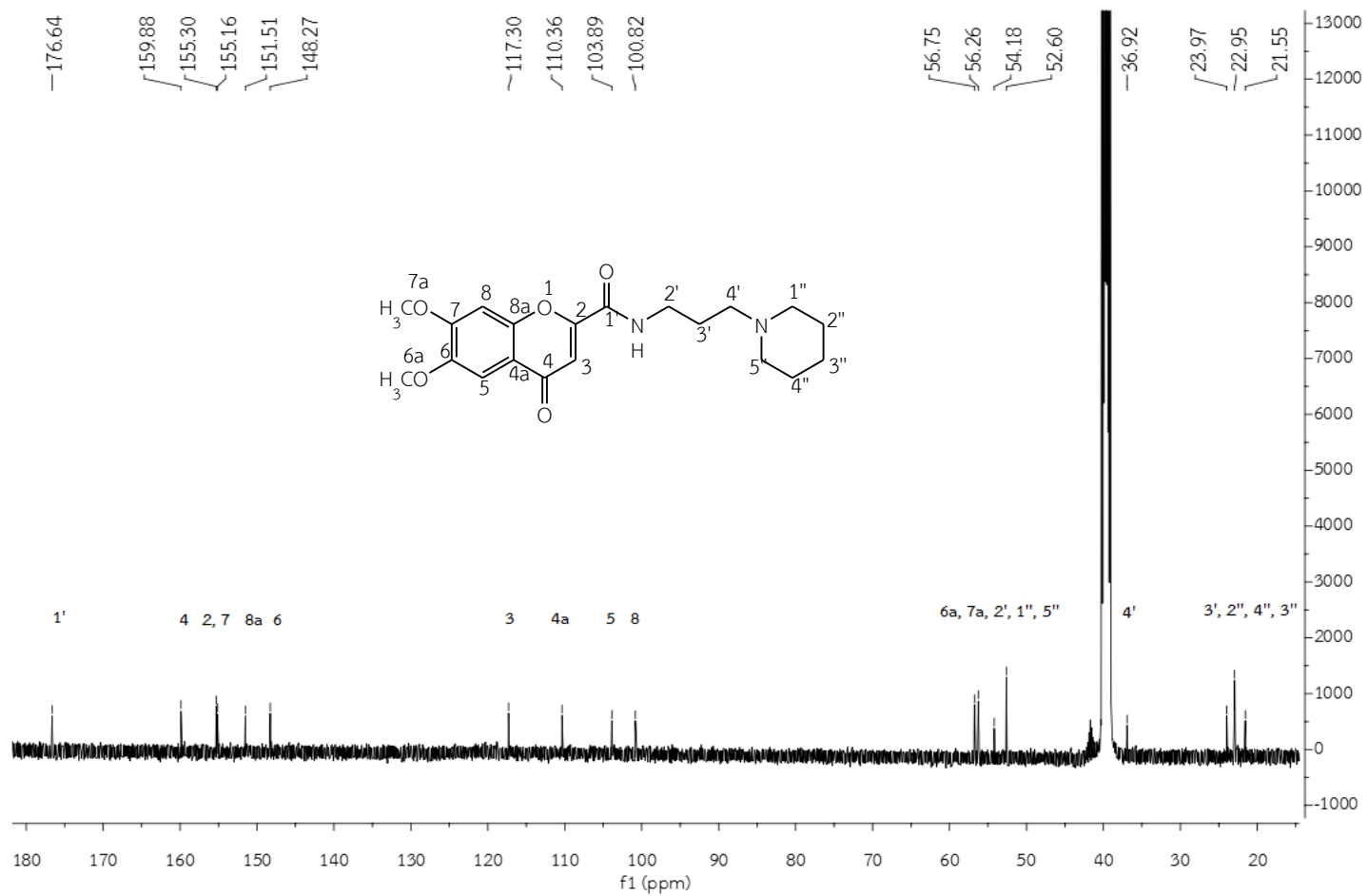


Figure 95. The ¹³C-NMR spectrum of 6, 7-dimethoxy-4-oxo-N-(3-(piperidin-1-yl)propyl)-4H-chromene-2-carboxamide (18) in DMSO-*d*₆

VITAE

Name Miss Paptawan Suwanhom

Student ID 5710720010

Educational Attainment

Degree	Name of Institution	Year of Graduation
Bachelor of Science (Chemistry)	Prince of Songkla University	2013

Scholarship Awards during Enrolment

This work was supported by the budget revenue of Prince of Songkla University (Project No. PHA590412S).

List of Publication and Proceedings

Paptawan Suwanhom, Vannajan Sanghiran Lee, Chatchai Wattanapiromsakul, Luelak Lomlim. Acetylcholinesterase Inhibitory Activity and Molecular Docking of Chromone Derivatives. The 13th Asian Conference on Analytical Sciences (ASIANALYSIS XIII), 8-11 December 2016 at the Empress International Convention Center, Chiangmai University.

P. Suwanhom, V. S. Lee, T. Nualnoi, L. Lomlim. Computational Docking Study of 4-oxo-*N*-(2-(piperidin-1-yl) ethyl)-4*H*-chromene-2-carboxamide as Acetylcholinesterase and Butyrylcholinesterase Inhibitors. The 21st International Annual Symposium on Computational Science and Engineering (ANSCSE21) at Thailand Science Park, Pathum Thani, Thailand.